ULTRASHORT PULSE GENERATION FROM DIODE LASER DEVICES

Youfang HU

Doctor of Philosophy

ASTON UNIVERSITY

May 2005

ABSTRACT

ULTRASHORT PULSE GENERATION FROM DIODE LASER DEVICES

Youfang HU
Doctor of Philosophy
May 2005
ASTON UNIVERSITY

This thesis presents a detailed, experiment-based study of generation of ultrashort optical pulses from diode lasers. Simple and cost-effective techniques were used to generate high power, high quality optical short pulses at various wavelength windows. The major achievements presented in the thesis is summarised as follows.

High power pulses generation is one of the major topics discussed in the thesis. Although gain switching is the simplest way for ultrashort pulse generation, it proves to be quite effective to deliver high energy pulses on condition that the pumping pulses with extremely fast rising time and high enough amplitude are applied on specially designed pulse generators. In the experiment on a grating-coupled surface emitting laser (GCSEL), peak power as high as 1W was achieved even when its spectral bandwidth was controlled within 0.2nm. Another experiment shows violet picosecond pulses with peak power as high as 7W was achieved when the intensive electrical pulses were applied on optimised DC bias to pump an InGaN violet diode laser. The physical mechanism of this phenomenon, as we considered, may attributed to the self-organised quantum dots structure in the laser.

Control of pulse quality, including spectral quality and temporal profile, is an important issue for high power pulse generation. The ways to control pulse quality described in the thesis are also based on simple and effective techniques. For instance, GCSEL used in our experiment has a specially designed air-grating structure for out-coupling of optical signals; hence, a tiny flat aluminium mirror was placed closed to the grating section and resulted in a wavelength tuning range over 100nm and the best side band suppression ratio of 40dB. Self-seeding, as an effective technique for spectral control of pulsed lasers, was demonstrated for the first time in a violet diode laser. In addition, control of temporal profile of the pulse is demonstrated in an overdriven DFB laser. Wavelength tuneable fibre Bragg gratings were used to tailor the huge energy tail of the high power pulse. The whole system was compact and robust.

The ultimate purpose of our study is to design a new family of compact ultrafast diode lasers. Some practical ideas of laser design based on gain-switched and Q-switched devices are also provided in the end.

Keywords: ultrashort pulse generation, diode lasers, high power

ACKNOWLEDGEMENTS

I would like to take this opportunity to express my gratitude to my supervisor, Dr. Igor Khrushchev. He showed me the first step of experiment ever since I came to Aston, discussed with me most of the problems I encountered in the experiments, helped me to write and successfully publish the first academic journal paper in my life. He tried his best to make me motivated in research area, and always offered smiles and encouragements for any minor achievements I had ever made. Under his help, I successfully won the highly competitive ORS award and financial support from Aston University. If it were not for his help, many of my dreams would not have come true.

I would like to thank Prof. Ian Bennion, who fully supports my study in Aston despite of my weak academic background at the beginning and helped me to get the funding both from ORS scheme and Aston University.

I would like to thank Mr. Michael Dubov, who gave me very specific guidance from the single step of the experiment to the theoretical explanation of the experimental phenomenon. He set a good example as a researcher with superb experimental skills as well as solid theoretical background. The discussion between Michael and me always went deep. Under his guidance, I saved a lot of time to get used to the complicated devices and equipments, to choose the proper direction of research, and to get the first valuable experimental result. From him, I acquired a large amount of knowledge and skills and was able to do research independently.

I would also like to thank Dr. Lin Zhang, who gave me a lot of general guidance of research, helped me to choose research area and apply for financial supports. I would like to thank Mr Bert Biggs, who offered highly professional technical support for my research work. My gratitude also goes to, Dr Zhijian Huang, Dr David Birkin, Dr Donghui Zhao and Dr Yicheng Lai, who are always generous to offer help either in research or in my daily life. All the three years' PhD study was full of joyfulness and I really enjoyed my stay in Aston.

The work presented in Chapter 2 is collaboration with Dr Alexei Gubenko from Ioffe Institute in Russia. He offered the GCSEL laser samples and helped to build the experimental set-up. The work presented in Chapter 5 is in collaboration with Mr Fillip Floreani, who offered great help for fabricating the 860nm fibre Bragg gratings. He endeavoured to align the fabrication system to improve the gratings' quality, which contributed to the success of our experiments.

Finally, I would like to express the deepest gratitude to my parents, who worked so hard to support my study in England and never asked for reward. They believe I will realize my dream one day. They are the best parents in the world.

LIST OF CONTENTS

LIST OF FIGURES

LIST OF TABLES

Chapter 1

Introduction

1.1 Perspective

As a part of ultrafast laser technology, ultrashort pulse generation from diode lasers is probably the most efficient and cost-effective way to produce picosecond or femtosecond pulses. It contributes to build extremely compact ultrafast diode lasers. Compared with bulky ultrafast lasers, like solid-state, gas and dye lasers, they have the advantages of high efficiency, low threshold, high repetition rate, excellent wavelength tuneability, extremely low loss, as well as extremely small size. Such compact ultrafast lasers are of great practical importance in modern optoelectronics with the applications covering optical communications, optical signal processing, optoelectronic measurement, optical sensing, high-resolution spectroscopy, bio-medical analysis etc.

Until recently, research in ultrafast diode lasers was mainly driven by the expansion of telecommunications market, for which optical pulses with pulse duration at range of picosend or subpicosecond, repetition rate more than dozens of gigahertz, timing jitter within subpicosecond, and there is no need for extremely high peak power, or femtosecond pulse duration. However, non-telecom applications, including sensing, medical diagnosis, spectroscopy, and biological imaging, are rapidly increasing in importance, and their further development is restricted largely by the lack of a simple, compact pulse source. Commonly, these applications require optical pulses with the shortest possible pulse duration, at various wavelength ranges, but not necessarily at ultrahigh repetition rates. In this thesis, high-quality ultrashort pulse generation from new types of diode lasers will be discussed for applications both within and beyond the area of telecommunication.

1.2 Thesis overview

The contents in the thesis are mainly based on experimental work about ultrashort pulse generation from three types of diode lasers, including InGaAs grating-coupled surface emitting lasers (GCSELs), InGaN violet diode lasers, and GaAs DFB lasers. The issues discussed about these lasers include high power pulse generation, wavelength tuning, linewidth narrowing, spectral filtering, pulse reshaping, etc. The structure of the thesis is shown in Fig. 1.1.

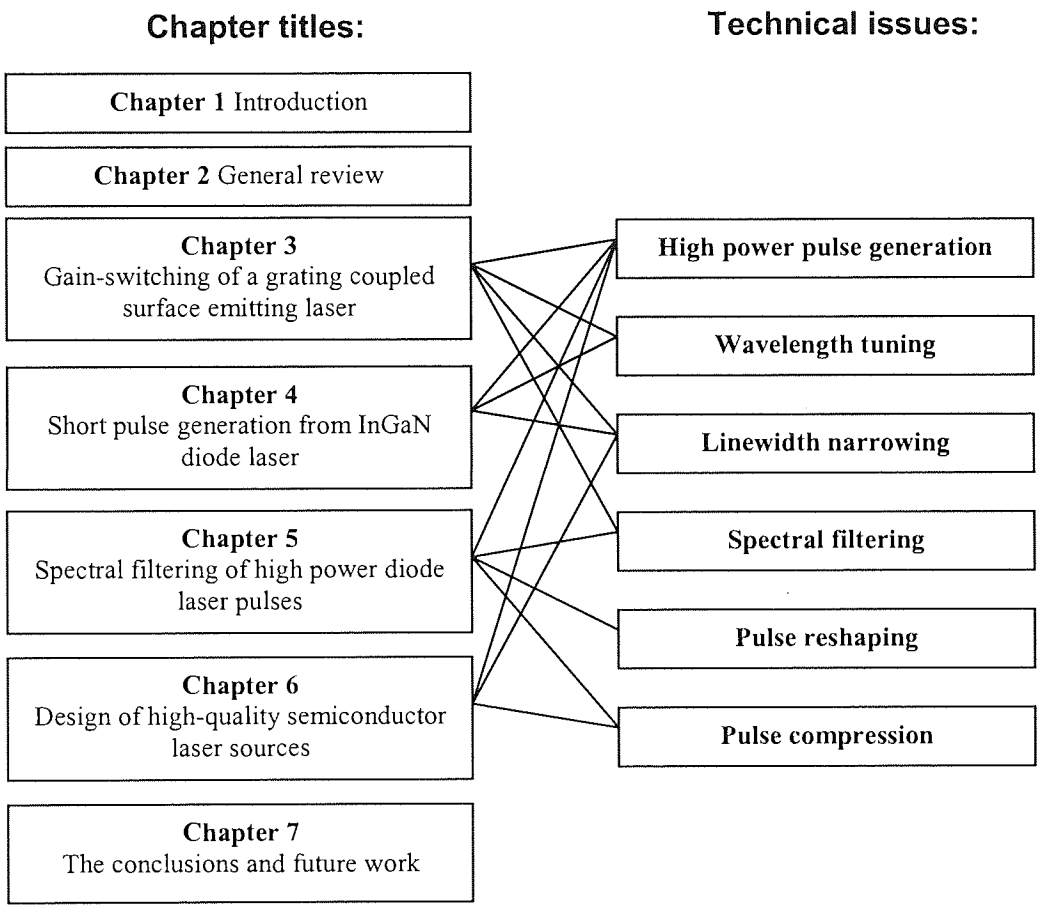

Fig. 1.1 Structure of thesis

Chapter 2 is the general review of ultrafast diode laser technology, it begins with some brief description of fundamental physics of semiconductor diode lasers and then describes the three main techniques for generating pulse trains from diode lasers, namely gain switching, Q-switching and mode-locking. Then, some key issues regarding increasing pulse energy, improving pulse quality, and the problems and new challenges in this field will be discussed. Those issues are also the main topics of the whole thesis.

Chapter 3 presents the detailed experimental study of a grating-coupled surface-emitting laser. The main achievements in this part of work include high energy optical pulses with peak power of 1W obtained by gain-switching, extremely wide wavelength tuning range over 100nm, excellent spectral filtering operation with single frequency output and high side band suppression ratio. The optical part of the pulse generation system has a footprint of only several millimetres. No other devices with similar size and performance are available at the moment.

Chapter 4 deals with experimental research of a commercial InGaN diode laser, operating within blue-violet spectral region. The laser of this type is new and has attracted considerable research attention. The purposes of our work are to control the spectrum as well as to obtain high output power from this laser. As a result, the peak power of the generated pulse was more than one order of magnitude higher than the previously reported. Highly stable, single frequency, wavelength tuneable optical pulses were also achieved using a relatively simple technique, named self-seeded gain switching.

Chapter 5 discusses the issue of spectral filtering of an overdriven GaAs DFB laser. A great deal of theoretical and experimental work shows the fact that, in a over-driven gain-switched pulse, spectral components of the main peak and relaxation tail are separated from each other. It will be a highly efficient way to eliminate the undesired energy tail by simply isolating its corresponding spectral components. In our experiment, fibre Bragg gratings manifested themselves to be the ideal spectral filters for this job. The experimental results qualitatively agreed with our previous work on an InGaAsP DFB laser.

In Chapter 6, the design consideration of a new type of ultrafast diode lasers is presented. It includes the design of pulse generators and auxiliary passive devices. All the techniques suggested are simple and cost-effective.

Finally, in Chapter 7, general conclusions are drawn and future work is suggested. The publications resulting from the work described in the thesis are listed in appendix.

Chapter 2

General review

This chapter presents the fundamental concepts of semiconductor lasers, ultrafast semiconductor lasers and the basic techniques used for ultrashort pulse generation in these lasers. High power ultrafast semiconductor lasers are specially highlighted in this chapter due to their great importance for future applications. In the end, we discuss several special issues associated with ultrafast semiconductor lasers, which are also the main issues of this thesis.

2.1 Introduction

Semiconductor laser was invented in 1962, only two years after the invention of the first ruby laser in the world. Ever since then, advances in material purity and epitaxial growth techniques have led to a variety of semiconductor lasers covering a wide wavelength range (0.3-100μm) with high output power and long lifetime. This kind of lasers has their unique advantages over conventional lasers, such as extremely compact size, cost-effectiveness and high wall-plug efficiency. Many technologies in our modern life like Internet, CD/DVD players and laser printers would be much more expensive and less practical if it were not for the use of semiconductor lasers. Their great commercial value together with tremendous potential of development means there is worldwide research interest in this topic.

Among their various applications, semiconductor lasers are considered to be the best light sources for high-bit-rate optical fibre communication systems and ultrafast optical data-processing systems, which were considered to be the backbone of modern information technology. The performance of those systems relies a great deal on the performance of optical pulses that are generated by diode lasers. Hence, ultrashort pulse generation from semiconductor diode laser becomes a rather practical and valuable topic of research. On the other hand, ultrafast diode lasers provide many other applications including time-resolved spectroscopy, optical computing, laser radar systems and optoelectronic measurement systems. Particularly, the advent of new laser materials and new laser structures in recent years offers an excellent opportunity and a great challenge of research in this field.

2.2 Fundamentals of semiconductor lasers

Comprehensive description of semiconductor physics and semiconductor lasers can be found in literature [2.1-2.4]. In this section, our discussion is focused on some key issues, including semiconductor materials, heterostructure, quantum confinement structures, and semiconductor laser cavity.

2.2.1 Semiconductor materials

It is the use of a large variety of semiconductor materials that makes the emission of diode lasers cover a wide wavelength range from UV to far infrared. Those materials suitable for use in lasers comply with some common characteristics. Fig. 2.1 is the plot of carriers' energy as a function of the crystal momentum wave vector **k** for semiconductor material *GaAs* and *Si*. The band structure depends on crystal direction. The upper bands are the conduction bands, while the lower bands are the valence bands. In *GaAs*, a direct energy gap material, the minimum energy in the conduction band and the maximum energy in the valence band both occur at the same value of **k** (k=0). For an indirect energy gap material, like *Si*, the minimum in the conduction band does not occur at the same value of **k** as the maximum in the valence band. In the direct energy gap material, an electron can make a transition from the valence to the conduction band (or vice versa) directly by the absorption (or emission) of a photon. For the indirect energy gap material, the minimum energy transition at a level of E_g must involve the emission or absorption of a phonon to conserve momentum; hence, the indirect transition is an inherently less probable process than the direct transition. Therefore the appropriate semiconductor materials for diode lasers are, indeed, with direct energy gap.

Fig. 2.1 Energy versus wave-vector diagram of (a) direct-band-gap semiconductor-GaAs and (b) indirect-band-gap semiconductor-Si [2.5].

Typically, one semiconductor laser, like heterostructure lasers, is composed of at least two alloy materials, e.g. $Al_{1-x}Ga_xAs/GaAs$, $In_{1-x}Ga_xAs_yP_{1-y}/InP$. In these types of lasers, lattice matched interface is formed between two semiconductors with different band gaps by varying the compositions x and y. The two materials should typically match to better than 0.1%. On the other hand, the bandgap is also determined by the composition of semiconductor elements. And it is possible to vary the bandgap energy of active layer material at a certain range without introducing lattice mismatch so as to obtain different lasing wavelength. For $In_{1-x}Ga_xAs_yP_{1-y}/InP$ lasers, a wavelength range of 1.1-1.65μm can by covered by choosing x and y with the active layer lattice-matched to InP (a=0.587nm). Semiconductor lasers emitting at 1.3μm and 1.55μm wavelength are of particular interest because of their application in optical fibre communications.

Recent advances in the epitaxial growth techniques permit a lattice mismatch of up to a few percent (<1.5%) without degrading the interface quality significantly. Such semiconductor lasers are referred to as strained-layer lasers and have attracted considerable attention because of their superior performance [2.6, 2.7].

Modern technology is able to make semiconductor lasers cover a very wide wavelength range. To date the longest wavelength of about 100μm is obtained using the semiconductor material $Bi_{1-x}Sb_x$. By contrast, short-wavelength

(ultraviolet/violet/blue) semiconductor lasers can use either II-VI semiconductors such as ZnS or ZnSe, doped with Cd [2.8] or III-V semiconductor, InGaN or AlGaN [2.9].

2.2.2 Heterostructure

Semiconductor lasers, at its early stage of development, had only one p-n junction formed by semiconductor materials with the same bandgap energy, named homostructure lasers. A common and discouraging problem of the laser was that the usual threshold current density for lasing was very high (>50,000A/cm^2) at room temperature. Most studies were done at liquid nitrogen temperature (<100K). Room temperature continuous operation was not feasible. Research on homostructure lasers started to diminish after 1963, when a suggestion was given that improved junction lasers could be achieved with a structure in which a layer of a semiconductor with a relatively narrow energy gap is sandwiched between two layers of a wider energy gap semiconductor. A junction of two such dissimilar semiconductors is called a heterojunction.

The properties of heterojunctions that permit much lower room temperature threshold current densities than homostructure lasers can best be illustrated with the double heterostructure (DH), shown in Fig. 2.2 with *P-p-N* structure. The heterojunctions serve to confine the injected carriers to the *p* active layer. Electrons and holes can move freely in the active region under forward bias. However, once there, they cannot cross over to the other side because of the potential build-up of the potential barrier resulting from the band-gap difference. This allows for a substantial build-up of the electron and hole populations inside the active region, where they can recombine to produce optical gain. The active layer thickness may be greatly reduced from the uncontrolled value of several microns to 0.1mm or less. On the other hand, the refractive index of the active layer is normally higher than that of cladding layer, which contributes to light confinement in the active layer. It was the adoption of heterostructure scheme that resulted in significantly lower threshold current densities and led to room-temperature operation of semiconductor lasers.

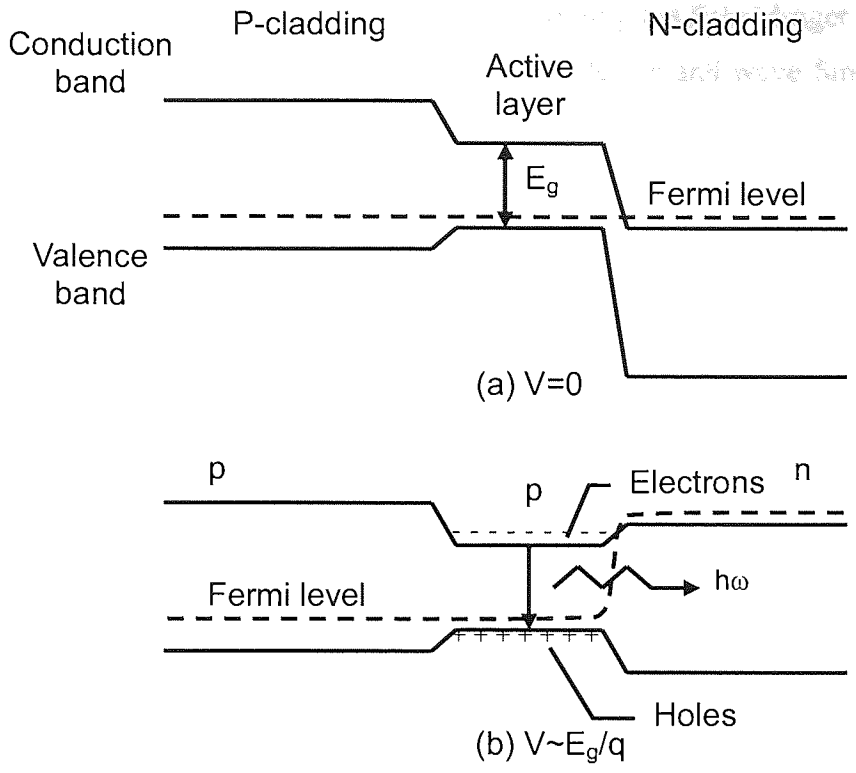

Fig. 2.2 Energy-band diagram of a double-heterostructure semiconductor laser at (a) zero bias and (b) forward bias

2.2.3 Quantum-confinement structures

The success of room temperature operation of DH lasers substantially broadened the application range of semiconductor lasers. There has been an immense amount of research on the DH laser to get better laser performance. It is natural to consider what would happen when the active layer in the DH lasers becomes extremely thin and spatial quantization occurred.

When the thickness of the active region (L_z) becomes comparable to the de Broglie wavelength ($\lambda=h/p$), quantum-mechanical effects are expected to occur. The kinetic energy corresponding to the carrier motion along the z direction is quantized. Along the x and y directions, the energy levels form a continuum of states given by

$$E = (\hbar^2 / 2m)(k_x^2 + k_y^2) \tag{2.1}$$

where m is the effective mass of the carrier and k_x and k_y are the wavevector components along the x and y directions, respectively.

The energy levels in the z direction are obtained by solving the Schrödinger equation for a one-dimensional finite potential well. The energy levels and wave function are then given by

$$\psi = \begin{cases} A\exp(k_1 z) & (z \le 0) \\ B\sin(k_2 z + \delta) & (0 \le z \le L_z) \\ C\exp(-k_1 z) & (z \ge L_z) \end{cases} \tag{2.2}$$

where

$$k_1 = \left[\frac{2m(V-E)}{\hbar^2}\right]^{1/2} \qquad k_2 = \left(\frac{2mE}{\hbar^2}\right)^{1/2} \tag{2.3}$$

The quantities A, B, C, and δ are constants. Using the boundary conditions stated above, the following eigenvalue equation is obtained:

$$\tan(k_2 L_z) = k_1 / k_2 \tag{2.4}$$

The eigenvalue equation is numerically solved to yield the energy levels E_n of a particle in a potential well.

Taking into account discrete states along the z direction and continuous states along the x and y directions, the energy eigenvalues for a particle confined in the quantum well are

$$E(n, k_x, k_y) = E_n + \frac{\hbar^2}{2m_n^*}(k_x^2 + k_y^2) \tag{2.5}$$

where E_n is the nth confined-particle energy level for carrier motion normal to the well and m_n^* is the effective mass for this level. Fig. 2.3 shows schematically the energy levels E_n of electrons and holes confined within a quantum well. The confined-particle energy levels E_n are denoted by E_{1c}, E_{2c}, and E_{3c} for electrons; E_{1hh}, E_{2hh}, and E_{3hh} for heavy holes; and E_{1lh} and E_{2lh} for light holes. These quantities can be calculated by solving the eigenvalue equation (2.4) for a given potential barrier (ΔE_c or ΔE_v)

Fig. 2.3 Schematic representation of the confined-particle energy levels of electrons, heavy holes (short dashes), and light holes (long dashes) in a quantum well [2.1].

This type of DH lasers, with active layer confined to L_z<10nm, are called quantum well lasers. An interesting feature of quantum well lasers is that the density of states in a quantum well is independent of the carrier energy. Fig. 2.4(b) shows the step-like profile of the density of states in a quantum well. Its most fundamental advantage over bulk material is improved optical gain. Optical gain in the material is attained when we inject a carrier density beyond transparent level such that the quasi-Fermi levels are separated by an energy gap greater than the band gap. The rate at which gain increases as we inject more carriers, known as the differential gain, *dg/dN*, is of great practical interest. At a forward bias condition, the increase of bias level has a much more profound effect on the band edge carrier density when the density of states has a steep profile. Thus, the step-like density of states in a quantum well is expected to result in a much higher differential gain than can be obtained in bulk material. Another advantage of quantum-well laser is that it delivers gain with less change in refractive index than bulk lasers, resulting in lower chirp and, accordingly, narrower linewidth.

Although quantum well laser was predicted to be much advantageous than bulk DH lasers, the first quantum well laser, demonstrated in 1975, was many times less efficient than a conventional laser [2.10], the situation was reversed by 1981 through the use of new materials growth capabilities (molecular beam epitaxy), and

optimisation of the heterostructure laser design [2.11, 2.12].

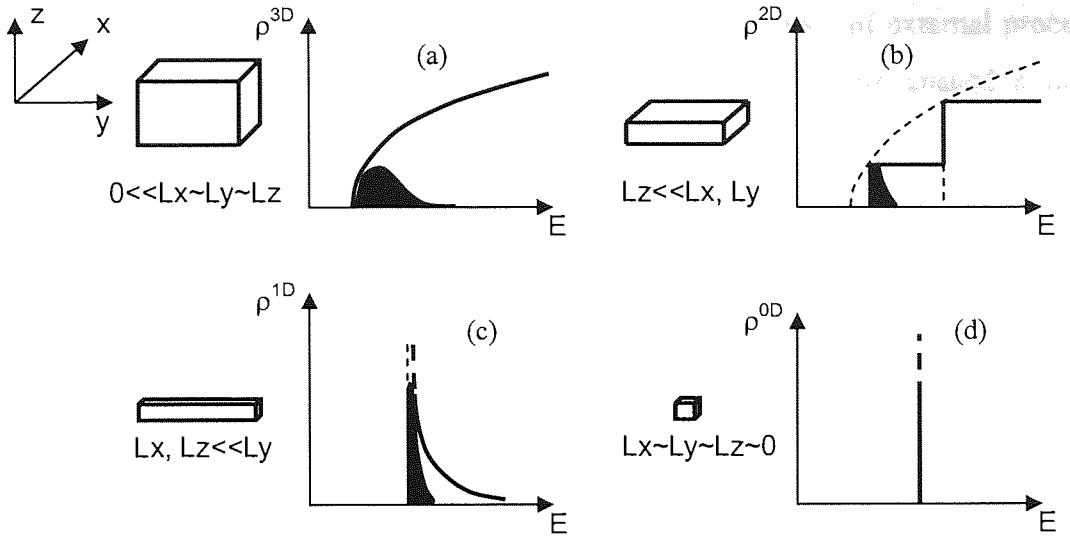

Fig. 2.4 Illustration of four typical crystal geometries: (a) bulk material, (b) quantum well structure, (c) quantum wire structure, (d) quantum dots structure, and their associated density of states as a function of energy. The solid areas indicate the real electrons/holes distribution in each case.

It is now possible to employ state-of-the-art technology to control the active region of semiconductor lasers at nanometre scale in three dimensions, i.e. to fabricate quantum dot lasers. In theory, quantum-dots lasers have a δ-function-like density of states, shown in Figure 2.4(d). The population inversion (creation of electrons and holes) necessary for lasing occurs more efficiently as the active layer material is scaled down from bulk (3-dimensional) to quantum dots (0-dimensional).

The benefits of quantum dot lasers include further reduction in threshold currents and an increase in differential gain, that is, more efficient laser operation. Quantum dot lasers also exhibit performance that is less temperature-dependent than other existing semiconductor lasers, and that will in particular not degrade at elevated temperatures. However, the advantages in operation depend not only on the absolute size of the nanostructures in the active region, but also on the uniformity of size. A broad distribution of sizes "smears" the density of states, producing behaviour similar to that of bulk material. Thus, the challenge in realizing quantum dot lasers with operation superior to that shown by quantum well lasers is that of forming high quality, uniform quantum dots in the active layer. Initially, the most widely followed approach to

forming quantum dots was through electron beam lithography of suitably small featured patterns (~300 Å) and subsequent dry-etch transfer of dots into the substrate material. With the demonstration of the high optical efficiency self-assembled formation of quantum dots [2.13, 2.14], formed without need of external processing and having the natural overgrowth of cladding material, there ensued a marked increase in quantum dot laser research.

2.2.4 Semiconductor laser cavity

The basic laser structure of edge emitting lasers can be represented by double-heterostructure lasers. Laser cavity structures in transverse and longitudinal directions will be introduced respectively.

The schematic draws of semiconductor laser cavity of DH lasers in transverse direction perpendicular to the junction plane are shown in Fig. 2.5. The use of a heterostructure device is twofold. The cladding layers surrounding the active layer have a higher band gap and at the same time a lower refractive index compared with those of the active layer. The band gap difference helps to confine electrons and holes to the active layer, where they recombine to produce the optical gain. At the same time the refractive index difference confines the optical mode close to the active layer, which acts as a dielectric waveguide. The optical mode confinement significantly reduces the internal loss that would otherwise occur in the absence of index guiding due to the spreading of the optical mode in the lossy regions.

Fig. 2.5 Schematic illustration of double-heterostructure laser in transverse direction perpendicular to the junction plane [2.1].

Field confinement in the lateral direction, which is parallel to the junction plane, can be either achieved in gain-guided and index-guided semiconductor lasers depending on whether it is the lateral variation of the optical gain or the refractive index that confines the mode. Index guided lasers can further be classified as weekly or strongly index guided depending on the magnitude of the lateral index step. In addition, semiconductor lasers without lateral confinement can be generally referred to as broad-area lasers. Fig. 2.6 shows schematically these four kinds of devices.

In the gain-guided structure, the width of the optical mode along the junction plane is mainly determined by the width of the optical gain region, which is determined by the width of the current pumped region (typically in the range of 5-10μm). In index-guided lasers, a narrow central region of relatively higher refractive index in the junction plane confines the lasing mode to that region. For weekly index-guided lasers, the active region is continuous and the effective index discontinuity is provided by a cladding layer of varying thickness. Depending on the specific design, these structures are known under various names, such as rib waveguide, ridge waveguide. By contrast, the strongly index-guided lasers employ a buried heterostructure. In these lasers, the active region is bounded by low-index, epitaxially grown layers both along and

normal to the junction plane. The lateral index difference is ~0.01 for weakly index-guided lasers and ~0.2 for strongly index-guided, buried-heterostructure lasers.

Fig. 2.6 Four kinds of laser structures without (a) and with (b)-(d) lateral confinement. The active-layer material has a smaller band gap compared with that of the surrounding cladding layers [2.1].

In general, gain-guided lasers are easier to fabricate than index-guided lasers. However, gain-guided lasers have a number of undesirable characteristics that become worse as the laser wavelength increases. Index-guided lasers, in spite of their difficulties in fabrication, have superior performance characteristics—low threshold current, stable fundamental-mode operation at high powers, and good high-speed modulation characteristics—making them a prime candidate for high-performance applications. In particular, their use as a source in lightwave transmission systems is highly attractive.

In longitudinal direction, a DH laser with a cavity length of L is shown in Fig. 2.7. The cleaved facets form a Fabry-Pérot (FP) cavity and provide the feedback for the

onset of laser oscillations. If R_1 and R_2 are the facet reflectivity at two ends, the amplitude after one round trip is set to unity at and above laser threshold. This leads to the condition

$$(R_1R_2)^{1/2}\exp(2i\tilde{\beta}L)=1 \tag{2.6}$$

where, β is the complex propagation constant which takes the form

$$\tilde{\beta}=\mu k_0+i\alpha/2 \tag{2.7}$$

and μ is effective refractive index, k_0 is the wave vector in vacuum, α is the net absorption coefficient which takes the form

$$\alpha=-\Gamma g+\alpha_{\text{int}} \tag{2.8}$$

From equation (2.7) we obtained

$$(R_1R_2)^{1/2}\exp(-\alpha L)=1 \tag{2.9}$$

$$\sin(2\mu k_0L)=0 \tag{2.10}$$

Equation (2.9) gives the threshold gain condition. Using equation (2.8), it can be written in the form

$$\Gamma g=\alpha_m+\alpha_{\text{int}} \tag{2.11}$$

where

$$\alpha_m=\frac{1}{2L}\ln\left(\frac{1}{R_1R_2}\right) \tag{2.12}$$

is the mirror loss and account for the radiation escaping from the FP cavity because of finite facet reflectivity.

The condition (2.10) governs light oscillation in longitudinal direction and can be used to obtain the laser frequency. It has multiple solutions

$$2\mu k_0L=2m\pi \tag{2.13}$$

where m is an integer. The lasing frequency is then given by

$$\nu=\nu_m=mc/(2\mu L) \tag{2.14}$$

where ν_m, referred to as the cavity-resonance frequency, is the frequency of the mth longitudinal mode of a FP cavity of the optical length μL.

Fig. 2.7 Schematic illustration of a semiconductor laser in longitudinal direction and its associated Fabry-Pérot (FP) cavity [2.1].

It is important to remember that in a semiconductor laser the refractive index μ varies with the frequency ν. Using the relation

$$\Delta(\mu\nu) = \mu(\Delta\nu) + \nu(\Delta\mu) \tag{2.15}$$

where Δ denotes a small change, the inter-mode spacing is given by

$$\Delta\nu = c/(2\mu_g L) \tag{2.16}$$

where

$$\mu_g = \mu + \nu(\partial\mu/\partial\nu) \tag{2.17}$$

is the group index of the dispersive semiconductor material. A feature unique to semiconductor lasers is that the longitudinal-mode frequencies and their separation vary with the external pumping because of the refractive-index variations.

2.3 Ultrashort pulse generation from diode lasers

There are three main techniques to generate ultrashort optical pulses in picosecond and sub-picosecond range from laser diodes. They are gain switching, Q-switching and mode locking. In following paragraphs, these techniques will be discussed respectively.

2.3.1 Gain switching

Gain switching can simply be achieved by driving the laser with electrical pulses or RF signal. Compared with mode locking and Q-switching techniques, it has the advantage that no external cavity and no sophisticated fabrication technology are required. The idea originated from observations of relaxation oscillation when turning on a laser from below threshold using electrical pulses with a fast leading edge. Gain switching is achieved by exciting the first spike of relaxation oscillation and terminating the electrical pulse before the onset of the next spikes. Electrical drive pulses typically range in width from 50 to 1000ps, while the generated optical pulses can be considerably shorter than the electrical ones. The fundamental reason for this is an extremely short photon lifetime in a diode-laser cavity due to very small cavity length and relatively high cavity losses.

The simplest analysis of basic dynamics of the generation of gain-switched pulses in a diode laser can be carried out by a set of nonlinear rate equations that connects the photon density S in the cavity with the carrier density n. They are written as,

$$\frac{dn}{dt} = \frac{j(t)}{ed} - g_0(n - n_t)S - \frac{n}{\tau_s} \tag{2.18a}$$

$$\frac{dS}{dt} = \Gamma g_0(n - n_t)S - \frac{S}{\tau_{ph}} + \frac{\beta\Gamma n}{\tau_s} \tag{2.18b}$$

where n_t is the transparency density, g_0 is the differential gain coefficient, β is the spontaneous coupling factor, e is the electron charge, d is the active layer thickness, $j(t)$

is the current density, Γ is the optical confinement factor, and τ_s and τ_{ph} are the carrier and photon lifetimes. Equation (2.18a) governs variation of carrier density with time. $j(t)/ed$ determines increase of carrier density for current injection; $g_0(n-n_t)S$ determines decrease of carrier density for stimulated emission; and n/τ_s determines decrease of carrier density for spontaneous emission. Equation (2.18b) governs variation of photon density with time. $\Gamma g_0(n-n_t)S$ determines increase of photon density for stimulated emission; S/τ_{ph} determines decrease of photon density for cavity loss; $\beta\Gamma n/\tau_s$ determines increase of photon density for spontaneous emission. These equations are single-mode, that is, they do not take into account the distribution of photons between cavity modes. However, the equations can be easily modified for the multimode case as,

$$\frac{dn}{dt} = \frac{j(t)}{ed} - \Sigma g_m S_m - \frac{n}{\tau_s} \tag{2.19a}$$

$$\frac{dS_m}{dt} = \Gamma S_m g_m - \frac{S_m}{\tau_{ph}} + \frac{\beta\Gamma n D_m}{\tau_s} \tag{2.19b}$$

where $g_m=g_0(D_m n-n_t)$; S_m is the photon density in the mth laser diode; the net photon density is given by the sum $S(t)=\Sigma S_m$ and D_m is the line shape factor.

Fig. 2.8 illustrates the evolution of ultrashort light pulses generated from a gain-switched diode laser pre-biased at a current, I_0, below threshold, I_{th}. The current pulse (a) quickly increases the carrier density (b) to a value greater than transparency, n_t, at which point lasing can commence. The carrier density follows the current pulse to reach a maximum value of n_i before decreasing to a value of n_f below the lasing threshold.

The gain-switched optical pulsewidth and peak power are mainly dependent on the electrical pumping conditions. Normally speaking, increasing the RF power causes the pulsewidth to decrease and the peak power to increase, and for a given drive pulse, there is an optimum DC bias level which contributes to the optical pulsewidth at a minimum value. On the other hand, gain compression has a strong influence on both

the pulsewidth and the peak power. Shorter pulsewidth and higher peak power can be achieved by quaternary material based laser diodes, like *InGaAsP* lasers, with a smaller nonlinear coefficient. In addition, increased differential gain coefficient can also improve the performance of gain-switched pulses for shorter pulsewidth and higher peak power. Hence, quantum well laser diode has a big advantage in this manner.

Fig. 2.8 (a) Electrical injection pulse, (b) carrier density and (c) optical output for a gain-switched diode laser [2.15].

Timing jitter is an important parameter of gain-switched pulses, as it dramatically affects system performance in many applications. It lies typically in range of 1-10ps

and originates from the random fluctuations of the photon density in the laser cavity. The laser emission contains phase noise, some of which is correlated with the phase noise of the electrical drive current, while some results from laser noise sources and is uncorrelated. The correlated phase noise do not depends on driving current and can be very low (the rms jitter << 1ps), however, uncorrelated jitter has been found to depend on the driving conditions and may drastically increase from 0.5ps to 2ps when the driving current is not optimised. This highlights the importance of using low-phase-noise electronics. Single-mode laser diodes, like DFB LDs, normally have a bigger value of timing jitter than multimode Fabry-Pérot LDs under gain-switched operation, due to the random fluctuations of photon density becoming much more obvious within only one lasing mode.

In typical gain-switched FP laser diodes, the dynamic overshoot of the carrier concentration causes more longitudinal modes to be generated than in CW operation, even when CW operation is single mode. The number of excited modes depends on the device structure, its spontaneous emission factor, the DC and pulse currents, and the modulation frequency. In addition to multimode operation, the spectral line of each mode is broadened. If a single-frequency laser diode is used for gain switching, the multimode operation can be avoided, however, the bandwidth under gain switching exceeds the bandwidth under CW operation. As the carrier concentration experiences large variations during the pulse, the refractive index in the laser cavity also varies and the laser spectrum is chirped. As a result of chirp, gain-switched pulses have a time bandwidth product, $\delta\gamma\delta\tau$, which is often far from the Fourier-transform limit. It is usually expressed as [2.15],

$$\delta\nu\delta\tau = \sqrt{k\left(1+\alpha^2\right)} \tag{2.20}$$

where k is a constant which depends on the pulse shape and α is the linewidth enhancement factor, which is defined by,

$$\alpha = -2k\frac{d\mu/dn}{dg/dn} \tag{2.21}$$

where $k=2\pi/\lambda$ is the free-space wave vector.

Single-frequency gain-switched operation can be achieved by using specific laser structures such as DFB lasers. Chirp reduction for single-frequency operation has

been achieved by driving DFB lasers with a strong RF modulation superimposed on a DC bias current. Fourier-transform-limited single-mode picosecond optical pulse generation by a distributed feedback InGaAsP diode laser has been reported [2.16]. Since then, DFB gain-switched lasers have become a popular means of generating single-frequency low-chirp pulses with pulse duration in the range of 25 to 30ps. Injection locking or using external cavity configuration can also reduce the number of modes as well as dynamic frequency chirp of each mode.

2.3.2 Q-switching

Q-switching, as a common way for high power short pulse generation both in microwave and bulk laser systems, is also widely used to generate picosecond optical pulses from diodes lasers. A Q-switched laser will consist of at least two discrete sections. One section of the laser is used to modulate the Q-factor of the cavity. The Q-switch is held in the "off" or high-loss state, ensuring a low-Q cavity while a population inversion is built up in the laser medium. As the carrier density reaches its peak, the cavity is switched to the high-Q condition and the stored energy is rapidly emitted as an optical pulse. When the switching is initiated externally, the technique is called active Q-switching. However, pulse generation can also be achieved by including a saturable absorber in the cavity and this is known as passive Q-switching. The absorber exhibits large optical attenuation at low optical power levels, which results in a low Q. As the gain medium is pumped and the optical intensity increases, the loss saturates and the cavity then develops a high Q-factor, allowing the rapid onset of lasing. In addition, a combination of the former two techniques can be achieved in a hybrid Q-switched device.

A typical actively Q-switched diode laser consists of a gain section, a modulator section and possibly a passive waveguide section in between. The gain section is forward biased to produce optical gain. The loss in the modulator section can be varied by applying an electric field to alter the band-gap energy. In bulk semiconductors, this is known as the Franz-Keldysh effect. In MQW lasers, the quantum-confined Stark effect further modifies the energy levels. As a result, the repetition rate of the pulses is variable according to that of the modulator. In this case, active Q-switched laser diodes have the same advantage as gain-switched ones. In

addition, active Q-switching can also be realised by modulating the phase of the optical waves propagating in the cavity. Fig. 2.9 shows the temporal evolution of optical pulses from an actively Q-switched diode laser, where the cavity loss is modulated by application of an electrical pulse to a loss section of a two-section

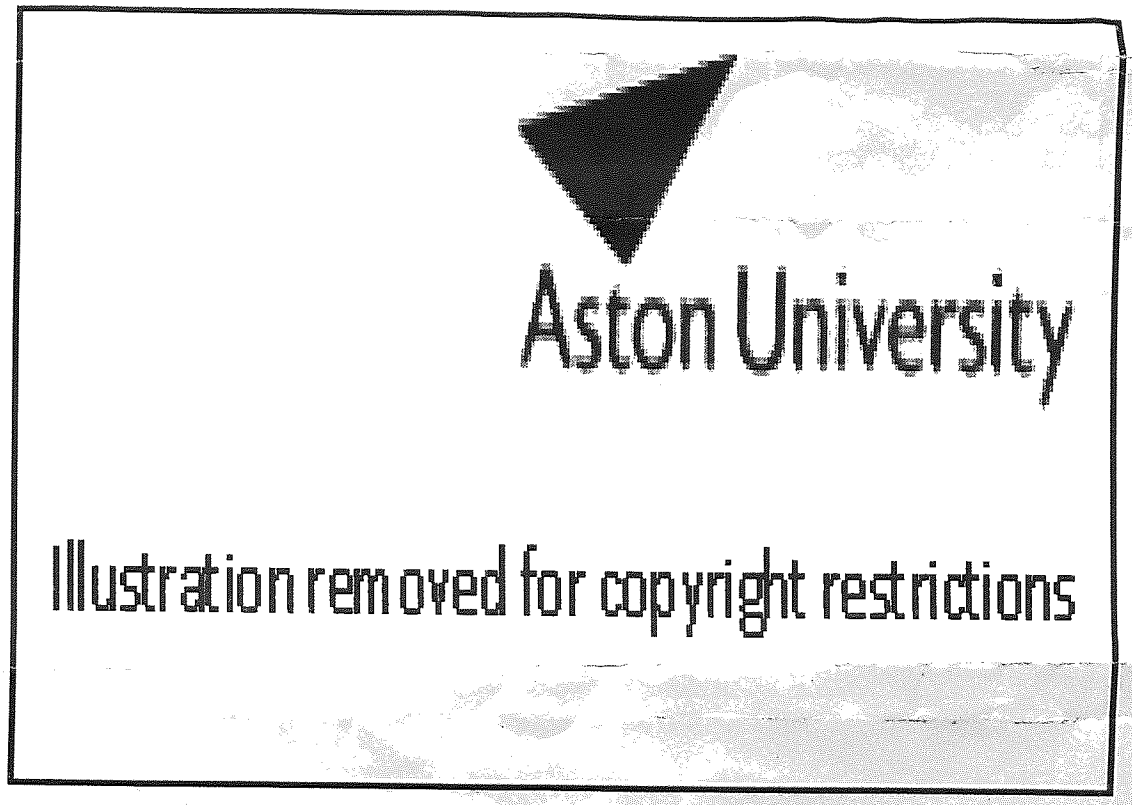

Fig. 2.9 The evolution of cavity loss, carrier density, and optical power for a two-section Q-switched diode laser. n_i is the initial carrier density just before the pulse emission [2.15].

Passive Q-switching is also widely used in ultrafast diode lasers. Similar to actively Q-switched diode lasers, passively Q-switched lasers are always multi-contact ones. Saturable absorbers, which can be unpumped sections or sections with a low pumping rate, incorporated in the laser cavity are responsible for the generation of ultrashort optical pulses in passively Q-switched lasers. The fundamental difference between the two techniques is that in contrast to active Q-switching no external electrical or optical modulation is required. In case of active Q-switching the pulse repetition frequency is set by an external RF or optical signal, whereas for passive Q-switching the frequency is governed by the laser parameters and pumping conditions.

To generate self-sustained pulsations or self-Q-switched pulses, the saturable absorber in the laser cavity must satisfy a number of conditions. The most important parameters that affect the dynamic behaviour of the laser are the ratio of the differential loss *da/dn* of the absorber to the differential gain *dg/dn* of the amplifier section and the ratio of the carrier lifetime in the gain τ_g and the absorber τ_a sections. It can be shown [2.17, 2.18] that in order to generate Q-switched pulses the following conditions should be satisfied:

$$\frac{da/dn}{dg/dn} > 1 \tag{2.22}$$

and

$$\tau_a / \tau_g < 1 \tag{2.23}$$

The value of *dg/dn* and *da/dn* can be readily controlled by using different current input applied to different sections of the laser. As a result, the pulse duration, the peak power, and the repetition rate are dependent on the electrical driving condition.

The spontaneous photons randomly generated during the build up of a passive Q-switched pulse give rise to a large timing jitter. Like gain switching, the turn-on of a Q-switched pulse relies on the amplification of these spontaneous photons. Whereas, under gain switching, the turn-on of the optical pulse is determined by the steep leading edge of the current pulse, in a Q-switched multiple-contact laser with a constant drive current, turn-on is random. Also, the repetition rate of Q-switched pulses is very sensitive to any variation in the applied bias currents and this also enhances timing jitter, which normally exceeds 6ps.

An obvious advantage of Q-switched laser diodes is the achievable peak optical power is higher than gain-switched and mode-locked ones by many times. The high-peak-power ultrashort optical pulses with good spatial mode quality are increasingly required for many scientific and industrial applications, including space communications and optical sensing. The simplest method of increasing the output power of Q-switched pulses is to increase the active-region volume of the laser, by increasing any or all of the spatial dimensions: thickness, width and length. In section 2.4, we will discuss the issue of high-energy pulse generation by Q-switching in detail.

2.3.3 Mode-locking

The fundamental advantage of mode locking is that it generates much shorter pulses with much lower timing jitter than those produced by gain or Q-switching. Mode locked optical pulses in laser diodes result from the realisation of the correlation in phase for a set of resonator modes in the laser cavity, hence the broadening of lasing spectrum and the narrowing of temporal pulse duration. Mode locked diode lasers offer a number of applications, typically, the light source of high-capacity, long-haul optical communication system.

We suppose the laser emission consists a set of resonator modes ω_m, m=1, 2, 3..., separated by $\delta\omega$. The output consists of a sum of frequency components that correspond to the oscillating modes, and the electric field is given as,

$$E(t) = \sum_m A_m \exp i[(\omega_0 + m\delta\omega)t + \phi_m] \tag{2.24}$$

Where A_m and ϕ_m represent the amplitude and phase of the mth mode. In general, relative phases between the modes are randomly fluctuating. If nothing fixes the phase ϕ_m, the laser output will vary randomly in time, the average power being approximately equal to the simultaneous one. On the other hand, if the modes are forced to maintain a fixed phase and amplitude relationship, for example,

$$\phi_m - \phi_{m-1} = \delta\phi \tag{2.25}$$

$$A_m \exp(i\phi_m) = A_0 \exp[i(\phi_0 + m\delta\phi)] \tag{2.26}$$

then the output of the laser will be a periodic function of time:

$$E(t) = A_0 \frac{\sin[(k+1)\delta\omega t_1 / 2]}{\sin(\delta\omega t_1 / 2)} \exp(i\omega_0 t) \tag{2.27}$$

where k is the number of locked modes and $t_1 = t + \delta\phi/\delta\omega$. The operation conditions given by (2.25) to (2.27) result in the generation of a train of regularly spaced optical pulses. The pulses have width $\Delta\tau$, which is proportional to $1/\Delta\omega_g$, where $\Delta\omega_g$ is spectral bandwidth. The pulse train has a temporal periodicity of $T = 2L\mu/c$. The ratio of the period T to the pulse duration $\Delta\tau$ is equal to the number of locked modes k.

Fig. 2.10 (a) electrical modulation current, (b) carrier density and (c) optical output for an actively mode-locked diode laser [2.15].

The principle of operation for active mode-locking is illustrated in Fig. 2.10. This involves modulating the gain (or loss) of the device at a frequency equal to the mode spacing. Typically a sinusoidal modulation is superimposed on a DC bias and applied to the device [Fig. 2.10(a)]. The current modulation causes the periodical modulation of the carrier density around the threshold value n_{th}. Both the amplitude I_1 of the current modulation and I_0 are chosen to create a very short time window of net gain in the laser. This implies that the carrier density $n(t)$ exceeds n_{th} for a very short period of time during each modulation period. The function of carrier density consists of a set of harmonics of the modulation frequency $2\pi/T$, where T is the period of modulation. Mode locking is ultimate provided that T is exactly equal to the round-trip time of the laser cavity, that is

$$T = \frac{1}{\delta\nu} \tag{2.28}$$

The repetition rate of mode-locked pulses is obviously equal to the driving current frequency. Detuning the modulation frequency from the resonance condition given by equation (2.28) leads to the degradation of mode-locked pulses, that is, the pulse duration increases while the peak power decreases with the increase of the frequency offset.

A limitation of active mode locking is the fact that the repetition frequency of a solitary diode laser cannot be varied since it is determined by the cavity round trip time. The short cavity lengths of diode lasers yield to a cavity frequency that can be prohibitively high. A straightforward decision of the problem is to increase the cavity length using an external cavity configuration. In fact, various external cavity schemes, shown in Fig. 2.11, have been employed. Prior to the implementation of external cavity elements one facet of the diode laser should be anti-reflection (AR) coated so as to suppress the undesired internal reflection.

(c) (d)

Fig. 2.11 External-cavity configuration of mode-locked diode lasers using (a) mirror, (b) grating, (c) Fabry-Pérot etalon and mirror, and (d) fibre [2.15].

The other mode-locking techniques include: (a) passive mode-locking when no external signal is used in a laser with a saturable absorber; (b) hybrid mode locking-when an external radio frequency (RF) signal is used for gain/loss modulation in multiple-contact laser diode or in laser with an intra-cavity element that exhibits the saturable absorption; (c) coupled-cavity or additive pulse mode-locking when an

external cavity that contains a nonlinear element is used to produce a pulse-shortening mechanism or to enhance mode locking.

2.4 Generation of high power ultrashort pulses

Obtaining high power ultrashort optical pulses from diode lasers is an issue of particular significance of research in ultrafast diode lasers. Relative low output power of ultrafast diode lasers restricts potential applications in nonlinear fibre optics, ultrafast opto-electronics, and instrumentation. Particularly, applications in laser tomography, laser metrology, laser radar and high-resolution spectroscopy call for the development of compact semiconductor sources of picosecond light pulses with peak power levels approaching those of solid-state lasers. Nowadays, it is possible to generate picosecond pulses with peak power in excess of 1W with all the three basic methods of ultrashort pulse generation with the highest achievable peak power by Q-switching.

In Q-switching mode, the common way of increasing the output energy of optical pulse is to augment the energy accumulated in the laser cavity by the moment of opening the optical shutter. The accumulated energy (Fig. 2.12) is directly determined by the quantity of non-equilibrium carriers, N, and modulation degree of the carrier concentration, ΔN, which depends on the quality of the saturable absorber inside the resonator of a semiconductor laser. An increase in the volume of the active layer causes a rise in the number of non-equilibrium charge carriers in the resonator. Accordingly, an increase both in the physical size of the active layer, V, and in its volume in energy space (i.e. concentration of non-equilibrium carriers, N) takes place. In this case, bulk structure lasers, like double heterostructure (DH) lasers or single heterosturcture (SH) lasers, have the advantage over quantum-well lasers. Here, the maximum thickness of the active region, while retaining zeroth-mode generation, can be achieved in asymmetric-waveguide lasers. The other ways to increase the active volume of diode lasers include using tapered-waveguide lasers or laser arrays [2.19, 2.20] and surface-emitting lasers [2.21, 2.22].

Fig. 2.12 Ways of increasing optical pulse energy from picosecond Q-switched diode lasers [2.23].

Fast switching time is also necessary for the generation of high power Q-switched pulse provided that enough non-equilibrium carriers are accumulated in the laser cavity. This requires a highly efficient saturable absorber. A conventional way of obtaining saturable absorber is to use multi-sectional quantum-well lasers with one or several reversely biased saturable absorber sections [2.24]. This method is not feasible for stable, high-speed Q-switching operation. It is mainly due to the low switching frequency of saturable absorber, as the thickness of the *p-n* junction is within 0.1μm, and the frequency is determined by the non-equilibrium carrier lifetime, which amounts to several nanoseconds in an active layer of about 2μm. A considerable increase of switching speed can be achieved by the use of a special technique, whereby an ultrafast saturable absorber is formed by implantation of heavy ions of high energy. This technique works best specifically on the laser having a thick active layer, like single-heterostructure (SH) laser, since, in this case, besides ultrashort

lifetimes, it is also possible to achieve a very high modulation degree of the non-equilibrium carrier concentration in the active layer. By applying this technique, a peak power approaching half a kilowatt was achieved in a broad-area laser [2.23]. Another study [2.25] shows much reliable high power picosecond pulse generation can be achieved in a specially designed laser structure, shown in Fig. 2.13. The main distinguishing feature of the structure is separation of the electron injector (*p-n* junction) from the active region by a potential barrier. The optical gain in the active region is controlled by the transverse electric field, which is determined by the magnitude of the current at each instant. Q-switching like behaviour occurred when the current stopped, i.e. the electric field is removed. At this moment, the carriers spread across the entire active region, which caused a significant increase in the overall gain. As a result, a 23ps long optical pulse with a peak power of 48W was achieved.

High power picosecond pulse generation can also be achieved in both gain-switching [2.26-2.28] and mode-locking [2.29-2.32] schemes. Gain-switching has the advantage that no special laser treatment and no sophisticated laser structure are needed to achieve high-power pulsed output, so long as the electrical pumping pulse has a very high *dI/dt* rate and its amplitude exceeds the laser threshold by a factor of at least 10. This issue will be discussed in detail in later chapters.

For a long time, mode locking was limited to relatively low output powers of typically only a few milliwatts. However, in recent years, several studies [2.29-2.32] show a peak power of >1W was achievable using vertical-cavity surface-emitting laser (VCSEL) with a semiconductor saturable absorber mirror (SESAM) in the external cavity. The pulse duration achieved can be less than 1ps.

2.5 Other problems and challenges

2.5.1 Increase of wavelength tuneability

Wavelength tunable, ultrafast diode lasers are an enabling technology that eliminate many of the limitations of fixed wavelength lasers, and enable new system architectures with increased functionality. In order to achieve effective wavelength tuning in semiconductor lasers, the spectral width and wavelength tuneability of the output pulses should be controlled at the same time.

Currently, there are four primary approaches to provide tuneability with semiconductor lasers, each with distinct advantages and disadvantages. Firstly, tuneable distributed feedback (DFB) lasers use temperature to tune the wavelength; secondly, distributed Bragg reflector (DBR) lasers extend the available tuning range beyond that of a tuneable DFB lasers using additional elements on the same

semiconductor; thirdly, micro-electrical mechanical systems (MEMS) technology can be used in surface-emitting lasers, like VCSELs and GCSELs to manipulate a movable top mirror so as to achieve wavelength tuning. Finally, external-cavity diode lasers (ECL) technology provides wide tuning range with high output power [2.46]. The last two techniques are more widely used than the former two, especially for pulsed diode lasers, and will be discussed in detail in Chapter 3 and Chapter 4.

2.5.2 Suppression of pulse tail

Pulse tail structures or sub-pulses always appeared in high power pulsed diode lasers and are hazardous for many applications. In gain-switched mode, increasing the signal power by driving the laser with higher current results in degradation of the pulse quality. In the most severe case of an overdriven laser, the useful laser signal in the form of short pulses carries only a small fraction of the total output power, the main contribution arising from the relaxation oscillation tail. For Q-switched diode laser pulses, their pulse shape is much cleaner. Strong dynamic gain saturation, a low level of the carrier density just after the emission of the pulse, and an additional loss due to the absorber are main reasons for the clean shape of output pulses. Ultrashort pulses with the best pulse shape quality are obtained in mode-locked lasers. However, the low output power is the main limitation for mode-locked lasers in many applications.

It is observed, both theoretically [2.33] and experimentally [2.27], that transient spectrum broadening effect can be so significant under high current pumping condition that simple spectral filtering allows the first optical side-mode relaxation oscillation to be efficiently separated from the steady-state lasing mode. It offers a practical way to suppress the pulse tail structures by spectral filtering with auxiliary devices. Such devices can be a conventional band-pass filter [2.27, 2.34] or a robust and compact fibre Bragg grating [2.35]. In Chapter 5, we will demonstrate the spectral filtering technique applied on an overdriven DFB laser using tuneable fibre Bragg gratings.

2.5.3 Ultrashort pulse generation in short wavelength range

Compact short wavelength ultrafast diode laser sources covering the wavelength

range from 350-450nm are now commercially available [2.36-2.38]. For most of those laser sources, the build-in semiconductor chips are made from GaN-based materials. In recent years, the quality of GaN-based laser chips has greatly improved in terms of lifetime, output power, spatial modes, spectral purity etc. As a result, picosecond blue/violet/ultraviolet laser pulses with peak power up to half a watt can be directly generated from these laser sources [2.39, 2.40]. It is an alternative way to the traditional frequency-doubled solid-state lasers for ultrashort pulse generation in short wavelength range.

Previous studies show gain-switched GaN diode laser produced picosecond pulse with peak power in range of 400~500mW [2.39, 2.40]. Mode locking has also been demonstrated for a GaN diode laser with pulse duration of 30ps and time-bandwidth product of 1.2 [2.41]. In our investigation, we were able to produce picosecond blue laser pulses with one order of magnitude increase of peak power from a high quality GaN diode laser. On the other hand, spectral control and wavelength tuning were achieved at the same time for self-seeded gain-switched operation. Chapter 4 presented the details of our study.

2.5.4 Femosecond pulse generation from diode lasers

Compact and cost-effective femtosecond diode laser sources are of particular interest for tomorrow's applications. Special techniques are required either to compress picosecond pulses to femtosecond ones or to generate femtosecond pulses directly from diode lasers.

The techniques used for compression of picosecond diode laser pulses down to femtosecond include fibre-grating pulse compression, grating pair pulse compression, nonlinear fibre loop mirror, soliton compression, and combination of these techniques. Sub-100-fs pulse generation of high quality has been reported using these auxiliary devices [2.42, 2.43]. In addition, sub-ps pulses generation directly from mode-locked diode laser has also been reported [2.29-2.32, 2.44, 2.45].

With the advent and quality improvement of new type of semiconductor lasers represented by VCSELs, GCSELs, GaN lasers etc., femtosecond pulse generation from these types of diode laser devices is of great potential. The aims of today's research in this field are not only to achieve femtosecond pulse duration with good pulse quality but also to increase the output power and to cut down the cost and spatial size of the whole femtosecond pulse generation systems. It will substantially broaden the application range of compact femtosecond laser sources.

2.6 Conclusion

As a general review of the thesis, we discussed the basic physics of semiconductor lasers and ultrafast semiconductor lasers. The three basic methods, gain switching, Q switching and mode locking, for ultrashort pulse generation from semiconductor lasers are introduced respectively. Gain switching is the simplest way to generate ultrashort optical pulses from diode lasers with flexible control of repetition frequency; Q switching produces the highest output power, but its timing jitter is poor; Mode-locking produces ultrashort pulses with the shortest pulse duration, small time-bandwidth product, and good timing jitter, however, the pulse energy is limited.

Today's ultrafast diode lasers are able to generate high quality pulses with pulse energy comparable with solid-state lasers. It is now a possibility to use ultrafast diode lasers as an alternative to traditional bulk laser system for ultrashort pulse generation. The challenges here are to further increase pulse energy and compress pulse duration, to achieve ultrashort diode laser pulses at various wavelength range, to broaden the achievable wavelength tuning range, to maintain good pulse quality, etc. Discussions in the following chapters are mainly focused on these issues.

References

[2.1] G. P. Agraval and N. K. Dutta, *Semiconductor Lasers*, 2nd edition, Kluwer Academic Publishers Group, Boston, 1993

[2.2] P. S. Zory, *Quantum Well Lasers*, Academic press, San Diego, 1993

[2.3] H. C. Casey and M. B. Panish, *Heterostructure Lasers, Part A: Fundamental Principles*, Academic press, San Diego, 1978

[2.4] A. E. Siegman, *Lasers*, University Science Books, Mill Valley, 1986

[2.5] http://people.deas.harvard.edu/~jones/ap216/images/bandgap_engineering/bandgap_engineering.html

[2.6] P. J. A. Thihs, L. F. Tiemeijer, P. I. Kuindersma, J. J. M. Binsma, and T. van Dongen, "High-performance 1.5 μm wavelength InGaAs-InGaAsP strained quantum well lasers and amplifiers", *Journal of Quantum Electronics*, **QE-27**, pp. 1426-1439, 1991

[2.7] D. P. Bour, D. B. Gilbert, L. Elbaum, and M. G. Harvey, "Continuous, high-power operation of a strained InGaAs/AlGaAs quantum well laser", *Applied Physics Letters*, **53**, pp. 2371-2373, 1988

[2.8] M. A. Haase, J. Qiu, J. M. DePuydt, and H. Cheng, "Blue-green laser diodes", *Applied Physics Letters*, 59, pp. 1272-1274, 1991

[2.9] S. Nakamura, G. Fasol and S. J. Pearton, *The Blue Laser Diode: The Complete Story*, 2nd edition, Springer-Verlag, Berlin, 2001

[2.10] J. P. van der Ziel, R. Dingle, R. C. Miller, W. Wiegmann, and W. A. Nordland, Jr. "Laser oscillation from quantum states in very thin GaAs–Al0.2Ga0.8As multilayer structures", *Applied Physics Letters*, **26**, pp. 463-465, 1975

[2.11] W. T. Tsang, "Extremely low threshold (AlGa)As modified multiquantum well heterostructure lasers grown by molecular-beam epitaxy" *Applied Physics Letters*, **39**, pp. 786-788, 1981

[2.12] W. T. Tsang, "Extremely low threshold (AlGa)As graded-index waveguide separate-confinement heterostructure lasers grown by molecular beam epitaxy", *Applied Physics Letters*, **40**, pp. 217-219, 1982

[2.13] D. Bimberg, M. Grundmann, and N. N. Ledenstov, *Quantum Dot Heterostuctures*, Wiley, Chichester, UK, 1998

[2.14] K. Hoshino, S. Kako, and Y. Arakawa, "Formation and optical properties of stacked GaN self-assembled quantum dots grown by metalorganic chemical vapor deposition", *Applied Physics Letter*, **85**, pp. 1262-1264, 2004

[2.15] P. P. Vasil'ev, I. H. White and J. Gowar., "Fast phenomena in semiconductor lasers", *Reports on Progress in Physics*, **63**, pp. 1997-2042, 2000

[2.16] N. Onodera, H. Ito, and H. Inaba, "Fourier-Transform-Limited Single-Mode Picosecond Optical Pulse Generation by a Distributed Feedback InGaAsP Diode Laser", *Applied Physics Letters*, **45**, pp. 843-845, 1984.

[2.17] R. Dixon and W. Joyce, "A possible model for sustained oscillations (pulsations) in (Al,Ga)As double-heterostructure lasers", *Journal of Quantum Electronics.*, **15**, pp. 470-474, 1979

[2.18] M. Ueno and R. Lang, "Conditions for self-sustained pulsation and bistability in semiconductor lasers", *Journal of Applied Physics.*, **58**, pp. 1689-1692, 1985

[2.19] K. A. Willams, J. Sarma, I. H. White, R. V. Penty, I. Middlemast, T. Ryan, F. R. Lauguton, J. S. Roberts, "Q-switched bow-tie lasers for high-energy picosecond pulse generation", *Electronics Letters*, **30**, pp. 320-321, 1994

[2.20] I. Y. Khrushchev, D. J. Kitcher, K. A. Williams, I. H. White, F. R. Laughton, and R. V. Penty, "Picosecond Q-switched bow-tie laser diode array", *Electronics Letters*, **33**, pp. 426-428, 1997

[2.21] J. Furst, T. Schwarzl, M. Boberl, H. Pascher, G. Springholz, W. Heiss, "Vertical-cavity surface-emitting lasers in the 8-μm midinfrared spectral range with continuous-wave and pulsed emission", *IEEE Journal of Quantum Electronics*, **40**, pp. 966-969, 2004

[2.22] A. J. Fischer, W. W. Chow, K. D. Choquette, A. A. Allerman, K. M. Geib, "Q-switched operation of a coupled-resonator vertical-cavity laser diode", *Applied Physics Letters*, **76**, pp. 1975-1977, 2000

[2.23] E. L. Portnoi, G. B. Venus, A. A. Khazan, I. M. Gadjiev, A. Yu. Shmarcev, J. Frahm, and D. Kuhl, "Superhigh-power picosecond optical pulses from Q-switched diode laser", *IEEE Journal of Selected Topics in Quantum Electronics*, **3**, pp. 256-260, 1997

[2.24] B. Zhu, I. H. White, K. A. Williams, F. R. Laughton, and R. V. Penty, "High-peak-power picosecond optical pulse generation from Q-switched bow-tie laser with a traveling wave amplifier", *IEEE Photonics Technology Letters*, **8**, pp. 503-505, 1996

[2.25] S. Vainshtein, J. Kostamovaara, L. Shestak, M. Sverdlov, V. Tretyakov,

"Laser diode structure for the generation of high-power picosecond optical pulses", *Applied Physics Letters*, **80**, pp. 4483-4485, 2002

[2.26] M. Kume, H. Naito, J. Ohya, I. Ohta, H. Shimizu, M. Kazumura, I. Teramoto, "A high-power short-pulse laser diode for wave-guide 2nd harmonic-generation", *Solid-State Electronics*, **34**, pp. 1329-1333, 1991

[2.27] S. N. Vainshtein, G. S. Simin, J. T. Kostamovaara, "Deriving of single intensive picosecond optical pulses from a high-power gain-switched laser diode by spectral filtering", *Journal of Applied Physics*, **84**, pp. 4109-4113, 1998

[2.28] Y. Hu, A. Gubenko, G. Venus, I. Gadjiev, N. Il'inskaja, S. Nesterov, E. Portnoi, M. Dubov, I. Khrushchev, "Gain switching of an external cavity grating-coupled surface emitting laser with wide tunability", *Applied Physics Letters*, **82**, pp. 4236-4237, 2003

[2.29] R. Haring, R. Paschotta, E. Gini, F. Morier-Genoud, D. Martin, H. Melchior, U. Keller, "Picosecond surface-emitting semiconductor laser with > 200 mW average power", *Electronics Letters*, **37**, pp. 766-767, 2001

[2.30] A. Garnache, S. Hoogland, A. C. Tropper, I. Sagnes, G. Saint-Girons, J. S. Roberts, "Sub-500-fs soliton-like pulse in a passively mode-locked broadband surface-emitting laser with 100 mW average power", *Applied Physics Letters*, **80**, pp. 3892-3894, 2002.

[2.31] R. Haring, R. Paschotta, A. Aschwanden, E. Gini, F. Morier-Genoud, U. Keller, "High-power passively mode-locked semiconductor lasers", *IEEE Journal of Quantum Electronics*, **38**, pp. 1268-1275, 2002

[2.32] S. Hoogland, A. Garnache, I. Sagnes, B. Paldus, K. J. Weingarten, R. Grange, M. Haiml, R. Paschotta, U. Keller, A. C. Tropper, "Picosecond pulse generation with 1.5 μm passively mode-locked surface-emitting semiconductor laser", *Electronics Letters*, **39**, pp. 846-847, 2003

[2.33] T. Sogawa and Y. Arakawa, "Picosecond spectral dynamics of gain-switched quantum-well lasers and its dependence on quantum-well structures", *Journal of Applied Physics*, **67**, pp. 2675-2677, 1990

[2.34] S. N. Vainshtein and J. T. Kostamovaara, "Spectral filtering for time isolation of intensive picosecond optical pulses from a Q-switched laser diode", *Journal of Applied Physics*, **84**, pp. 1843-1847, 1998

[2.35] M. Dubov, D. Giannone, I. Khrushechev, I. Bennion, "Pulse tail suppression in laser diode output by tunable notch filter", *Electronics Letters*, **37**, pp. 1404-1405, 2001

[2.36] http://www.ibh.co.uk/products/light_sources/nanoled/heads/blue_laser_heads

.htm

[2.37] http://www.picoquant.com/_products.htm

[2.38] http://www.laser2000.co.uk/lasers/modules/bluemod.htm

[2.39] S. Nakamura, M. Senoh, S. Nagahama, N. Iwasa, T. Yamada, T. Matsushita, Y. Sugimoto, and H. Kiyoku, "Longitudinal mode spectra and ultrashort pulse generation of InGaN multiquantum well structure laser diodes", *Applied Physics Letters*, **70**, pp. 616-618, 1997

[2.40] C. Marinelli, I. Khrushchev, J. Rorison, R. Penty, I. White, Y. Kaneko, S. Watanabe, N. Yamada, T. Takeuchi, H. Amano, I. Akasaki, G. Hasnain. R. Schneider, S. Wang, and M. Tan, "Gain-switching of GaInN multiquantum well laser diodes", *Electronics Letters*, **36**, pp. 83-84, 2000

[2.41] S. Gee and J. Bowers, "Ultraviolet picosecond pulse generation from a mode-locked InGaN laser diode", *Applied Physics Letters*, **79**, pp. 1951-1952, 2001

[2.42] M. Tsuchiya, K. Igarashi, R. Yatsu, K. Taira, K. Y. Koay, M. Kishi, "Sub-100 fs SDPF optical soliton compressor for diode laser pulses", *Optical and Quantum Electronics*, **33**, pp. 751-766, 2001

[2.43] R. Yatsu, K. Taira, M. Tsuchiya, "High-quality sub-100-fs optical pulse generation by fiber-optic soliton compression of gain-switched distributed-feedback laser-diode pulses in conjunction with nonlinear optical fiber loops", *Optics Letters*, **24**, pp. 1172-1174, 1999

[2.44] J. P. Vanderziel, W. T. Tsang, R. A. Logan, R. M. Mikulyak, W. M. Augustyniak, "Subpicosecond pulses from passively mode-locked GaAs buried optical guide semiconductor lasers", *Applied Physics Letters*, **39**, pp. 525-527, 1981

[2.45] P. P. Vasilev, V. N. Morozov, Y. M. Popov, and A. B. Sergeev, "Subpicosecond pulses generation by a tandem-type AlGaAs DH laser with colliding pulse mode-locking", *IEEE Journal of Quantum Electronics*, **22**, pp. 149-151, 1986

[2.46] T. Day, C. Thompson, J. Lee, "Widely tunable laser technologies: Meeting the needs of tomorrow's networks", *Proceedings of SPIE*, **4652**, pp. 186-192, 2002

Chapter 3

Short pulse generation in grating-coupled surface emitting lasers

In this chapter, a detailed study of picosecond pulse generation from a grating-coupled surface emitting laser (GCSEL) is presented. We firstly introduce the background of recent research in GCSELs. It shows a great potential of building a new type of ultrashort optical pulses sources based on this type of lasers. Then, experimental investigation of a gain-switched GCSEL with off-resonance grating structure is demonstrated under external cavity configuration. The generated picosecond pulses are characterised by high output power up to 1W, wide wavelength tuneability of 100nm, and single-frequency spectrum. Based on the laser structure and the phenomena observed in the experiment, we also discuss the fundamental physical mechanisms attributed to our experimental results. Finally, conclusion is given.

3.1 Introduction

The grating-coupled surface emitting lasers (GCSELs) are a type of devices where the active region has the conventional waveguide form, but the light is deflected with a certain angle to the surface using a diffraction grating fabricated adjacent to the laser waveguide. This type of laser structure was initially demonstrated in 1975 [3.1, 3.2], and a range of GCSEL configurations have been developed since then [3.3-3.9]. These devices possess interesting characteristics such as higher output power, wavelength selectivity and low divergent optical beam. These properties make GCSELs suitable for free-space communication, optical data processing, photonic integrated circuits and optical interconnects, printing, and pumping applications.

In a typical GCSEL, one or several distributed Bragg reflector (DBR) sections are utilised in the device acting as the end mirror as well as output coupler. Due to the inherently lossy nature of the distributed Bragg reflector/output couple waveguide, one major task for fabricating a GCSEL is to reduce the threshold current. The end losses in a GCSEL result from the dielectric discontinuity at the active/DBR transition region and the distributed optical losses (due to absorption and output coupling) in the DBR waveguide itself. The use of graded-index separate confinement heterostructure single quantum well (GRINSCH) structure for the waveguide layer in both the gain section and the passive DBR section can reduce both the discontinuity loss and the absorption losses of the DBR section [3.5, 3.6]. The discontinuity loss can be further reduced using tapered waveguide transition in the active-passive boundary [shown in Fig. 3.1(b)]. In addition, studies on surface-emitting distributed feedback (DFB) lasers [3.7-3.9] show that intra-cavity dielectric discontinuities were totally eliminated in these lasers, and the output coupling performed in the gain section.

The performance of a GCSEL is largely determined by the structure of its passive grating sections, which has close relationship with the laser's threshold current, output

coupling efficiency, and spectral purity. Recently, a specially designed "off-resonance" grating structure occurred in GCSELs [3.10-3.12]. Although these special lasers demonstrated very high threshold current, they are extremely suitable for external cavity operation. They have two–fold advantages over traditional external cavity Fabry-Pérot (FP) diode lasers. Firstly, Bragg reflection is greatly compressed with a properly designed off-resonance grating, i.e. there is no internal feedback mechanism; hence, no anti-reflection (AR) coating is required for external cavity operation. Secondly, the wide-area GCSEL beam divergence is much lower; hence, beam coupling optics and mounting mechanics are less stringent than for conventional FP devices. Indeed, broadband, continuous tuning in CW regime over a range of 115nm has been demonstrated based on a GCSEL with off-resonance grating structure, where only a tiny mirror acted as the external feedback element. In another study, a tuneable dual wavelength terahertz oscillator was demonstrated using this kind of GCSEL in a simple external cavity [3.11].

One aspect of particular interest is to build compact, wavelength tuneable ultrashort optical pulse sources based on the above mentioned external cavity GCSELs. A preliminary study shows the GCSELs can be easily gain-switched and tuned over 60nm spectral span to produce relatively long, 160ps pulses [3.12]. It is of great practical importance to improve the quality of the output pulse generated from this type of lasers, since they may represent a new generation of compact and low-cost ultrashort optical pulse sources suitable for commercialisation. In our experiment, we demonstrated optimised, pulsed operation of a GCSEL in external cavity configuration resulting in increased output power, reduced pulse duration, expanded wavelength tuning range, and greatly improved spectral features.

3.2 Gain-switched operation of external cavity grating-coupled surface emitting lasers

3.2.1 Laser sample

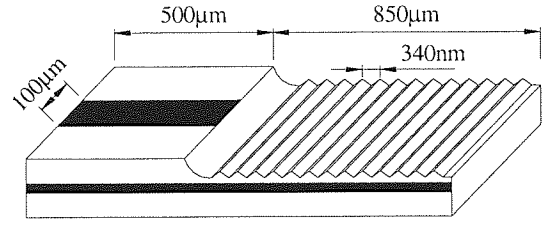

(a)

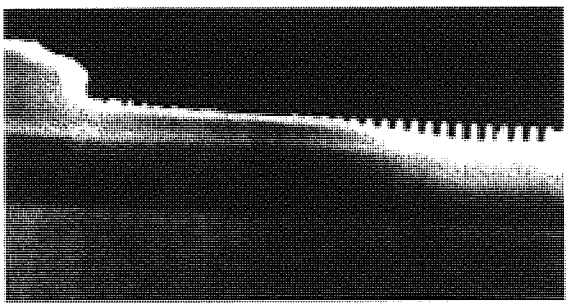

(b)

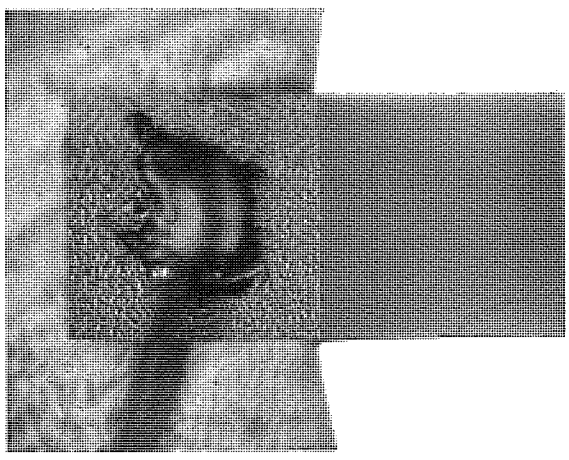

(c)

Fig. 3.1 GCSEL sample
(a): Diagram of the structure of GCSEL;
(b): Electron microscope image of smooth transition region between the active region and grating in the longitudinal slit of off-resonance GCSEL;
(c): Optical microscope image: top view of the GCSEL.

The laser used in our experiment was provided by Ioffe Institute, Russian Science Academy. Fig. 3.1 shows the structure and microscope images of the laser sample. It has a single quantum well graded-index (SQW GRIN) InGaAs structure, composed of a 100μm-wide, 500μm-long active region with electrical confinement provided by SiO_2 stripes. The active layer is followed by an 850μm long off-resonance grating section with the grating period of 340nm.

Parasitic optical feedback in the device is substantially suppressed even at high pumping levels, which results from the following two facts: Firstly, the grating period is detuned from second order Bragg reflection feedback, and Bragg resonance at 0° is not achieved in the grating for any frequencies inside the gain band; hence, almost no signal is reflected back into the laser from the grating. The grating only serves as the first order output coupler, and the light in the grating is coupled out of the laser under a certain angle to the surface of the wafer. (A detailed output coupling feature of the grating section will be discussed later.) Secondly, the optical feedback at active-passive boundary is almost zero (10^{-9}, theoretical approximation) due to the smooth transition between the active region and grating, shown in Fig. 3.1(b).

The laser sample was mounted p-side [bottom side of Fig. 3.1(a)] down to the ground for efficient heat dissipation. It was also connected in series with a 47Ω surface mounted resistor for impedance match. There was no thermal control for the laser.

3.2.2 Experimental set-up

For an off-resonance grating structure, lasing can only be achieved when an external feedback element was used. In the experiment, the external cavity was formed by a small (1mm by 1mm approximately) 100% reflecting aluminium flat mirror, placed in the vicinity of the grating section, as shown in the Fig. 3.2. It was possible to vary the distance d and the angle θ between the surfaces of mirror and the grating. The output was taken from the cleaved facet on the edge of the active region.

Pulse characterization (sampling oscilloscope, OSA);
Optical power measurement (optical power meter);
Near filed pattern measurement (CCD camera);

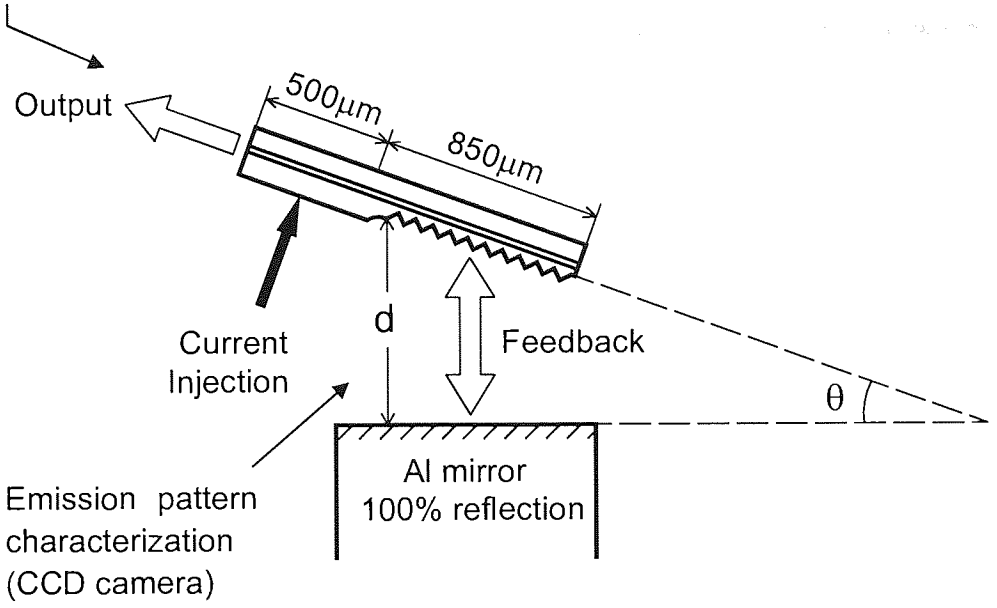

Fig. 3.2 External cavity configuration

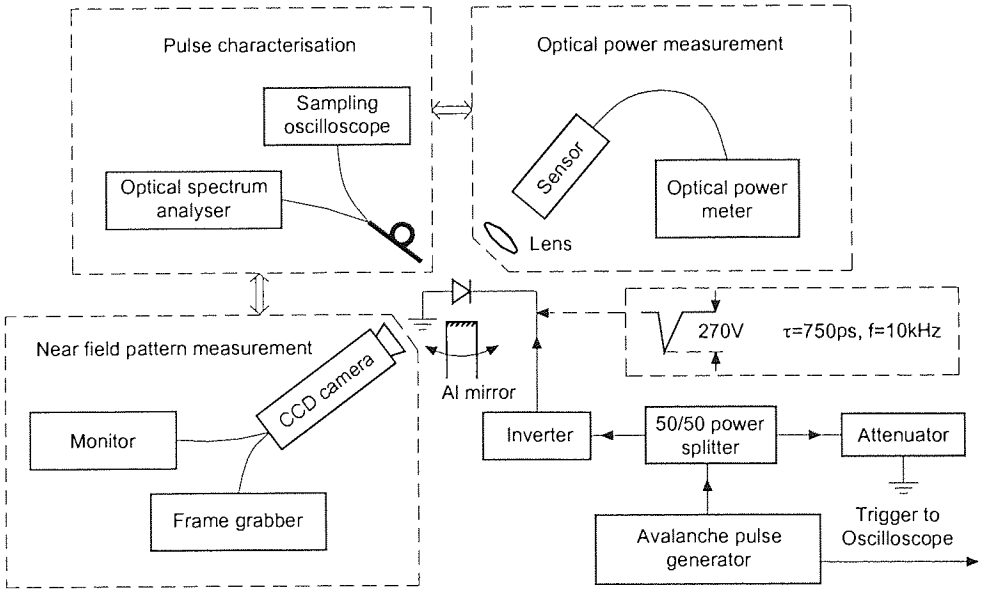

Fig. 3.3 Experimental set-up (for laser structure and external cavity configuration see Fig. 3.2). Pulse characterization, optical power measurement and near field pattern measurement were carried out separately.

Lasing was not achieved until the Al mirror was placed at a proper angle and was moved close enough to the grating section ($15^{\circ}<\theta<35^{\circ}$, $d<2mm$). In order to align the external cavity in an efficient way, Quasi-CW electrical signal (rectangular wave) with a peak voltage of 20V, a pulse duration of 200ns, and a duty cycle of 2% was used to pump the laser. Meanwhile, A CCD camera was also used to monitor the light emission from the grating substrate. For a well-aligned cavity, the emission pattern on the grating substrate was switched from short rectangular spot (spontaneous emission) to several long filaments (stimulated emission), shown in Fig. 3.4. The filaments had a width of 20-30μm each.

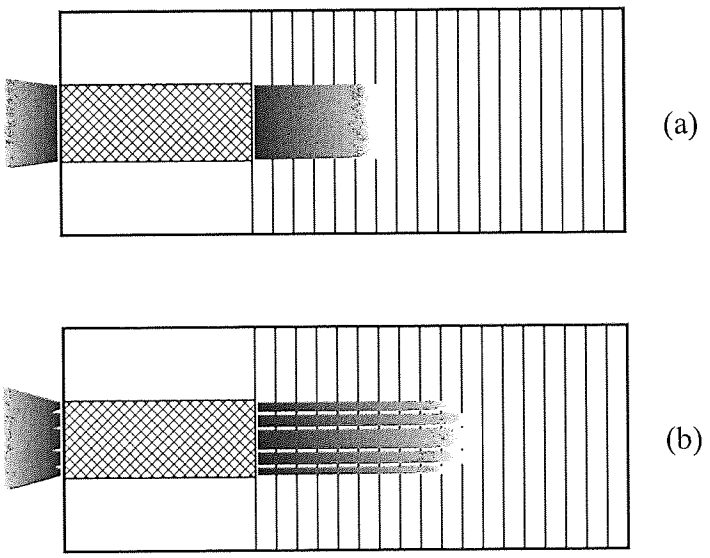

Fig. 3.4 Illustration of spontaneous emission (a) and stimulated emission (b) of the GCSEL

After the external mirror was properly aligned, the pumping signal was replaced by an avalanche pulse generator (Kentech APG1). The electrical pulse had a repetition rate of 10 kHz, a rise-time of 150ps, a fall-time of 850ps, and the peak current was attenuated to approximately 5A before applied on the laser, shown in Fig. 3.5. No DC bias was applied. For this pumping condition, the emission pattern shown in Fig. 3.4 was invisible from the CCD camera due to the low output power (<1μW). Thus, the laser performance can only be monitored from the output end (cleaved facet) with the output signal detected on optical spectrum analyser and sampling oscilloscope.

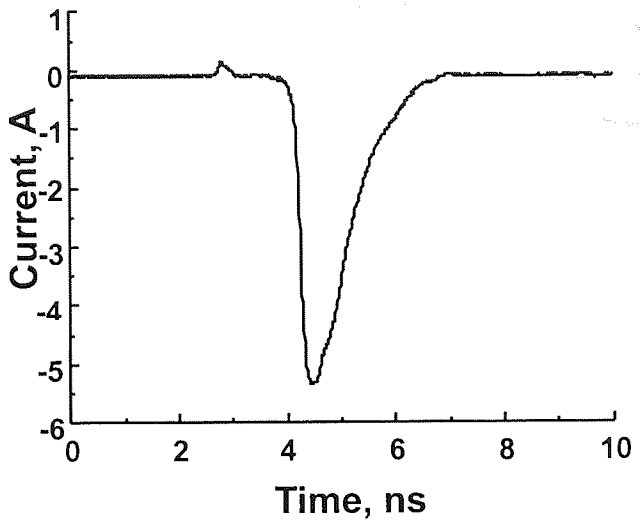

Fig. 3.5 Electrical pumping pulse of the GCSEL

The overall experimental set-up was shown in Fig. 3.3. With a properly aligned external cavity configuration, three tasks, including pulse characterisation, output power measurement, and near field pattern characterisation, were carried out separately.

3.2.3 Experimental results

The output power increased as the mirror was moved closer to the laser. The signal wavelength was tuned by adjustment of the mirror angle θ. The spectral bandwidth of the laser output was not affected by the distance to the mirror d. We therefore kept the length of the external cavity very short, 800μm approximately, in order to provide strong optical feedback. The corresponding longitudinal mode spacing of the compound cavity was about 0.16nm.

When the angle of the external aluminium mirror, θ, was adjusted from 15.9° to 35.0°, the generation wavelength changed by 100nm (902-1002nm). The temporal and spectral profiles of the generated pulses were detected by a 40GHz digital sampling oscilloscope (Agilent 86100A) and an optical spectrum analyser (Hewlett-Packard 70950, resolution: 0.06nm) respectively.

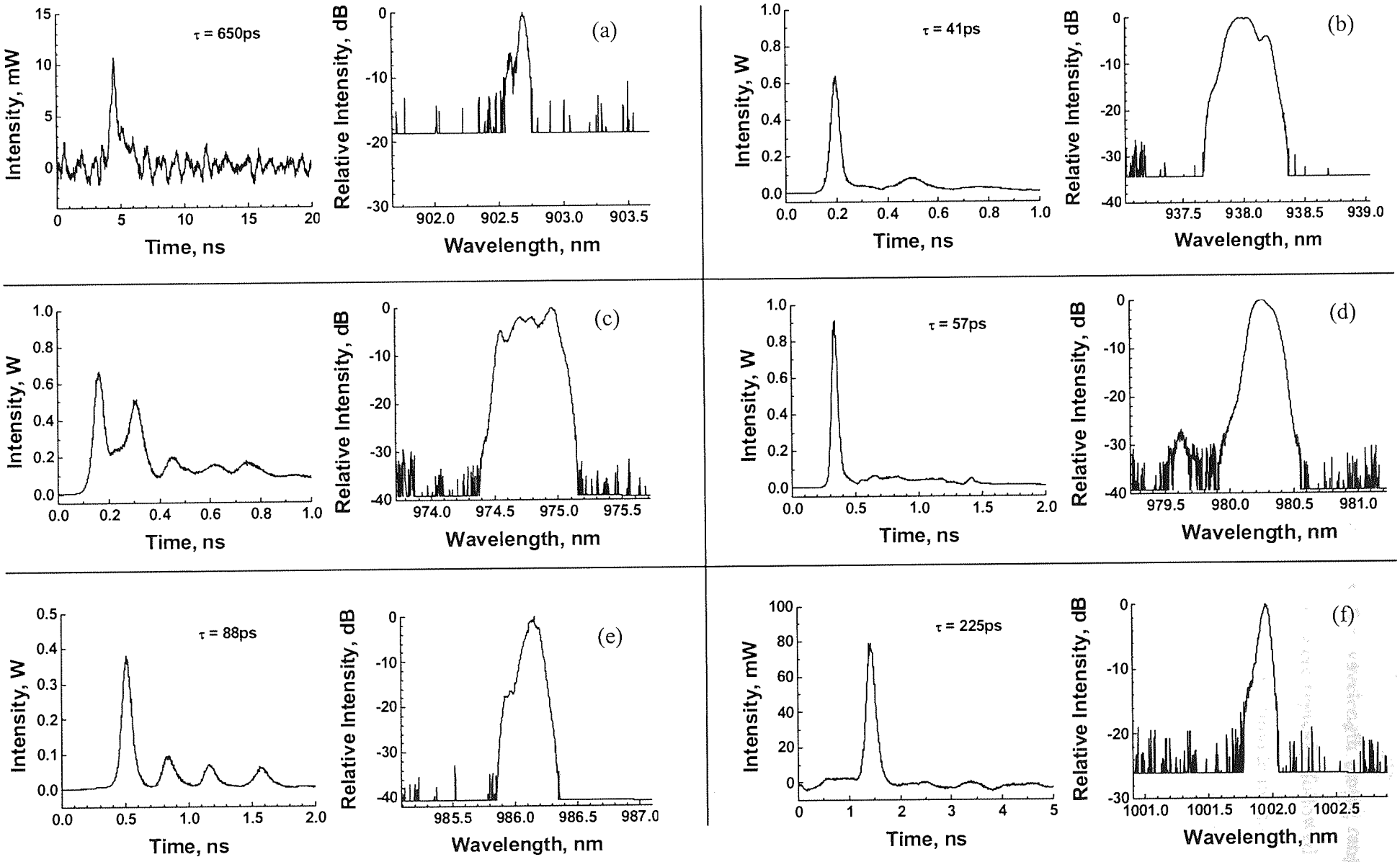

Fig. 3.6 Oscilloscope traces (left) and spectra (right) of gain switched pulses generated from external cavity GCSEL at different wavelength positions across the whole tuning range. Lasing wavelength increases from 902nm (a) to 1002nm (f).

Fig. 3.6 showed several typical signals obtained across the wavelength tuning range. At high level of pumping current, the gain switched pulses were typically followed by pronounced relaxation tails, and the pulse spectra were always multimode in that case [Fig. 3.6(c)]. However, in our experiment, we found the relaxation tail of the gain-switched pulse was greatly suppressed at some points within the wavelength tuning range [Fig. 3.6(b), (d)]. These pulses had very narrow spectrum (λ_{FWHM}<0.3nm) with a side-band suppression ratio of 35-40dB. There were also some points where the pulses possess narrow spectra and low energy sub-pulses [Fig. 3.6(e)]. These facts indicate, as the laser was tuned, the pulses were tailored according to spectral components of the feedback signal from the external mirror. A similar spectral filtering effect was also reported by using a tuneable fibre Bragg grating [3.13]. More detailed discussion of spectral filtering mechanism in our laser will be presented in Section 3.3.

The wavelength tuning curves, showing the peak power and the pulse duration as functions of wavelength, are presented in Fig. 3.7.

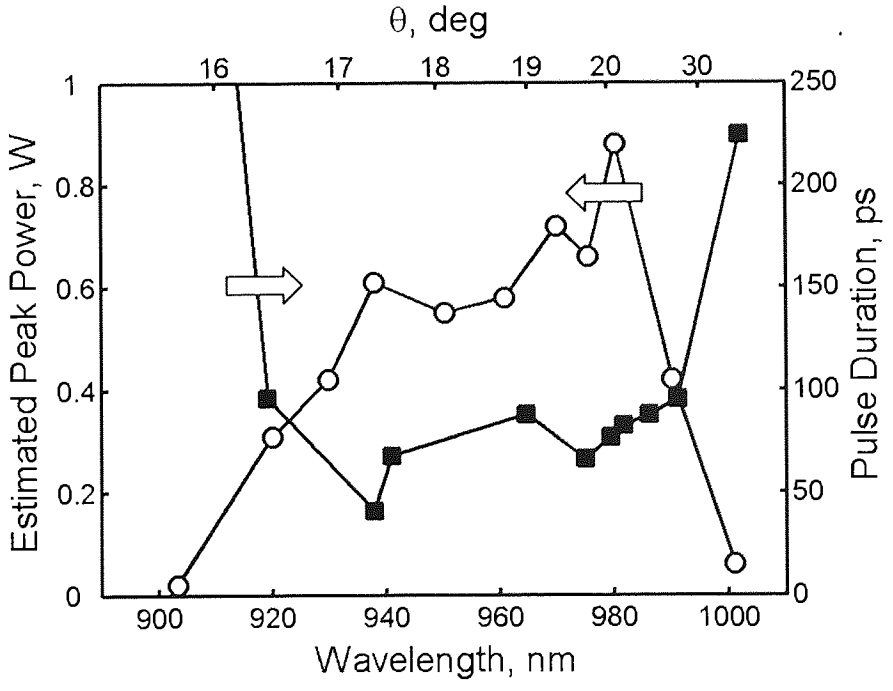

Fig. 3.7 Tuning curves of the laser. Peak power and the pulse duration are shown over the entire wavelength tuning range.

The pulse duration increased towards the edges of the tuning curve. The pulse duration shorter than 100ps was observed within a 70nm-wide spectral window (920-990nm). The shortest pulse duration of 41ps was obtained at a wavelength of 938nm with the corresponding peak power of 0.64W [Fig. 3.6(b)]. The maximum peak power of 0.88W was obtained at a wavelength of 980nm [Fig. 3.6(d)]. At this point, good pulse quality with substantial tail suppression was also achieved.

As the laser was tuned, the spectra changed in a periodic manner, switching between single frequency and the multimode operation with a period of 1.2nm. Fig. 3.8 shows 3 periods of this spectral switching behaviour in the central gain band of the laser, ~980nm. In the case of single frequency operation [Fig. 3.8(a),(c),(e),(g)], laser spectra had exceptionally good side-band suppression ratio in excess of 32dB [Fig. 3.8(h)] and FWHM linewidth around 0.2nm. In the case of multimode operation [Fig. 3.8(b),(d),(f)], 3-6 laser modes can be observed at lower reference levels (-6dB and -10dB). This phenomenon was likely to be caused by the additional resonances in an etalon formed by the grating/air interface and the bottom of the wafer. The wafer itself served as a periodical band-pass filter due to the etalon effect. At the edges of the tuning range, the multimode operation did not occur, instead, dark zones between the adjacent single-frequency points were observed, indicating that the multimode operation corresponds to the minima of the substrate etalon reflection. Assuming the refractive index of the wafer media is 3.5, the depth of the etalon was estimated at 150μm, which matches the structure parameter of our laser.

The lateral intensity profile from the output facet measured in the near field with a CCD camera is presented in Fig. 3.9. Similar to broad-area diode lasers, filamentation in the GCSEL was evident. The spectral profiles of the emission in different filaments were almost identical (Fig. 3.10), however, the near-field mode pattern changed substantially with tuning of the laser.

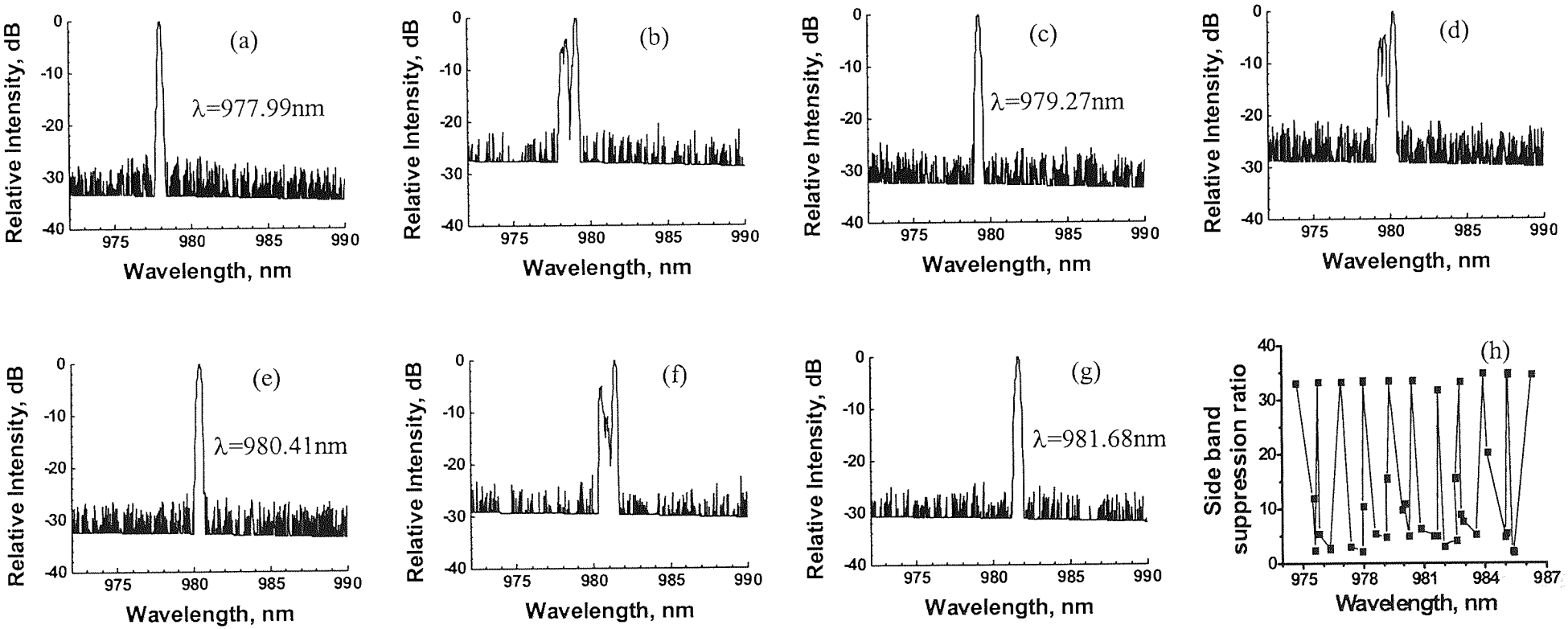

Fig. 3.8 Periodical switching between single-frequency (a), (c), (e), (g) and multi-mode spectra (b), (d), (f) at a lasing wavelength around 980nm. Single-frequency lasing appeared at a wavelength interval of 1.2nm and had a side band suppression ratio in excess of 32dB (h).

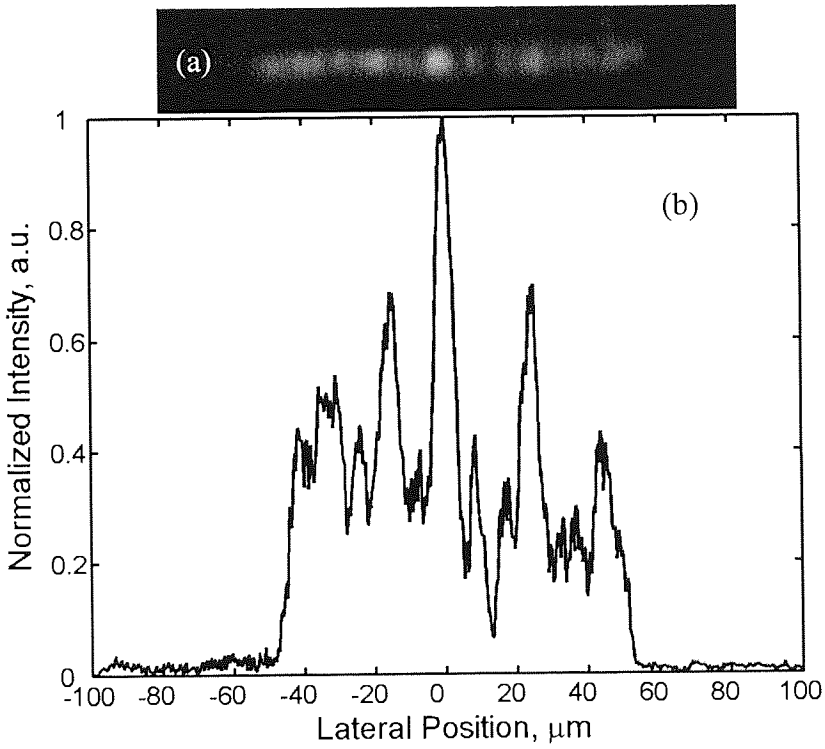

Fig. 3.9 (a) Near-field pattern and (b) lateral profile of the laser beam, obtained from the output facet by a CCD camera.

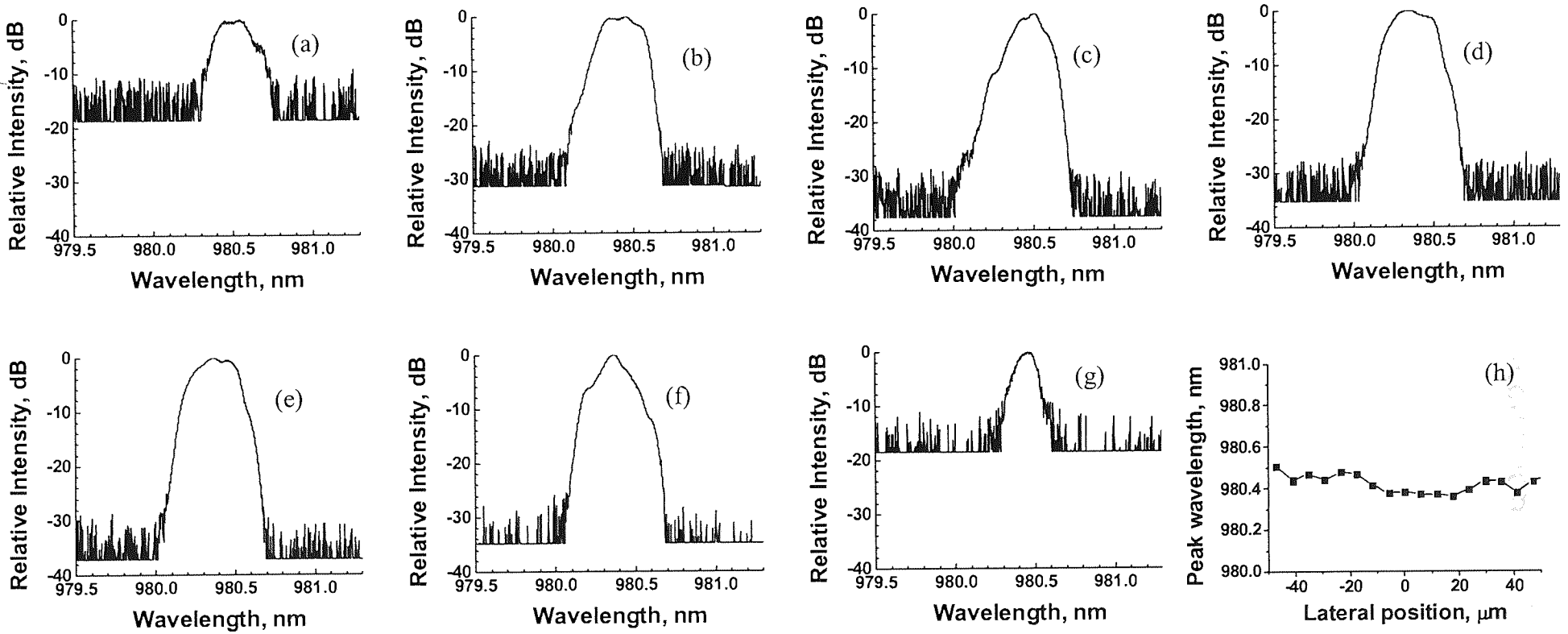

Fig. 3.10 Spectra obtained by scanning the coupling fiber along the lateral direction, from (a) to (g), of the output facet. The laser was tuned at a single-frequency lasing point around 980nm. There was no substantial change of peak wavelength along the lateral position (h).

3.3 Discussion

A notable feature of the experiment described above is that no sophisticated configuration was required to obtain experimental results of great practical value, such as a wavelength tuneability of 100nm, a high output power of nearly 1W, substantially suppressed relaxation tail, and single frequency spectra. The simplicity of the system offers a good opportunity to analyse the fundamental physics mechanism behind the observed phenomena. In this section, analytical modes are used to discuss the spectral filtering effects attributed to single-frequency spectrum, suppression of relaxation tail, wide wavelength tuneability etc., while, a numerical mode is presented to analyse the filamentation formed in the grating substrate.

3.3.1 Spectral filtering

Spectral filtering in the laser was realised through the interaction between the grating substrate and the external mirror. The interaction of light waves in the passive grating section is depicted in Fig. 3.11.

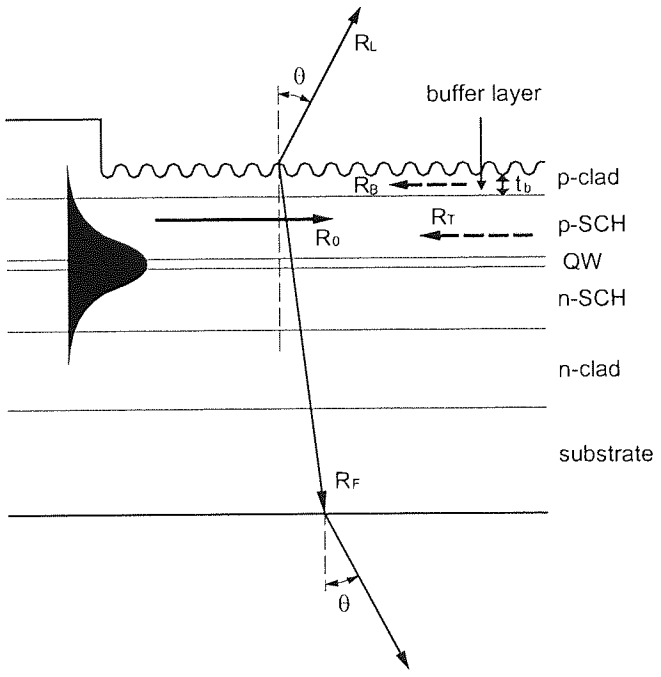

Fig. 3.11Illustration of wave propagation and transition in off-resonance grating section.

In the above passive grating substrate, there exists a TE_0 wave propagating in the waveguide from the active section towards the grating section, R_0. In theory, there is also a TE_0 wave within the waveguide, S_0, propagating opposite to R_0, However, it is neglectable due to the following two reasons. Firstly, Bragg reflection, R_B, was not achieved due to the off-resonance grating with detuned grating period. Secondly, all the light was coupled out of the laser within a short distance from the active/passive boundary; hence, there is no termination reflection, R_T. In the air-grating interface, the power of forward propagating wave, R_0, was distributed to transition reflection wave, R_F, and leaky wave, R_L. The latter is coupled out of the grating at an angle of θ.

The m-line spectroscopy technology [3.14-3.16] can be utilized to describe the transition in the air-grating interface. The leaky wave generated from power in the propagating mode of the grating waveguide leaves the device at a well-defined direction, θ_m^q , given by,

$$\sin\theta_m^q = n_g \sin\theta_{Bm} + q\lambda_m / d \equiv n_m + q\lambda_m / d \tag{3.1}$$

In this equation, which is derived from the diffraction grating equation and Snell's law, n_g is the refractive index of the grating layer. θ_{Bm} is the mode bounce angle, n_m is the mode guide index, λ_m is the vacuum wavelength of the mth mode, d is the grating period, and q is an integer corresponding to the diffraction order of the grating.

By substituting the laser parameters and experiment data to equation 3.1, real value of θ_m^q can only be obtained when q=-1, and only fundamental waveguide mode, TE_0, is supported in our laser. Hence, the emission angle for the leaky waves, in our case, is given by,

$$\sin\theta_0^{-1} = n_0 - \frac{\lambda_0}{d} \tag{3.2}$$

The beam divergence depends on a superposition of two divergence functions: $\Delta\theta(A)$, the divergence due to the finite spatial width A of the output aperture; and $\Delta\theta(\Delta\lambda)$, the divergence due to the finite spectral width $\Delta\lambda$ of the laser oscillation. An approximate

expression for Δθ(A) is,

$$\Delta\theta(A) \cong \lambda / A \tag{3.3}$$

and an approximate expression for Δθ(Δλ), obtained from (3.2), is

$$\Delta\theta(\Delta\lambda) \cong |\Delta n(\Delta\lambda)| + |\Delta\lambda / d| \tag{3.4}$$

In our laser, the mode dispersion is assumed to be normal, i.e. n increases as λ decreases, so that the two terms on the right-hand side of (3.4) always add. In the AlGaAs grating substrate of our laser, the dispersion term $\Delta n(\Delta\lambda)$ is dominated by $\Delta\lambda/d$ term. If the output aperture is small and the emission bandwidth is large, highly divergent beam will be obtained. In our experiment, the value of Δθ is in the range 15°~20°.

Large bandwidth emission without external feedback was achieved in our experiment, which was essentially attributed to the off-resonant grating structure. The grating period had a value of 340nm, which was highly detuned from the second order Bragg resonant wavelength of the central gain band of the laser. Hence, there was almost no Bragg reflection in the waveguide. Without external feedback, only broad-band amplified spontaneous emission (ASE) was obtained even at very high pumping levels, i.e. this device was actually a superluminescent LED. The spectrum dispersion induced beam divergence angle, governed by the $\Delta\lambda/d$ term in equation (3.4), was estimated at 16°, and dominated the whole divergence angle.

The output beam aperture, A, in the grating section can be controlled by varying the thickness of buffer layer, t_b, in the passive section, shown in Fig. 3.11. Theoretical analysis [3.17] shows, due to first-order leaky-wave excitation, the power-loss coefficient of TE_0 mode, α_0^{-1}, increases exponentially as the thickness, t_b, decreases. Therefore, a shallow buffer layer would result in the light coupled out of the grating substrate within a short distance, i.e. a small beam aperture, and thus a wider beam divergence angle. In our experiment, a beam aperture of 100~150μm for spontaneous emission was observed. It corresponded to a limited-aperture-induced beam divergence angle of 0.4°~0.6°, which contributed very little to the overall beam

divergence angle.

With highly efficient out-coupling of light into the air at a wide range of angle, stimulated emission could be achieved by using properly designed external feedback element. In our experiment, a single, 100% reflection aluminium flat mirror was used. It not only provided optical feedback but also was essential for spectral filtering and wavelength tuning. The role of the aluminium flat mirror can be explained by the dynamics of in-coupling behaviour from the mirror to the grating as presented below.

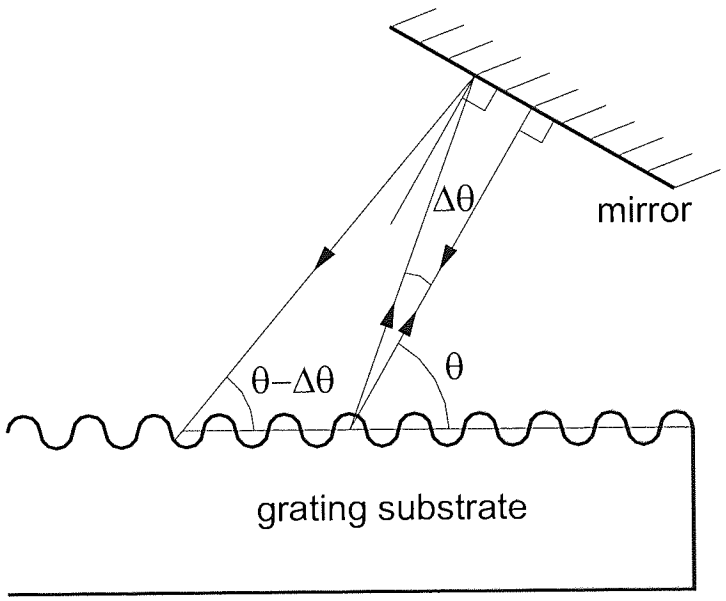

Fig. 3.12 Illustration of light propagation between grating substrate and mirror.

Fig. 3.12 illustrates the light propagation between the grating and the mirror. We assume the out coupling beam from the grating at an angle of θ is perpendicular to the external mirror. The exit angle for a wavelength λ+Δλ is then θ+Δθ with Δθ=−Δλ/(*d**cosθ), and the beam reflected by the mirror is incident back on the grating at an angle of θ−Δθ with deviation from the coupling angle by 2Δθ. Expressions for the dependence of the input coupling efficiency η on the phase mismatch can be derived based on the reciprocity theorem [3.18], given by

$$\eta/\eta_0=\mathrm{sinc}^2(L\Delta\beta/2) \tag{3.5}$$

where, $\Delta\beta = k\cos\theta\Delta\theta$, $k=2\pi/\lambda$, , L is the aperture of the output beam from the

grating, and η_0 is the input coupling efficiency for $\Delta\lambda=0$.

The wavelength dependence of η, in our case, can be approximately written as

$$\eta/\eta_0=\text{sinc}^2(kL\cos\theta\Delta\theta)=\text{sinc}^2(kL\Delta\lambda/d) \quad (3.6)$$

where, d is grating period.

The spectral filtering characteristic of the mirror-grating-mirror coupling is dominated by equation (3.6). Substituting our experimental data into equation (3.6), we obtained the estimated FWHM spectral bandwidth as 0.5~0.6nm. The theoretical result accurately matches the bandwidth for multimode operation observed in our experiment. Such sharp wavelength selectivity assured precise wavelength control.

On the other hand, the feedback efficiency for the lasing wavelength, η_0, stays nearly constant when the device angle is changed for tuning within the gain bandwidth [3.19], therefore, the wavelength tuning bandwidth is not limited by the dependence of the feedback efficiency on the beam angle. From this point of view, the maximum achievable range of wavelength tuning for this external cavity GCSEL is simply determined by the bandwidth of the gain spectrum of the laser material. Besides, highly intensive electrical driven signal will cause large modulation depth of carrier density in the laser media, thus a large portion of spectral components within the gain band will participate in lasing and a wide wavelength tuning range will be achieved. Above all, the simple external cavity configuration was extremely suitable for broadband wavelength tuning of pulsed operation. This fact was also justified in our experiment, noticing that the wavelength tuning range had achieved 100nm (900-1000nm).

In addition, there was another spectral filtering mechanism in the GCSEL caused by Fabry-Pérot etalon effect of the grating substrate. Resonance was achieved due to reflection from the bottom surface of the wafer, shown in Fig. 3.11. As a result, the modulated transmission spectrum from the grating was characterised by narrow peaks

at an interval (free spectral range) of

$$\Delta\lambda = \frac{\lambda^2}{2n_F D} \tag{3.7}$$

where, n_F is the refractive index of the wafer for the reflected wave R_F, D is the thickness of the wafer. The sharpness of the peaks in transmission spectrum is given by,

$$\delta\lambda=\Delta\lambda/F \tag{3.8}$$

where, F is the sharpness factor given by,

$$F=4R/(1-R)^2 \tag{3.9}$$

and R is the reflectivity from the laser media to the air.

By substituting our experimental data into equation (3.7)-(3.9), the sharpness of the transmission spectrum was estimated at 0.4-0.5nm. In our experiment, the linewidth for single-frequency operation was measured at 0.2-0.3nm, which was considered to be the superposition of two spectral filtering effects induced by the substrate etalon and the external flat mirror, respectively.

The above mentioned effect of spectral filtering could also be used to explain the effect of tail suppression of the output pulses. For intensively driven gain switched pulses, there is substantial blue shift of the spectral components for the first peak so that the spectral components for the rest part of the pulse are isolated. Therefore, pulse tail could be substantially suppressed if proper spectral filtering mechanism is used. (More detailed theoretical discussion will be presented in Chapter 4 and Chapter 5.) The built in spectral filter in our external cavity configuration proved to be well suited to eliminate the huge relaxation tail of the gain-switched pulses. It was evidently shown in our experiment by noticing compressed pulse tails with single frequency output and side band suppression ratio in excess of 40dB [Fig. 3.6(d)] and uncompressed pulse tails corresponding to multimode output [Fig. 3.6(c)].

3.3.2 Filamentation

In a typical grating coupled surface emitting laser, the light beam coupled out of the grating section should be wide enough to assure small divergence angle in lateral direction. In order to obtain a wide out-coupled beam, the lateral size of the active section is relatively large, or at least, the active/passive boundary is wide. Filamentation was always an inevitable phenomenon in this kind of wide-strip lasers. This phenomenon was evidently shown in our experiment by multi-lobe lateral profiles (Fig. 3.10) and the stimulated emission pattern in the grating substrate [Fig. 3.4(b)].

There are three nonlinear mechanisms that can lead to filamentation in semiconductor lasers: gain-saturation-induced changes in refractive index through the linewidth-enhancement factor, self-focusing due to heat-induced index changes, and self-defocusing through intensity-dependent index changes in the cladding layer. As we considered the theoretical analysis based on broad-area lasers [3.20] is also suited to qualitatively explain the phenomenon observed in our experiment.

Theoretically, filamentation can be demonstrated by solving the lateral distribution (along the x axis) of the intra-cavity field. The electric field in terms of counter-propagating waves can be given as

$$\vec{E}(\vec{r},t)=\frac{1}{2}\hat{x}\phi(y)\left[E_f(x,z)\exp(ikz)+E_b(x,z)\exp(-ikz)\right]\exp(-i\omega t)+c.c. \quad (3.10)$$

where, E_f and E_b represent the forward and backward travelling waves of frequency ω, respectively, k is the mode propagation constant. Since the active layer is planar, the x and z dependence of the transverse field distribution $\phi(y)$ can be neglected. The laser field in the cavity must satisfy the wave equation

$$\nabla^2\vec{E}(\vec{r},t)-\frac{\varepsilon(\vec{r})}{c^2}\frac{\partial^2\vec{E}}{\partial t^2}=0 \quad (3.11)$$

where $\varepsilon(\vec{r})$ is the complex dielectric constant whose y dependence is responsible for waveguiding in the transverse direction.

Substituting (3.10) into (3.11), making the paraxial approximation, and using the fact that $\phi(y)$ satisfies a Helmholtz equation, the counter-propagating waves are found to satisfy a set of two coupled equations given by

$$\frac{\partial E_f}{\partial z} = \frac{i}{2k}\frac{\partial^2 E_f}{\partial x^2} + \left[\frac{1}{2}\Gamma(1-i\alpha)g(N) - \frac{\alpha_{\text{int}}}{2} + in_2 k_0\left(|E_f|^2 + 2|E_b|^2\right)\right]E_f \qquad (3.12a)$$

$$-\frac{\partial E_b}{\partial z} = \frac{i}{2k}\frac{\partial^2 E_b}{\partial x^2} + \left[\frac{1}{2}\Gamma(1-i\alpha)g(N) - \frac{\alpha_{\text{int}}}{2} + in_2 k_0\left(|E_b|^2 + 2|E_f|^2\right)\right]E_b \qquad (3.12b)$$

where Γ is the transverse confinement factor, α is the linewidth-enhancement factor, α_{int} is internal loss, n_2 is the Kerr coefficient, and $g(N)$ is the local carrier-dependent gain assumed to be $g(N)=a(N-N_0)$. Here, a is the differential gain coefficient, and N_0 is the transparency value for the carrier density. Equations (3.12) not only account for coupling between counter-propagating waves but also includes diffraction, carrier-induced index variations, free-carrier absorption, material gain, and self-focusing ($n_2>0$) or self-defocusing ($n_2<0$) through a Kerr-type nonlinearity.

The carrier density distribution can be accounted for by solving the diffusing equation,

$$D\nabla^2 N(\vec{r}) = -\frac{J(\vec{r})}{qd} + \frac{N(\vec{r})}{\tau_{nr}} + BN^2(\vec{r}) + \frac{g(N)}{\hbar\omega}\left|\vec{E}(\vec{r},t)\right|^2 \qquad (3.13)$$

where D is the diffusion constant, $J(\vec{r})$ is the injected current density, q is the magnitude of electron charge, d is the active-layer thickness, τ_{nr} is the nonradiative lifetime, and B is the spontaneous emission coefficient. The first term accounts for carrier injection, while the second and third terms account for the nonradiative and spontaneous recombinations, respectively. The last term is due to stimulated recombination and accounts for gain saturation.

The forward and backward propagating beams at the facets can be related by the boundary conditions

$$E_f(x,0) = \sqrt{R_0}E_b(x,0) \qquad (3.14a)$$

$$E_b(x,L)=\sqrt{R_L}E_f(x,L) \qquad (3.14b)$$

Here, in our case, R_0 and R_L represent the facet power reflectivities at x=0 (output facet) and x=L (grating-air interface), respectively.

In [3.20], equations (3.12) and (3.13) were solved iteratively assuming initially a rectangular lateral profile at z=0. Depending on the laser parameters, the iteration procedure either converges or fails to converge. The lateral mode is identified as unstable in the latter case, i.e. filaments occur in the waveguide.

Several general conclusions can be drawn from the numerical simulation in [3.20], as is considered to be also applicable to our grating coupled surface emitting laser: (1) For a given linewidth enhancement factor, α, the value of the critical stripe width ω_c, below which the device will operate stably, depends on the level of pumping; increased levels of pumping reduces the critical width at which a laser can operate stably. (2) For a given pump level, variation in α around typical device values ($2<\alpha<5$) do not change this critical width much; (3) for narrow stripe width ($\omega<6\mu m$), laser is stable for any value of α and any level of pump; and for small linewidth enhancement factor ($\alpha<0.4$), laser is stable for any stripe width and any level of pump; (4) both self-focusing and self-defocusing, governed by the parameter n_2, can also destabilize the lateral laser mode. The dependence of n_2 on critical stripe width, ω_c, has a close similarity with the dependence of as linewidth enhancement factor, α, on ω_c. However, the influence of α is the most dominant mechanism.

Several considerations could be given to eliminate filamentation in such wide strip lasers. First, it may be possible to design a broad area grating coupled laser such that the effective α is below the critical value. Such laser will be stable without filamentation, regardless of stripe width or injection current. Second, a source for self-defocusing ($n_2<0$) may come from the cladding layers, hence, by a proper design of the cladding layer, the self-defocusing nonlinearity may help to offset or even

cancel the filamentary self-focusing effects caused by the linewidth-enhancement factor.

In practice, suppression of filamentation in wide stripe grating coupled surface emitting laser has been demonstrated using an unstable resonator [3.21-3.23], which supports non-conterpropagating waves. In such lasers, it is possible to have a single, broad lateral mode. On the other hand, due to the introduction of off-resonance grating there is almost no backward propagating wave in the absence of external cavity, then it is possible to suppress filamentation using specially designed unstable external cavity, say, using convex mirror as the external feedback element.

3.4 Conclusion

In conclusion, we present experimental investigation of a grating-coupled surface emitting laser (GCSEL). The laser was used in a very simple external cavity configuration for high power gain-switched operation. The wavelength tuneability has reached 100nm (900~1000nm) by simply adjusting the angle between the laser wafer and the external mirror. The pulse duration was maintained below 100ps at a wavelength range of 70nm (920~990nm). Within the wavelength tuning range, the shortest pulse duration of 40ps was obtained at a wavelength of 940nm, and the highest peak power output up to 1W was obtained at a wavelength of 980nm. Under high power pumping condition, relaxation oscillation tail of gain switched pulse was greatly compressed and good pulse quality was maintained.

Investigation shows output spectral filtering mechanism existed in the external cavity and was of great importance to achieve single-frequency operation with wide wavelength tuning range for pulsed operation. Filamentation observed in the device was discussed using the theoretical model of broad-area diode lasers taken from

literature, which qualitatively explained the phenomena in our experiment. Further improvement of laser design is of great practical value for building compact ultrashort optical pulses sources.

References

[3.1] Z. Alferov, V. Andreyev, S. Gurevich, R. Kazarinov, V. Larionov, M. Mizerov, and E. Portnoy, "Semiconductor lasers with the light output through the diffraction grating on the surface of the waveguide layer", *IEEE Journal of Quantum Electron.* **QE-11**, 449-451, 1975

[3.2] P. Zory and L. Comerford, "Grating-coupled double-heterostrucuture AlGaAs diode lasers", *IEEE Journal of Quantum Electronics*, **QE-11**, pp. 451-457, 1975

[3.3] K. Kojima, S. Noda, K. Mitsunaga, K. Kyuma, K. Hamanaka, and T. Nakayama, "Edge- and surface-emitting distributed Bragg reflector laser with multiquantum well active/passive waveguides", *Applied Physics Letters*, **50**, pp. 227-229, 1987

[3.4] G. Evans, N. Carlson, J. Hammer, M. Lurie, J. Butler, S. Palfrey, L. Carr, F. Hawrylo, E. James, C. Kaiser, J. Kirk, and W. Reichert, "Efficient 30mW grating surface-emitting lasers", *Applied Physics Letters*, **51**, pp. 1478-1480, 1987

[3.5] G. Evans, N. Carlson, J. Hammer, M. Lurie, J. Butler, L. Carr, F. Hawrylo, E. James, C. Kaiser, J. Kirk, and W. Reichert, "Efficient, high-power (>150mW) grating surfact emitting lasers", *Applied Physics Letters*, **52**, pp. 1037-1039, 1988

[3.6] G. Evans, D. Bour, N. Carlson, R. Amantea, J. Hammer, L. Hao, M. Lurie, R. Lai, P. Pelka, R. Farkas, J. Kirk, S. Liew, W. Reichert, C. Wang, H. Choi, J. Walpole, J. Butler, W. Ferguson, R. Defreez, M. Felisky, "Characteristics of coherent 2-dimensional grating surface emitting diode-laser arrays during CW operation", IEEE Journal of Quantum Electronics, **27**, pp. 1594-1608, 1991

[3.7] N. Carlson, S. Liew, R. Amantea, D. Bour, G. Evans, E. Vangieson, "Mode-discrimination in distributed feedback grating surface emitting lasers containing a buried 2nd-order grating", *IEEE Journal of Quantum Electronics*, **27**, pp. 1746-1752, 1991

[3.8] P. Kellermann, A. Golshani, A. Kock, E. Gornik, H. Gauggel, R. Winterhoff, M. Pilkuhn, "Single-mode and single-beam surface emission from visible red GaInP/AlGaInP laser diodes", *Applied Physics Letters*, **70**, pp. 2374-2376, 1997

[3.9] J. Lopez J, G. Witjaksono, D. Botez, "Single-mode, single-lobe operation of surface-emitting, second-order distributed feedback lasers", *Applied Physics Letters*, **75**, pp. 885-887, 1999

[3.10] J. Jiang, O. Smolski, C. Roychoudhuri, E. Portnoi, G. Venus, I. Gadjiev, and J. McKillop, "Broad tenability of grating coupled surface-emitting laser with external cavity", *Electronics Letters*, **35**, 1847-1848, 1999

[3.11] A. Gubenko, G. Venus, I. Gadzhiev, G. Zaboev, E. Portnoi, "Tunable dual wavelength grating coupled surface emitting diode laser for Thz frequency optoelectronics", *Submitted to LAT Conferences on Lasers*, Moscow, Russia, 2002

[3.12] O. Smolski, J. Jiang, C. Roychoudhuri, E. Portnoi, G. Venus, and J. Bullington, "Tunable picosecond pulses from gain-switched grating coupled surface emitting laser", *Proceedings of the society of photo-optical instrumentation engineering (SPIE)*, edited by J. Meyer and C. Gmachl, **4651**, pp. 59-62, 2002

[3.13] M. Dubov, D. Giannone, I. Khrushchev, I. Bennion, "Pulse tail suppression in laser diode output by tuneable notch filter", *Electronic Letters*, **37**, pp.1404-1405, 2001

[3.14] P. Tien, R. Ulrich, and R. Martin, "Modes of propagation light waves in thin deposited semiconductor films", *Applied Physics Letters*, **14**, pp. 291-294, 1969

[3.15] M. Dakss, L. Kuhn, P. Heidrich, and B. Scott, "Grating coupler for efficient excitation of optical guided waves in thin films", *Applied Physics Letters*, **16**, pp. 523-525, 1970

[3.16] P. Zory, "Laser oscillation in leaky corrugated optical waveguides", *Applied Physics Letters*, **22**, pp. 125-128, 1973

[3.17] P. Zory and L. Comerford, "Grating-coupled double-heterostructure AlGaAs diode lasers", *IEEE Journal of Quantum Electronics*, **QE-11**, pp. 451-457, 1975

[3.18] T. Suhara, H. Ishimaru, S. Ura, and H. Nishihara, "Integration of detection optics for magnetooptical disk pickup", *Transactions of IEICE*, **E73**, pp. 110-115, 1990

[3.19] M. Uemukai, T. Suhara, K. Yutani, N. Shimada, Y. Fukumoto, H. Nishihara, and A. Larsson, "Tunable external-cavity semiconductor laser using monolithically integrated tapered amplifier and grating coupler for collimation", *IEEE Photonics Technology Letters*, **12**, pp. 1607-1609, 2000

[3.20] J. Marciante and G. Agrawal, "Nonlinear mechanisms of filamentation in broad-area semiconductor lasers", *IEEE Journal of Quantum Electronics*, **12**, pp. 590-596, 1996

[3.21] N. Eriksson, P. Modh, and A. Larsson, "Grating-coupled surface-emitting laser with a hyperbolic unstable resonator producing a stable focused output beam", *IEEE Photonics Technology Letters*, **11**, pp. 1366-1368, 1999

[3.22] N. Eriksson N, P. Modh, A. Larsson, "Design optimization of a hyperbolic unstable-resonator semiconductor laser", *IEEE Journal of Quantum Electronics*, **37**, pp. 1095-1102, 2001

[3.23] P. Modh, J. Backlund, J. Bengtsson, A. Larsson, N. Shimada, T. Suhara, "Multifunctional gratings for surface-emitting lasers: design and implementation", *Applied Optics*, **42**, pp. 4847-4854, 2003

Chapter 4

Short pulse generation in InGaN diode lasers

In this chapter, we discuss experimental research on picosecond pulse generation from an InGaN multi-quantum well diode laser, which operated at a central wavelength of 402nm. This laser was a commercial sample based on advanced fabrication technology. It was suitable for pulsed operation at high level of pumping current as well as room temperature CW operation. For picosecond pulse generation, particularly high power was obtained by simply gain switching the laser with highly intensive electrical pulses. For spectral control of generated pulses, the technique of self-seeded gain switching was used. This technique, previously demonstrated in near-infrared region, proved to be effective in "blue" or "violet" region. Finally, the conclusion is presented.

4.1 Recent advances of GaN-based diode lasers

The development of GaN based lasers has progressed rapidly in the last few years. Room temperature gallium nitride based lasers with lifetime more than 10,000 hours have already been demonstrated. Commercial gallium nitride lasers are now available for purchase. One of the greatest commercial values for blue and violet GaN based lasers is optical reading and writing of data in compact disk memories and opto-magnetic memories. Since the storage density in these memories is largely determined by the wavelength of the light, it is expected that blue lasers will increase the storage density by about a factor of four compared to presently employed red and infrared lasers. In addition to data storage and read-out, there are many other possible markets, for example, in spectroscopy, metrology, and bio-medical field.

These developments are a result of the realisation of high-quality epilayers of AlGaN and InGaN, and p-type conduction in AlGaN [4.1]-[4.5]. Recombination of localised exitons was proposed as an emission mechanism for the spontaneous emission of the InGaN quantum-well-structure LDs. The radiative recombination of the spontaneous and stimulated emission of the InGaN MQW LDs was attributed to excitons (or carriers) localised at deep traps, which was verified by measuring Stokes shift between the exciting and the emission energy of the InGaN MQW LDs as large as 100-250meV at room temperature. Using high-resolution cross-sectional transmission electron microscopy (TEM), a periodic indium composition fluctuation was observed, which was probably caused by InGaN phase separation during growth. Based on these results, the laser emission is considered to originate from the In-rich region in the InGaN quantum wells acting as quantum dots [4.6-4.8]. These InGaN quantum dots were self-organised due to phase separation during InGaN growth. It should be noted that the process for self-formation of quantum dots may not be due to interface fluctuation as was reported in narrow GaAs/AlAs or CdSe/ZnSe QWs, but may be a result of the intrinsic nature of InGaN ternary alloys since the compositional modulation due to phase separation would be energetically favoured in this system.

The formation of quantum dot-like structure governed the main operational properties of the diode lasers, optical gain for example, and resulted in commercial products with low threshold current density (<50mA), high slope efficient (>1W/A), high output power (>30mW) for room temperature CW operation [4.9].

In addition, commercialisation of GaN diode lasers greatly attributed to the increased lifetime of InGaN laser diode which is due to use of epitaxially laterally overgrown (ELOG) substrates and AlGaN/GaN modulation-doped, strained-layer superlattices as cladding layers [4.10, 4.11]. In the latest studies [4.12-4.14], epitaxially laterally overgrown GaN on free-standing GaN was used to reduce the threading dislocations which were widely scattered over the entire surface. InGaN multi-quantum-well diode lasers grown on these low-dislocation-density GaN substrates exhibited an estimated lifetime of 15,000h under 30mW CW operation at 60°C. Other improved operation characteristics, such as a kink level of 100mW [4.13, 4.14], a low aspect ratio of 2.3 for the far field [4.14], and a low relative intensity noise (RIN) of –125dB/Hz [4.13, 4.14] have also been reported.

Blue InGaN/GaN diode lasers are now commercially available with wavelengths in the range of 380-450nm [4.9], however, few LDs with emission wavelengths longer than 420nm have been reported yet because the threshold current density increases dramatically with increase of emission wavelength from 390 to 450nm by increasing the In mole fraction of InGaN well layers. Thus, it has been difficult to achieve room temperature operation of blue LDs with an emission wavelength of 450nm. However, for practical application, LDs working at around 450nm are of great importance for laser full colour displays. Recent study shows InGaN single quantum well structure diode lasers working at 450nm were grown on an epitaxially laterally overgrown GaN substrate by a metalorganic chemical vapour deposition (MOCVD) method. The threshold current was reduced to 4.6kAcm^{-2}. The estimated lifetime was approximately 200h for room temperature CW operation at an output power of 5mW [4.15].

4.2 Characterisation of InGaN violet diode lasers

Our experimental study was based on a commercial InGaN violet diode laser, (Nichia, model number: NLHV 3000E), which has a CW output power more than 30mW and a fundamental lateral mode over the entire driving range of CW operation.

We measured steady-state power-current (P-I) curve and voltage-current (V-I) curve of this laser with temperature controlled at 25°C. The LD was driven by a precision current source (Newport model 505 laser diode drive, resolution: 0.1mA). Meanwhile, the operation voltage was measured by a multimeter. The output power of the LD was taken by a high aperture (ϕ = 9mm) optical power sensor (Anritsu, model number: MA9411A), placed closed to the laser output window. Fig. 4.1 shows the measured P-I and V-I curves of the LD.

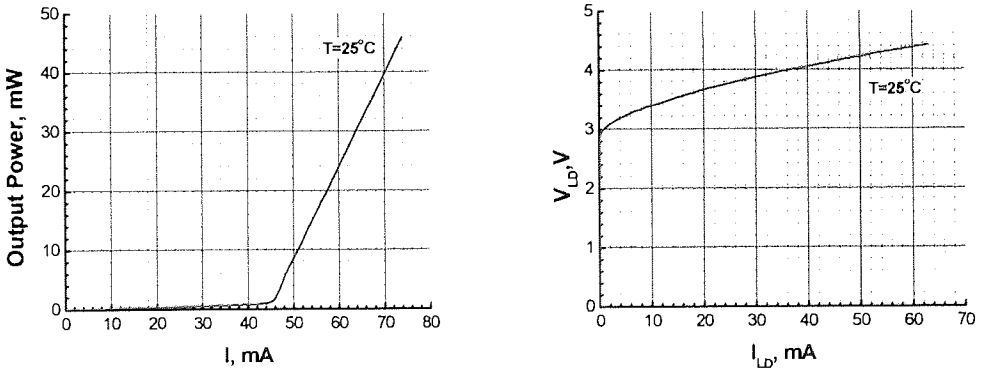

(a) (b)

Fig. 4.1 P-I curve (a) and V-I curve (b) of Nichia violet laser diode (NLHV3000E) for room temperature CW operation

From the above figures, the threshold current was estimated at 44.5mA, and slope efficiency at 1.6W/A. The differential resistance of the LD was estimated at 15.5Ω. For impedance match 50Ω system, we used two 68Ω surface mount resistors connected in parallel to form an identical 34Ω resistor. It was then connected closed to the LD in series, which resulted in a differential resistance of 50Ω approximately (Fig. 4.2).

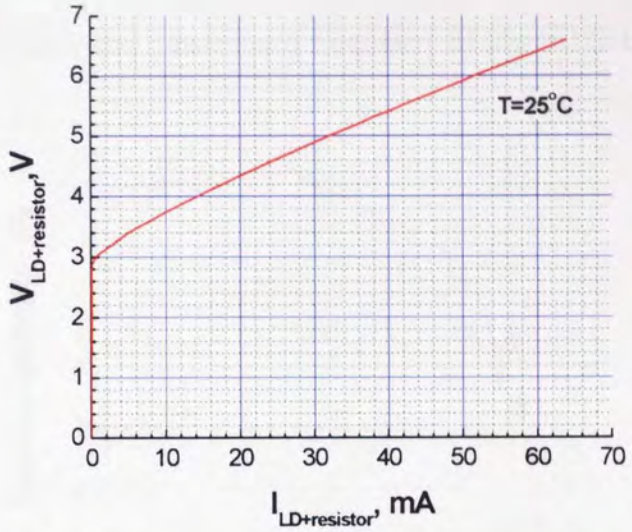

Fig. 4.2 V-I curve of the LD after impedance match

A broadband (350~1700nm) optical spectrum analyser (Ando 6310C) with resolution of 0.1nm was used for characterisation of the steady state spectrum of the laser. In Fig. 4.3, the laser output shows typical multimode spectrum at high driving levels. Red shift of peak lasing wavelength was observed at a high pumping level (I>50mA). FWHM spectral width lies in the range 0.3~0.6nm. Longitudinal mode spacing was estimated at 0.25nm, which corresponded to a laser cavity length of 130μm, assuming the effective refractive index is 2.5.

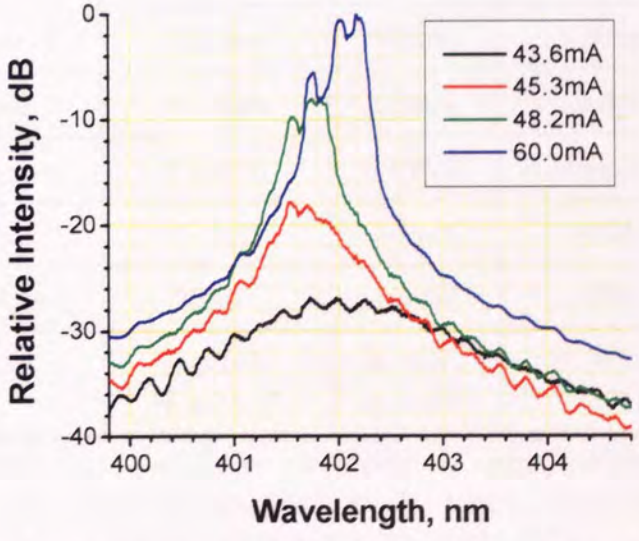

Fig.4.3 Steady state spectra of violet LD pumped at different driving currents

Fig. 4.4 shows small signal frequency response of the LD when it was DC biased well above threshold current. The laser had –3dB bandwidth of 200MHz, –10dB bandwidth of 700MHz, and a resonance frequency of about 1GHz at a DC bias level of 70mA.

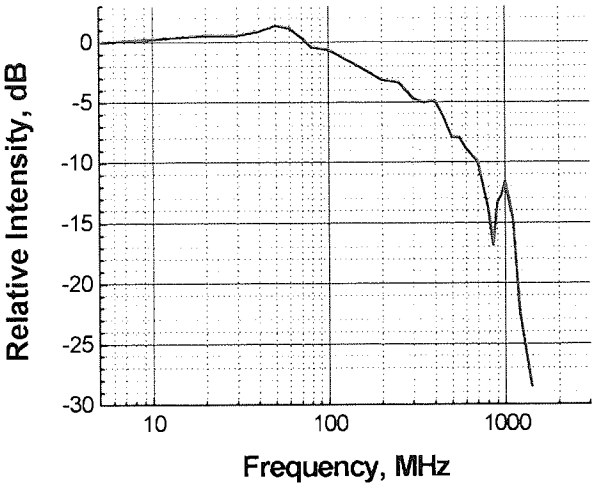

Fig. 4.4 Small signal frequency response of the diode Laser (DC bias: 70mA)

Table 4.1 gives a comparison of primary specifications of Nichia laser NLHV 3000E with three commercial high power diode lasers. It manifests the quality of Nichia laser is comparable with nowadays commercial LDs at long wavelength range. Particularly, Nichia laser has an outstandingly high quantum efficiency.

Model number (company)	NLHV 3000E (Nichia)	HL6321G (Hitachi)	SDL-6380-A (JDSU)	C-15-001-E-A (Laser 2000)
Material	InGaN	AlGaInP	InGaAs	InGaAsP
Peak wavelength, λ	402nm	635nm	980nm	1550nm
Threshold current, I_{th}	44.7mA	50mA	0.4A	12mA
Slope efficiency, η	1.6W/A	0.5W/A	0.9W/A	0.25W/A
Operation current, I_o	65.5mA	80mA	4.8A	20mA
Output power P_o at I_o	30mW	15mW	4W	5mW
FWHM beam divergence	$\theta_{//} = 6.5^\circ$, $\theta_{\perp} = 26.6^\circ$	$\theta_{//} = 8^\circ$, $\theta_{\perp} = 30^\circ$	$\theta_{//} = 12^\circ$, $\theta_{\perp} = 28^\circ$	$\theta_{//} = 20^\circ$, $\theta_{\perp} = 40^\circ$

Table 4.1 Comparison of room temperature specifications of Nichia laser NLHV3000E with three commercial diode lasers, Hitachi HL6321G, JDSU SDL-6380-A, and Laser2000 C-15-001-E-A, T=25°C

4.3 Generation of high power picosecond pulses from InGaN violet diode lasers

4.3.1 Introduction

As mentioned in Chapter 2, generation of high power picosecond pulse is of particular interest for a variety of applications. Ever since the advent of GaN based diode lasers, great efforts have been made to generate short wavelength (350~450nm) highly intensitive picosecond pulses from this type of lasers. Its applications cover high-resolution fluorescence spectroscopy, bio-chemical analysis, metrology etc.

Traditionally, ultrashort laser pulses in blue-violet wavelength regime were generated by frequency-doubling of ultrafast solid-state lasers working at near-infrared wavelength range [4.17-4.20], which requires extensive maintenance and considerable experience to run in daily work. In one research [4.21], 30ps long blue light pulses were generated by frequency-doubling of a gain-switched GaAlAs diode lasers with saturable absorber. However, a peak power of only 7.88mW was achieved due to the low nonlinear conversion rate. The occurrence of commercially available blue-violet diode lasers offers the possibility to build cheap, compact and highly efficient turn-key systems for generating blue-violet picosecond pulses. Indeed, compact picosecond blue/violet diode laser sources are now also commercially available [4.22-4.24], which cost only about one tenth of traditional blue/violet pulses sources, like argon ion lasers and frequency doubled Ti:Sapphire lasers, however, the spatial dimension of the devices was substantially reduced.

Since the first demonstration of picosecond pulse generated from a violet diode laser [4.25], pulse duration lies in the range 50-70ps and peak power is up to 500mW [4.25], [4.26]. Further improvement of pulse quality is of great practical importance. Indeed, recent progress in fabrication of GaN-based diode lasers, as mentioned in section 4.1, shows great possibility to increase output power from pulsed blue/violet diode lasers.

Here, we firstly introduced the dynamics of high power picosecond pulses generation by gain switching, followed by experimental investigation of generating picosecond violet pulse from our laser sample, mentioned in section 4.2, which demonstrated increase of peak power by one order of magnitude compared with previous reported results.

4.3.2 Dynamics of high power gain switching

The technique of gain switching based on directly driving the laser with large amplitude and short electrical pulses is the simplest way to generate picosecond optical pulses with the outstanding advantage of flexibly tuneable repetition frequency. It has been demonstrated in Chapter 2 that a lot of research work based on gain switching was concerned about compression of pulse duration, reduction of timing jitter and increase of repetition frequency. It has also been demonstrated that this technique has a close similarity with the conventional Q switching and is suitable for generating high power picosecond pulses [4.27].

The following theoretical analysis of high power gain switched process is based on the generally used rate equations (2.18). We define threshold carrier density n_{th}, peak inversion carrier density n_i, peak inversion ratio r, modified gain compression factor F, and energy extraction efficiency η as follows:

$$n_{th}=1/g_0\tau_p \tag{4.1}$$

$$r = n_i/n_{th} \tag{4.2}$$

$$F = \frac{\varepsilon}{g_0\tau_{ph}} \tag{4.3}$$

$$\eta = \frac{1}{F}\left[\left(\frac{1}{r}-1\right)(F-1)-1\right]\left[(1-\eta)^F-1\right] \tag{4.4}$$

Derived from equations 2.18, the analytical expressions for peak photon density N_{ph}, total number of photons E contained in the optical pulse, and optical pulse duration τ_ω of gain switched pulse can be given as follows [4.28]:

$$\frac{N_p}{n_i}=\frac{1}{F-1}\left(-1+\left[\frac{1}{r}+\left(\frac{N_p}{n_i}\right)F\right]+\frac{1}{F}\left[\left(\frac{1}{r}-1\right)(F-1)-1\right]\left\{\left[\frac{1}{r}+\left(\frac{N_p}{n_i}\right)F\right]^F-1\right\}\right) \quad (4.5)$$

$$E=\eta n_i \quad (4.6)$$

$$\tau_\omega=\tau_{ph}\eta\left(\frac{n_i}{N_{ph}}\right) \quad (4.7)$$

Equation (4.6), (4.8) convert into the standard Q-switching formula [27] in the limit of F=0, which take the forms:

$$N_{ph}=\frac{r-1-\ln r}{r}n_i \quad (4.8)$$

$$\tau_\omega=\frac{r\eta}{r-1-\ln r}\tau_{ph} \quad (4.9)$$

Numerical calculation [4.28] based on equations (4.5)-(4.7) gives some general conclusions for gain-switched operation: (1) A higher peak inversion ratio will lead to shorter pulse duration and higher pulse energy; (2) A smaller value of F will lead to shorter pulse duration and higher peak power; (3) A slower buildup of lasing photons will allow the carriers a longer time to build up to a higher inversion level.

Similar to Q-switching, the key issue for generating high-power, short pulses in gain switched devices is to increase peak inversion ratio, r. In Q-switched process, the limitation in the peak inversion can be overcome by introduction of a saturable absorber which serves to suppress the initial buildup of photons. Light will be emitter only when saturable absorber becomes transparent. At this moment, laser gain still maintains at initial level, i.e. there is no gain compression. As a result, a huge optical spike is formed. For gain-switched devices, theoretical analysis [4.28], [4.31]-[4.33] shows a large peak inversion can also be achieved provided the following conditions are satisfied: (1) The current pulse amplitude should exceed the threshold current by a factor of at least 10; (2) The time when peak injection current occurs should roughly be equal to or shorter than the turn-on delay time of the laser; (3) The current pulse should be switched off shortly after the first laser spike to prevent the excitation of residual relaxation oscillation tail.

Simulation in [4.28] also shows the peak inversion ratio, r, is a very weak function of pump current and does not exceed 2 even at a pumping level of $J/J_{th} = 20$. In fact, if the electrical pump pulse contains an amount of charge many times larger than that for threshold inversion, the increase of output power becomes more sensitive to the change of DC bias level rather than the amplitude of electrical pump pulse. For a fixed amplitude of electrical pump pulse, increase of DC bias works in two ways: firstly, it results in a higher spontaneous emission in the laser before the pump pulse was applied, thus, the initial photons in the laser will lead to gain compression; secondly, the amount of injection carriers need to reach threshold level is reduced, thus, a higher peak inversion ratio is achieved. The interaction of this two effects lead to an optimum level of DC bias corresponding to the maximum output power. This fact was justified in our experiment discussed below.

Above all, gain switching is an efficient way to generate high power picosecond laser pulses. The mechanism to achieve high power output pulse is different from Q-switched operation, which requires saturable absorber in the laser for the accumulation of upper level carriers before the onset of laser spike. This technique does not require special treatment of the laser and is suitable for a large variety of diode lasers. The achievable maximum output power and shortest pulse duration is largely dependent on the electrical pumping pulses and DC bias levels.

4.3.3 Experiment

A high-power avalanche pulse generator (Kentech APG-1) was used to drive the Nichia LD, mentioned in section 4.2, for gain-switched operation. The electrical pulse signal from the generator was shown in Fig.4.5. It has a pulse duration of 750ps, a rising time of 140ps and a failing time of 1.1ns. The peak voltage was estimated at 780V. The repetition frequency was 10kHz. DC bias was applied to the laser together with electrical pulses. The electrical pumping pulse was attenuated to the range 25~50V for LD pumping, which corresponded to a LD current in the range 0.5-1A.

Temperature was controlled at 25°C.

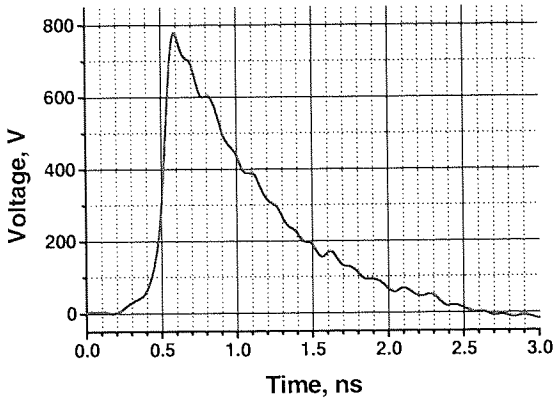

Fig.4.5 Electrical pulse signal for LD pumping

The generated optical pulse signals were coupled into a single mode fibre, which has a cut-off wavelength of 350nm and a core diameter of 2.2μm. The pulse signals were then launched into a Newfocus 1431 wide bandwidth (400-1650nm) photodetector with impulse response of 17ps for detection of pulse temporal profile on an Agilent 86100A 40G wide-bandwidth digital sampling oscilloscope. Two different techniques were used to calibrate peak output power of the laser pulses: (1) measure the output average power, the peak power was deduced according to the pulse shape; (2) calibrate the photodetector and system couple efficiency, the peak power was deduced according to the peak-to-peak voltage measured on the oscilloscope. Pulse spectra were measured by an Ando 6310C optical spectrum analyser with spectral width covering 350~1700nm.

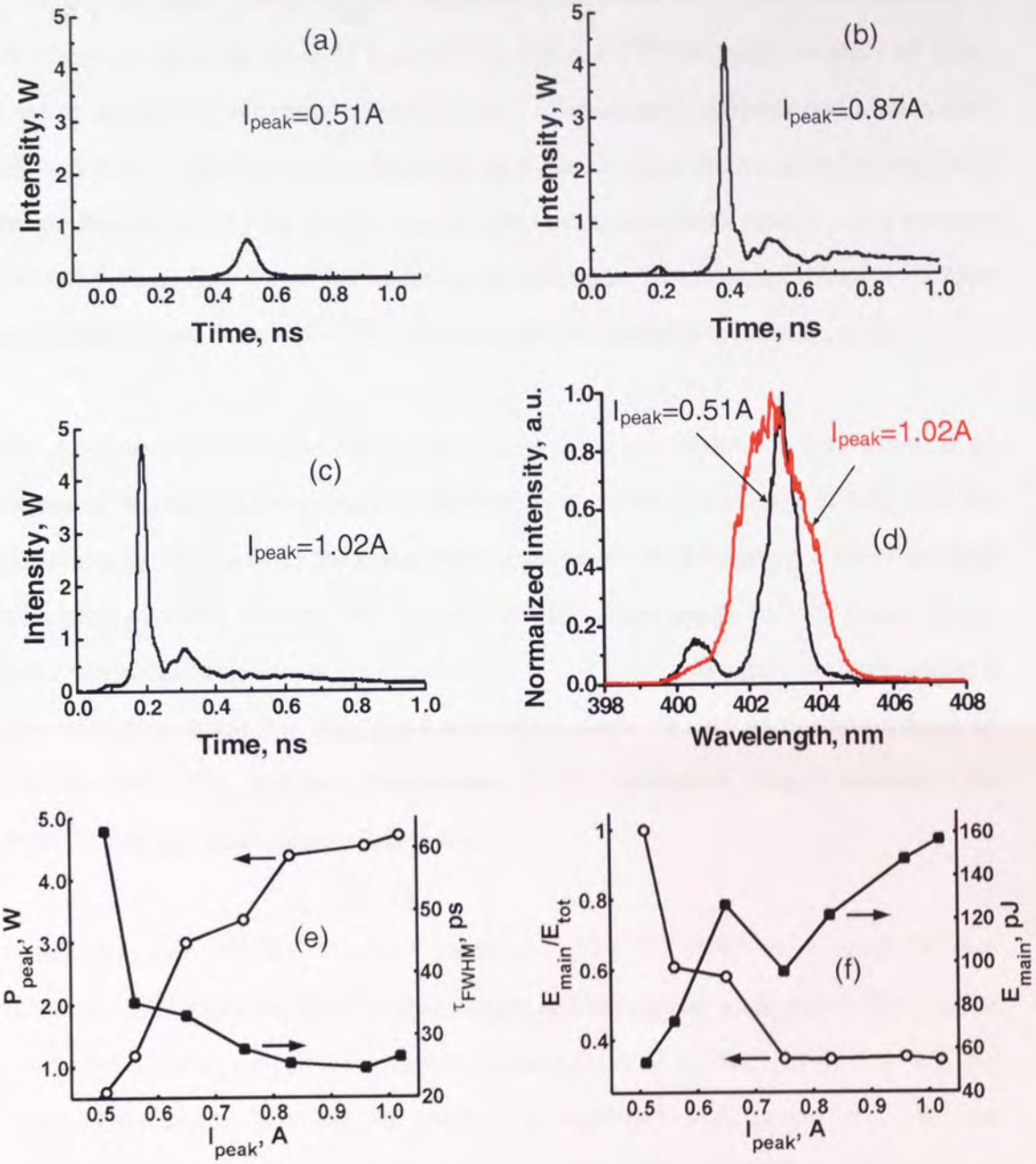

Fig. 4.6 Pulsed operation of Nichia violet diode laser without DC bias.
(a)-(c): Gain-switched pulses obtained at different levels of peak pumping current, I_{peak};
(d): Spectra of the pulses for high (red line) and low (black line) pumping levels;
(e): Dependence of peak output power and pulse duration on pumping level;
(f): Dependence of energy distribution in laser pulses on pumping level.

We firstly investigated pulsed operation of the laser without DC bias, shown in Fig. 4.6. Tail-free optical pulse with the maximum peak power of 730mW was achieved at an electrical pumping level of I_{peak}=0.51A. It has a FWHM pulse duration of 61ps. Further increase of pumping current induced a broadened spectrum and a relaxation tail followed by the main peak, however, its pulse duration decreased substantially to below 35ps at a pumping level of I_{peak}>0.55A. Increase of peak output power became saturated when I_{peak}>0.8A. An intensive optical pulse with a pulse duration of 25ps and a peak output power of 4.2W was achieved at a pumping level of I_{peak}=1A.

Fig. 4.6(f) shows total pulse energy and energy fraction contained in the main peak as functions of peak pumping current. Noticeably, at a high pump level of I>0.75A, the pulse energy contained in the main peak of the pulse shows almost a linear relation with peak pumping current, and the ratio of main peak energy to total pulse energy was maintained at an almost constant value of 0.34. (The pulse duration kept almost a constant value when I>0.75A (Fig.4.6e), which could be due to resolution limit of photodetector.) The peculiar phenomenon, as we considered, was in relation with possible self-organised quantum dots structure.

Pulsed operation with DC bias was presented in Fig. 4.7. Applying a small DC bias below the CW threshold level initially increased the optical peak power for a given peak current level, as can be seen from comparison of (a) and (b) in Fig. 4.7. By optimisation of the bias and the pump, the maximum peak power of 7.3W was achieved, corresponding to a pulse duration of 24ps and a FWHM spectral width of 4.2nm [Fig. 4.7(b)].

Two different calibration techniques of peak output power was employed for more accurate measurement: 1) to measure the output average power, the peak power was deduced according to the pulse shape and pulse repetition frequency; 2) to calibrate the photodetector and system couple efficiency, the peak power was deduced according to the peak-to-peak voltage measured on the oscilloscope. A measurement

mismatch of <10% was obtained through the two approaches.

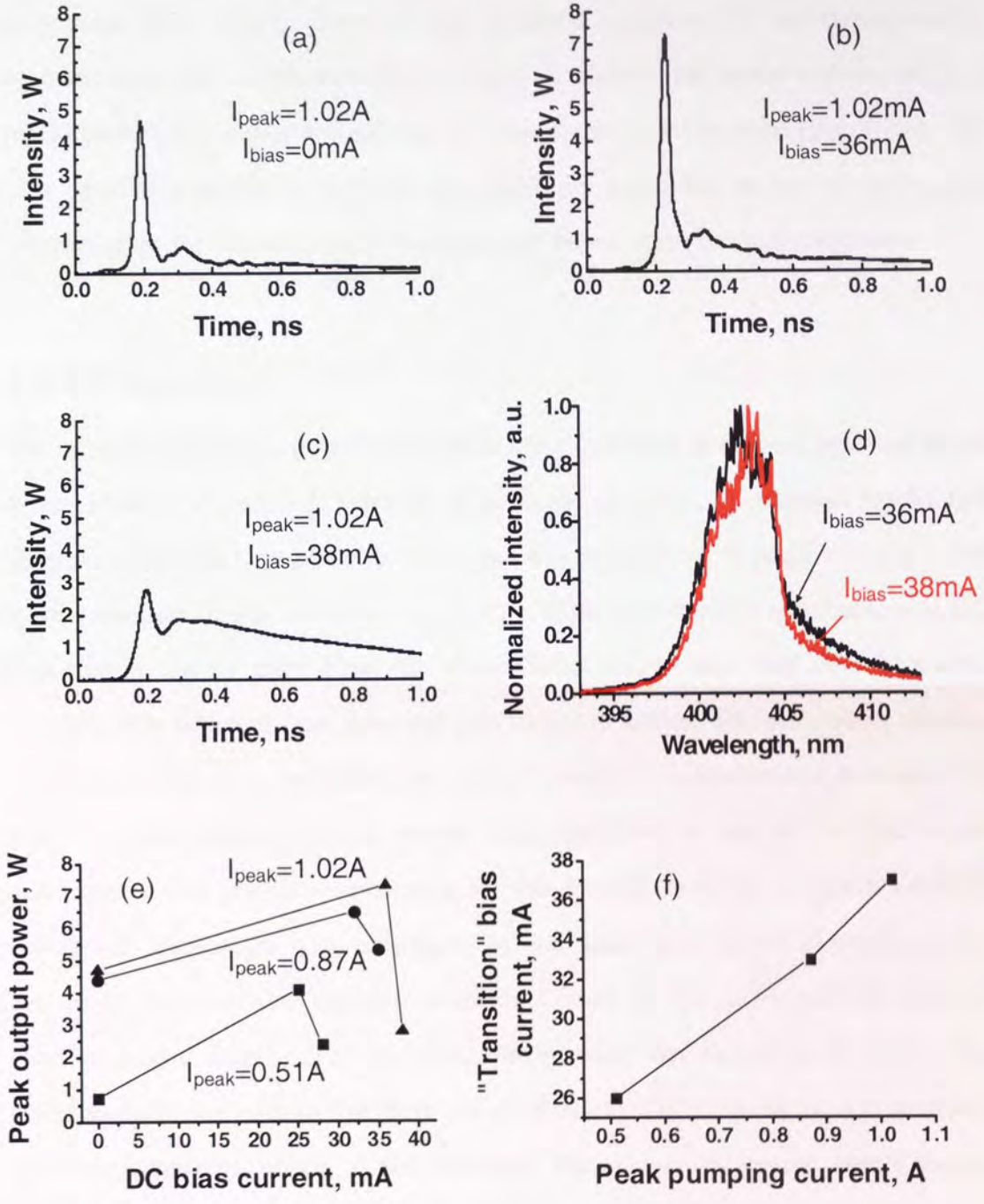

Fig. 4.7 Pulsed operation of Nichia violet diode laser with DC bias.
(a)-(c): Gain-switched pulses obtained at different levels of DC bias current, I_{bias}, where peak pumping current was maintained at I_{peak}=1.02A. Substantial change of pulse profile occurred when I_{bias} increased slightly from (b) 36mA to (c) 38mA
(d): Spectra corresponded to the pulses (b)-red line and (c)-black line;
(e): Dependence of peak output power on DC bias current at different levels of peak pumping current.
(f): The "transition" DC bias current as a function of peak pumping current.

Peculiar dynamics of the laser output was observed at a certain bias level, where a minor increase of bias from 36mA to 38mA produced a dramatic change of the pulseshape [Fig. 4.7(c)]. However, this temporal transition did not correspond to substantial change in spectrum [Fig. 4.7(d)]. A higher peak pump current led to a higher peak output power and a higher DC bias at the transition point [Fig. 4.7(e), (f)]. This peculiarity indirectly indicates the possibility that a self-switching mechanism contributed to the achievement of the high peak power at the optimal conditions.

4.3.4 Discussion

The unusual high output power achieved in our experiment is of great practical value. It may result in a number of potential applications. However, the physical mechanism for generating such high power optical pulse was still unclear. It could attribute to the special electrical pump condition: $I_{peak}/I_{th}>20$, $dI/dt>6$mA/ps, and optimisation of DC bias current. On the other hand, the experimental results show this laser behaviour was evidently different from a typical gain switched device. The differences include, low-energy relaxation oscillation tail, abrupt change of pulseshape at a certain DC bias level, and probably, a long turn-on delay (although it was not justified in our experiment). One possible explanation for this peculiarity is that a certain saturable absorption mechanism was introduced in our laser and led to Q-switched like behaviour. The saturable absorber could be formed by the self-organised quantum dots, as it was observed in InAs/InGaAs quantum dot lasers [4.34, 4.35]. The discrepancy in our laser is that there are no specially treated sections, e.g. reversely DC biased sections, acting as the absorber. This theory, of course, needs further verification.

4.4 Spectral control of InGaN diode lasers

4.4.1 Introduction

Under both CW and pulsed modes, spectral quality of output signals from Fabry-Pérot diode laser always deteriorates at high pumping levels. In the above mentioned experiment, the violet laser had multimode spectra with poor side-mode suppression for CW operation, and widely broadened spectra for high power pulsed operation. It will be highly advantageous to achieve narrow linewidth and wavelength tuneable violet laser signals with output power maintained at high level. Such kind of spectrally controlled high power violet diode laser sources are highly desirable for a large variety of applications, such as time-resolved fluorescence spectroscopy, semiconductor luminescence spectroscopy, etc.

Experimental investigations of steady state spectral control of GaN-based diode lasers have been demonstrated [4.36-4.38], typically in a Littrow external cavity configuration [4.36, 4.37]. One study [4.34] shows single frequency wavelength tuneable operation of a GaN laser in an external cavity. The laser was tuned discontinuously at a range of 2.7nm, centred at 393nm. A narrow linewidth of less than 5MHz was also achieved. The discontinuity of wavelength tuning was thought to be due to *In* compositional fluctuation within the InGaN quantum wells. Optimised results were achieved by D. J. Lonsdale et al [4.35]. An enhanced tuning range of 6.3nm was achieved, which was due to the high-quality anti-reflection coating on the laser. The linewidth achieved was less than 11MHz.

Spectral control of pulsed violet diode lasers was also reported. In actively mode-locked scheme of an InGaN laser [4.37], 30ps-long pulses with spectral width of 0.023nm were achieved. The duration-bandwidth product was as low as 1.2. However, the laser output power was as low as 2mW due to the imperfect anti-reflection coating of the laser sample, which caused residual reflection at the laser output facet. Like any other actively mode-locked lasers, the system required

precise control of the cavity length, and its performance was very sensitive to environmental change. Therefore, in consideration of high output power, simplicity and system stability, gain-switched or Q-switched violet diode lasers with spectral control would be advantageous. Until now, as far as we know, there are no reports on this kind of pulsed laser sources.

In this section, we present experiment study of spectrally controlled InGaN violet diode laser both under steady state and gain switched state, using a technique named injection locking, previously demonstrated in near-infrared wavelength regime.

4.4.2 Injection locking of steady state InGaN lasers

4.4.2.1. Introduction

Injection locking is a commonly used technique for steady state spectral control of diode lasers. Actually, this technique applies universally to virtually any kind of oscillators, whether laser, electronic, mechanical, or whatever. It is realised by using a weak and high-quality laser signal to control the spectrum, phase and spatial characteristics of a strong and poor-quality laser output.

We suppose the steady state laser is initially oscillating at an oscillation frequency of ω_0 and producing a coherent output intensity I_0 at that frequency. A very weak external signal with a low power of I_1 is injected into this laser at a frequency ω_1, which is close to but not exactly coincident with the oscillation frequency ω_0 of the laser. If this signal at ω_1 is weak enough, it can circulate around inside the cavity, and be regeneratively amplified by the laser medium, even in the presence of the much stronger oscillation already present at ω_0.

The power amplification for the weak signal at $\omega \neq \omega_0$, under oscillating conditions at ω_0, is approximately given by [4.27],

$$|\tilde{g}(\omega)|^2 \approx \frac{\gamma_e^2}{(\omega-\omega_0)^2} \tag{4.10}$$

where γ_e is the energy decay rate, and can be given by,

$$\gamma_e \approx \frac{1-R}{T} \tag{4.11}$$

where R is output mirror reflectivity, T is laser cavity round trip time.

When injected signal at ω_I, is approaching oscillation frequency of the laser, ω_0, there exist a point, where the amplified signal $|\tilde{g}(\omega_1)|^2 I_1$ begins to steal enough gain from the laser medium by just enough, so that the oscillation frequency ω_0 is turned off, leaving only the injected signal at ω_I. If signal ω_I is even closer to ω_0, the original oscillation frequency of the laser at ω_0 will be completely captured or "injection-locked" by the injected signal at frequency ω_I. This effect begins when the amplified signal just take over the original signal, given by,

$$|\tilde{g}(\omega_1)|^2 I_1 = \frac{\gamma_e^2}{(\omega_1-\omega_0)^2} I_1 \approx I_0 \tag{4.12}$$

Therefore, the locking range of the laser is given by,

$$\Delta\omega_{lock} = 2(\omega_1-\omega_0) \approx 2\gamma_e \sqrt{\frac{I_1}{I_0}} \tag{4.13}$$

From the above equations, we can easily find that the higher the power of the signal is injected, the wider wavelength tuning range will be achieved. On the other hand, the spectral quality of output signal can be improved by high quality of injected signal. In fact, at high power injection level and at the edges of locking range, some more subtle nonlinear effects will occur and more complex analysis is required.

4.4.2.2 Experiment

Experiment of steady state injection seeding of InGaN diode laser was based on the commercial Nichia laser used for high power gain-switched operation, as shown in section 4.3. The experiment setup was based on Littrow configuration (Fig.4.8), employing a self-injection-seeding scheme. The laser was driven by a precision

current supply with a resolution of 0.1A. It was mounted on a heat sink with temperature controlled at 25°C.

Two gratings, one with a resolution of 830 grooves/mm and a diffraction efficiency of 30% (#1) and the other with a resolution of 1100 grooves/mm and a diffraction efficiency of 60% (#2) were used respectively. A microscope objective (NA=0.54, f=8mm) was used to collimate the output light for the LD. The first order diffraction beam of the grating overlapped with the incident laser beam and was injected into the laser as feedback signal. The output was taken from a 50/50 beam splitter placed in the external cavity rather than from the zero-order of grating diffraction beam. This advantage of this is that output beam would be exempt from angular displacement when we adjusted the grating position for wavelength tuning. However, a reduction of feedback signal power by a factor of 4 due to the inset beam splitter was a drawback of this configuration. Improvement of experiment configuration will be discussed in section 4.6.

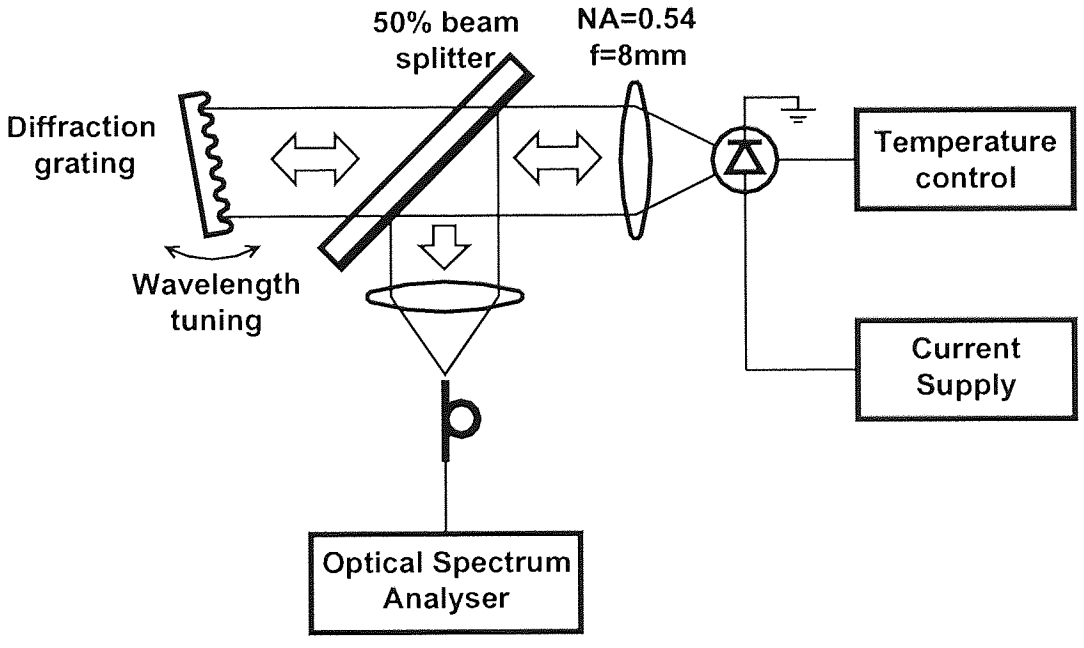

Fig. 4.8 Littrow configuration for steady state self-seeding operation of InGaN laser

Fig. 4.9 shows the effect of injection seeding under different DC pump levels when grating #1 was used. Under a well-aligned system, lasing threshold dropped from

44.5mA to 43.5mA. Single frequency operation with a maximum side band suppression ratio of 10dB was observed at a driving level of I=45.3mA [Fig. 4.9(b)]. At even higher DC pumping levels, laser spectrum became less sensitive to the injected signal [Fig. 4.9(c), (d)]. Single frequency wavelength tuning was hard to be achieved with this grating.

Better injection seeding performance was achieved using a grating #2 (Fig. 4.10). Lasing threshold became even lower at 41.2mA. Single frequency operation with side band suppression ratio above 20dB has been achieved at a driving level of 45-60mA. Wavelength tuning with the maximum range of 3.4nm (from 400.6nm to 404.0nm) was also achieved at a level of 45mA [Fig. 4.10(e)]. Side mode suppression ratio as a function of peak wavelength of single frequency spectra was plotted at different DC pumping levels [Fig. 4.10(f)].

From the experiment data, we may find that improved steady state injection seeding operation of InGaN diode laser can by achieved by using monochromatic feedback signal with increased power, which is in accordance with near-infrared diode lasers. On the other hand, the fundamental lateral mode of our laser also contributed to a continuous and stable wavelength tuning. As a result, the wavelength tuning range we have achieved is about 1.5 times wider than the early reported [4.36]. The performance of injection locking might be further improved if anti-reflection coating was applied on the laser.

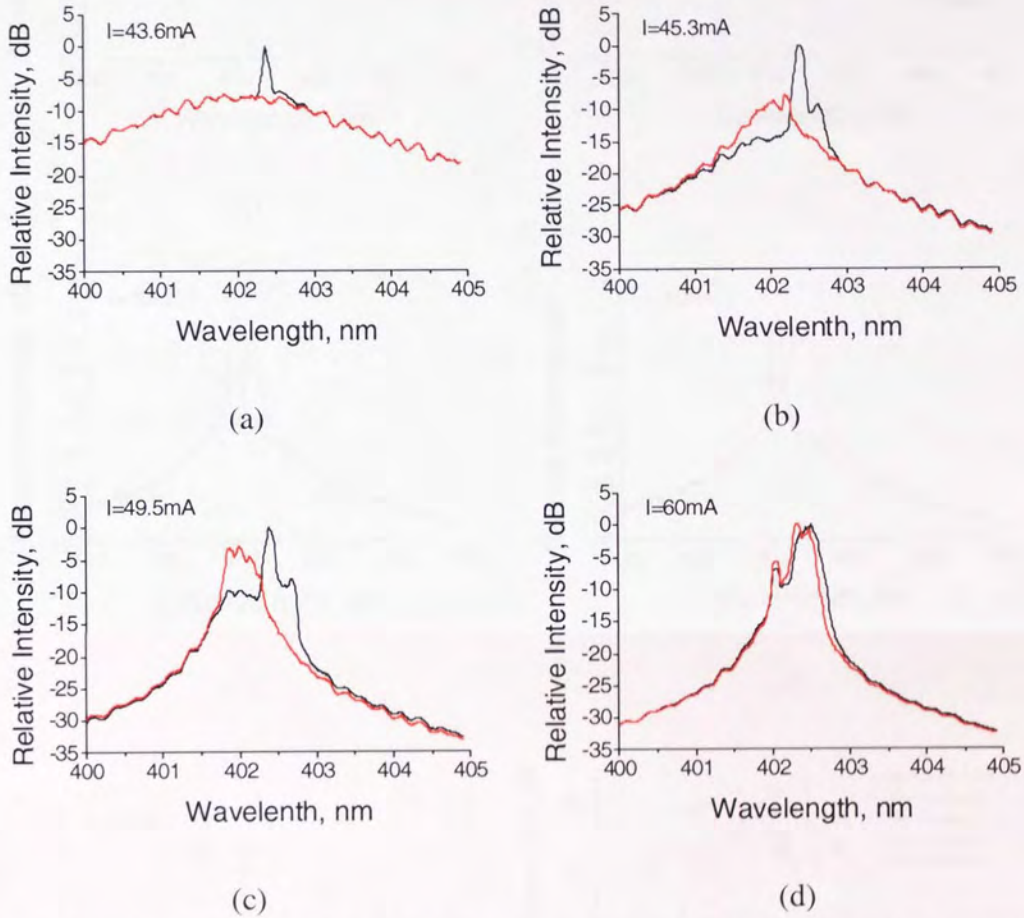

Fig. 4.9 Steady state injection locked spectra of Nichia violet laser using grating #1 (black line) and free running spectra (red line) at current injection levels of (a) 43.6mA, (b) 45.3mA, (c) 49.5mA, and (d) 60.0mA.

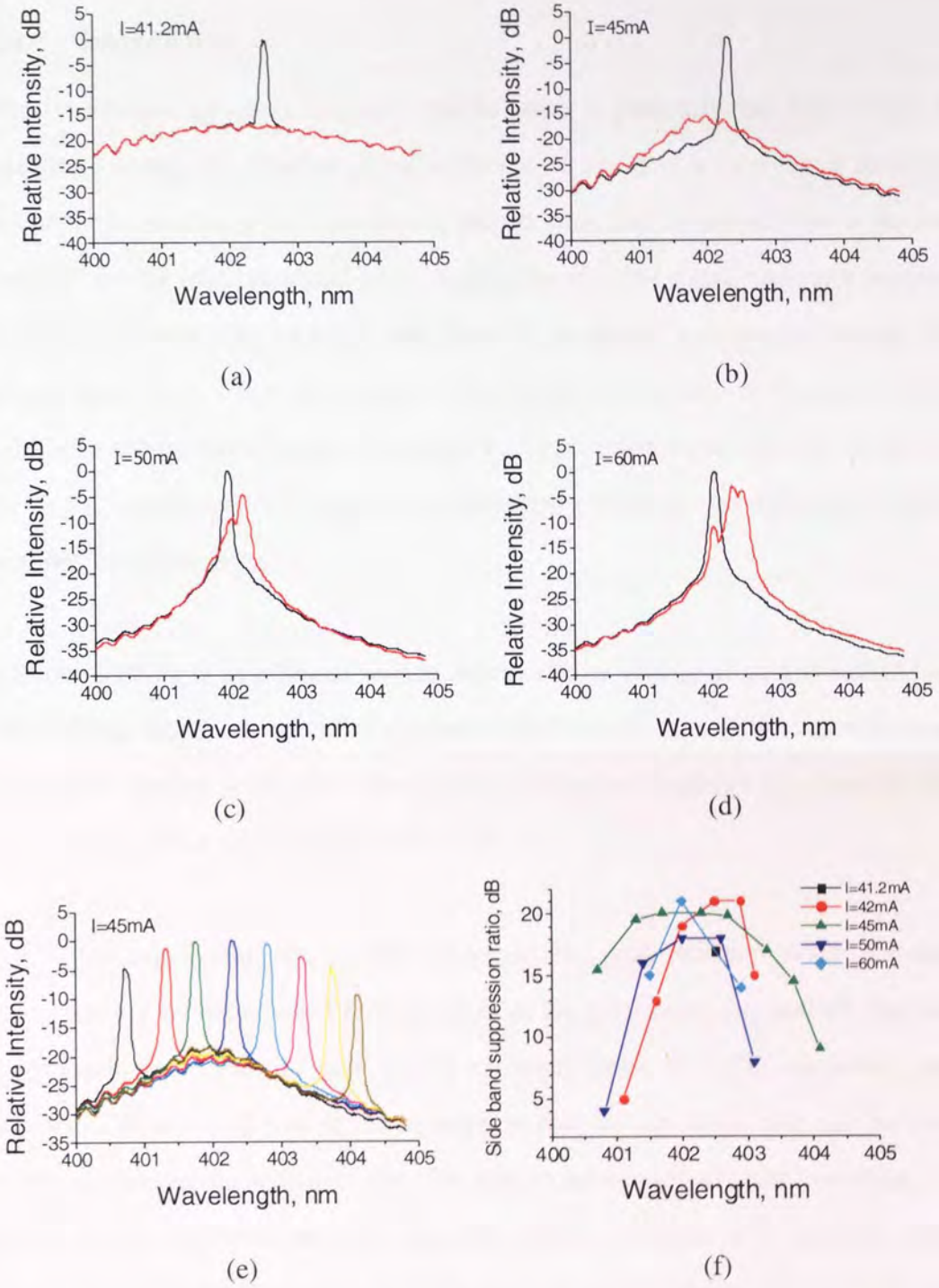

Fig. 4.10 Steady state injection locked spectra of Nichia violet laser using a grating #2 (black line) and free running spectra (red line) at current injection levels of (a) 41.2mA, (b) 45mA, (c) 50mA, and (d) 60mA; (e) single frequency wavelength tuning at DC pumping level of 45mA; (f) side band suppression ratio as a function of peak wavelength for single frequency wavelength tuning at different current injection levels.

4.4.3 Injection locking/seeding of pulsed InGaN lasers

4.4.3.1 Introduction

The dynamics of injection locking of pulsed lasers is quite different from steady state injection locking. The injected signal in the pulsed situation is so weak or so far from resonance in relation to the free running pulsed laser that the pulsed laser is not really "locked" by the injected signal at all. Rather the injected signal can more accurately be viewed as providing an initial condition on the spatial and spectral modes of the pulsed laser, from which these modes then grow and develop in the usual fashion, with little continuing influence or control by the injected signal beyond its setting of the initial conditions. We might more accurately refer to this effect as "injection seeding" of pulsed laser.

Injection locking is an efficient way to improve pulse quality of gain switched lasers. The seeding signal can be either a separate continuous-wave (CW) tuneable source, called CW seeding [4.40-4.44], or wavelength-selective feedback of a fraction of the output pulse, called self seeding [4.45-4.52].

In CW seeding regime, the generated poor quality gain switched pulses are seeded independently by the injected CW signal from the very beginning and all time along the pulse build-up process. The quality of output pulse is highly dependent on the external CW signal. It has the advantages in that the repetition rate can be chosen within a wide range, which is also the distinct advantage of gain switching. L. P. Barry et al. demonstrated, by injecting strong external CW seeding into a gain-switched laser with a repetition frequency exceeding 20 GHz [4.40, 4.43], which is far beyond the laser inherent bandwidth of 8GHz. The pulse has a duration of 12ps. Other interesting features, such as a wide wavelength tuning range up to 40nm [4.41], a reduction of pulse-to-pulse timing jitter to 160fs [4.42], and an increase of side band suppression ratio to 25dB [4.44] have also been demonstrated in CW seeded gain switched lasers.

In self-seeded gain-switched lasers, a small amount of quasi-monochromatic signal from the multimode output pulse is fed back into the gain-switched laser during the early stage of the build-up of optical pulses. A requirement for this process is that the pulse modulation frequency is close to but slightly lower than a multiple of the laser cavity round-trip frequency. The advantage of self seeding is that no additional light source is needed for spectral control and wavelength tuning, thus exhibiting better stability than CW seeding. Recent progress shows robust single mode and fast wavelength tuning operation of self-seeded diode lasers has been achieved by using advanced auxiliary devices, typically, linearly chirped fibre Bragg grating [4.45], Moiré grating [4.46], high-birefringence fiber loop mirror [4.47], and Fabry-Perot semiconductor filter [4.48]. Another advantage of self-seeding is fast wavelength switching behaviour. One study [4.49] shows the number of round-trips necessary to reach the single mode steady state after switch-on is in the range of 5-10, which is 1-2 orders of magnitude shorter than mode-locked lasers.

A large number of experiments about injection seeding were demonstrated on long wavelength diode lasers (>1.3μm) with the aim to develop high quality pulsed laser sources for applications on optical communication system. Very few studies are demonstrated on injection seeded pulsed diode lasers in short wavelength regime (<600nm), especially, in the "blue" or "violet" range. Here, we present, for the first time, an experiment investigation of external-cavity self-seeded gain-switched operation in violet wavelength range using an InGaN laser.

4.4.3.2 Experiment

The laser used in the experiment was the same sample mentioned in section 4.2, a NLHV3000E single mode device from Nichia Corporation. It produced a fundamental lateral mode across the whole range of operating current and was found to have a threshold current of 44.5mA, a CW output power of >30mW, and a resonance response frequency of 1.2GHz. The laser was driven by an amplified radio frequency (RF) signal imposed on a direct current (DC) bias. Temperature of the laser was

maintained at a level of 25°C.

The external cavity had Littrow geometry, as shown in Fig. 4.11. An aspheric lens with a numerical aperture of 0.5 was used to collimate the output diode laser beam, producing an elliptical beam with size of 9mm by 1mm, approximately. A diffraction grating with a resolution of 1200grooves/mm, a blazing wavelength of 393nm, and diffraction efficiency of 80% to the first order was placed at a distance of 240mm from the laser, so that the second harmonic of the external cavity round-trip frequency was close to the laser resonance frequency. Similar to our experiment for steady state injection locking of InGaN laser, the output was taken from a 50/50 beam splitter, which avoided angular displacement of the output beam when we tuned the grating.

Polarization of the laser output was perpendicular to the elliptical laser spot. Hence, in our experiment setup, the grating was oriented so that the grating grooves were parallel to the laser's polarisation and perpendicular to the long axis of the laser's elliptical spot, refer to as "s" geometry, shown in Fig. 4.12. In such a configuration, the feedback laser beam dispersed across the laser's junction plane, and a very small amount of feedback signal with narrow bandwidth was injected into the laser as the seeding signal. This assured a good spectral quality and wide wavelength tuning range of the output signals, as the effectiveness of injection seeding for gain-switched operation is largely determined by the "quality" rather than the "quantity" of the seeding signals.

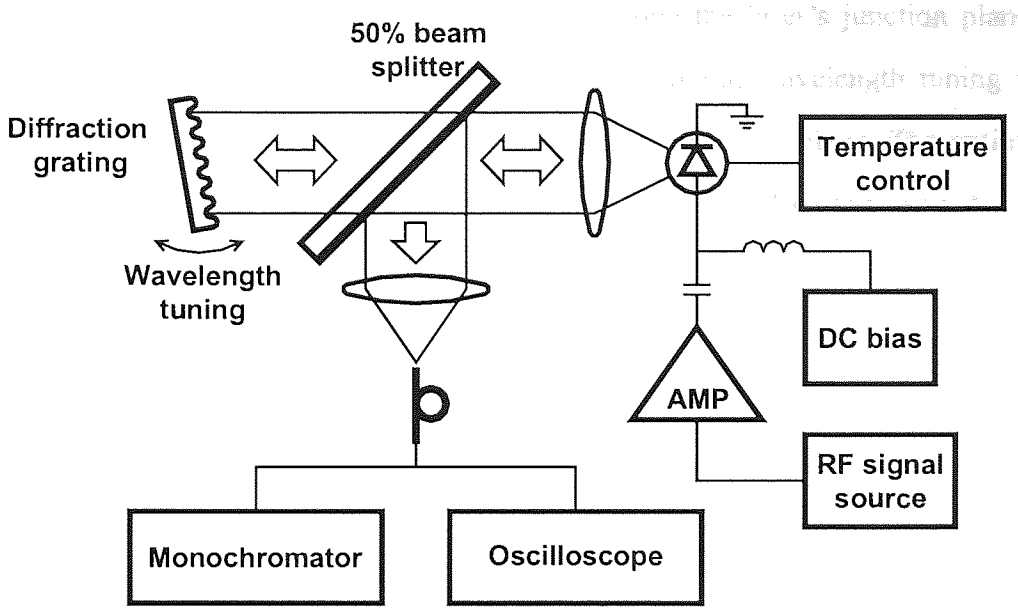

Fig. 4.11 Experimental set-up for self-seeded gain-switched operation of InGaN laser

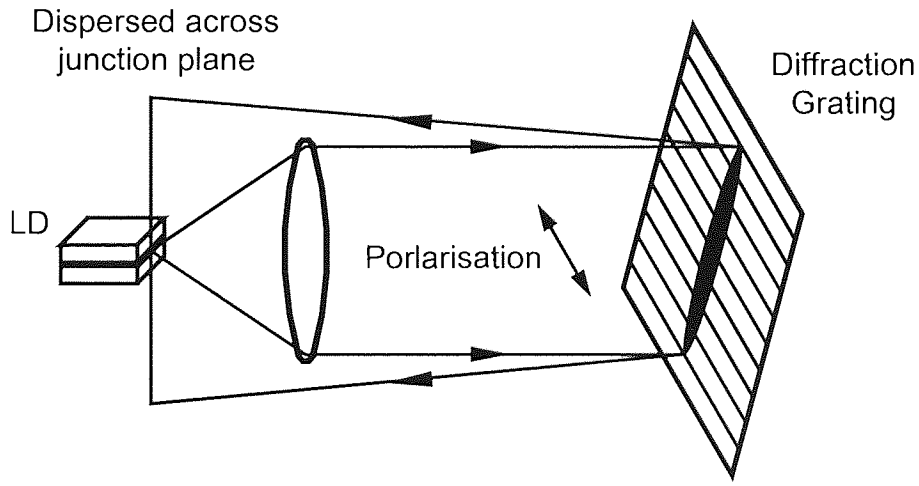

Fig. 4.12 Illustration of "s" geometry used in the self-seeding Littrow configuration

Without external cavity, the laser produced the shortest pulse duration of 49ps and the highest peak power of 460mW when driven by the maximum power of RF signal, approximately 1W. The driving frequency was 1.13 GHz, close to the laser resonance frequency of 1.0GHz. The DC bias was 80mA.

With the adjustment of external cavity feedback along the laser's junction plane, a very strong self-seeding point was obtained. At this point, wavelength tuning was achieved by adjusting the grating feedback across the junction plane. The optimum self-seeded gain-switched operation was shown in Fig. 4.13. The output pulse duration broadened to 60ps and the peak power reduced to 360mW, whilst the average power slightly increased from 45mW to 47mW [Fig. 4.13(a)]. The pulse spectrum changed dramatically from a broad, 1.5nm wide band to a line as narrow as 0.14nm, with the sideband suppression in excess of 20dB [Fig. 4.13(b)].

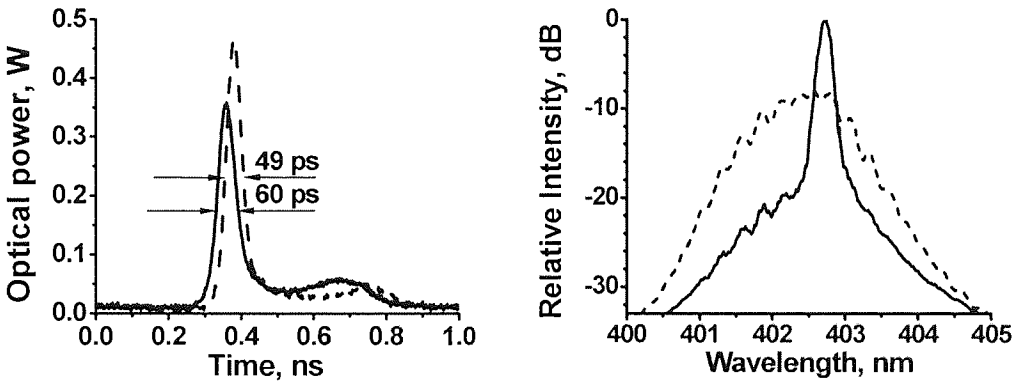

Fig. 4.13 (a) Oscilloscope traces and (b) spectra of the laser output without (dashed line) and with (solid line) self-seeding in a strong self-seeding region

At this strong self-seeding point, it was possible to continuously tune the laser wavelength within a 3.6nm range, from 401.1nm to 404.7nm and the linewidth was kept below 0.2nm, as shown in Fig. 4.14. At the edges of the tuning range, a broad, low intensity side band appeared at the centre of the laser's gain curve.

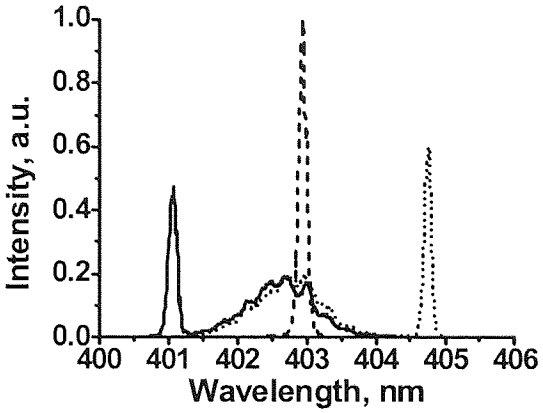

Fig. 4.14 Single frequency wavelength tuning of the laser pulses at a strong self-seeding point

By scanning the reflected beam along the laser's junction plane, we found another relatively weak self-seeding point. (i.e. spectral quality was relatively poorer and wavelength tuning range was relatively narrower.) At this point, we obtained single frequency output with maximum side band suppression ratio of 20dB, where the peak power of the output pulses dropped from 460mW to 380mW, and pulse duration broadened from 49ps to 54ps, shown in Fig. 4.15. Continuous single frequency wavelength tuning was achieved at a range of 3nm (400.9-403.9nm), shown in Fig. 4.16. The existence of two self-seeding points was probably due to multimode near field pattern of the laser, although it had a fundamental far field mode. Further investigation is required to justify this fact.

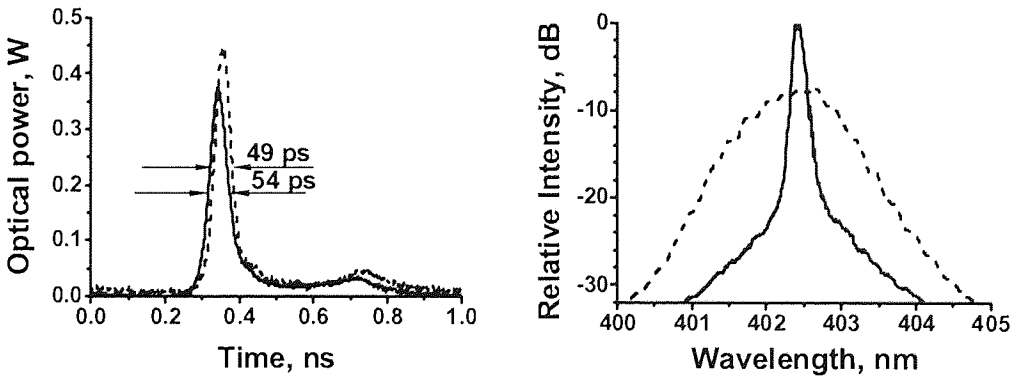

(a) (b)

Fig. 4.15 (a) Oscilloscope traces and (b) spectra of the laser output without (dashed line) and with (solid line) self-seeding in the second self-seeding point

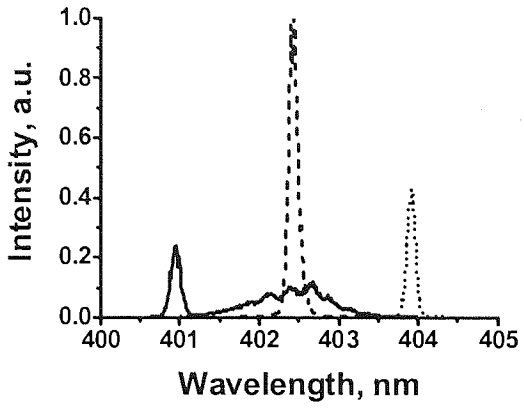

Fig. 4.16 Wavelength tuning of single frequency laser pulses in the second self-seeding point

4.4.3.3 Discussion

In previous studies of self-seeded gain-switched near-IR lasers, the time-windows, during which the feedback has to arrive back at the laser has a width of about 20ps [4.50, 4.51]. This leads to such an excellent stability that operation up to 3100th harmonic of the feedback loop has been demonstrated [4.52]. It is the most distinct advantage over mode locked lasers. Noticeably, our self-seeding system for gain-switched InGaN laser showed an even better stability. We varied the external cavity length between 235mm and 250mm, corresponding to a maximum of 50ps time offset between the feedback signal and the initial laser signal. This variation did not induce any noticeable changes in the temporal and spectral profiles of the laser output.

4.5 Conclusion

In conclusion, we demonstrated experimental research of a commercial InGaN multiquantum well diode laser. In order to generate high power, high quality picosecond pulse from InGaN laser with efficient and low-cost methods, gain switching was the mainly used technique. We have achieved highly intensive gain switched pulses and spectrally controlled gain switched pulses using the same laser

sample.

In the high power gain switched scheme, we used a high power avalanche pulse generator to pump the laser. With optimised pumping condition, a highly intensive (7.3W) violet laser pulse with a FWHM duration of 24ps was achieved, which corresponds to one order of magnitude increase of peak power than ever reported before. Peak power of the followed relaxation oscillation tail was only 1/5 of the main pulse's peak power. Moreover, an unusual self-switching phenomenon was observed at a certain DC bias level, as is thought to the mechanism contributing to the high peak power output. Further investigation of laser material and structure are required to clarify this mechanism.

Our studies also show spectrum of this commercial laser can be controlled under both CW and gain switched regime with a simple Littrow configuration. Single frequency continuous wavelength tuning operation was achieved at a range of 3.4nm and 3.6nm respectively. Noticeably, very stable wavelength tuneable operation was observed, which is a distinct advantage over mode locked InGaN laser and is of large practical importance. In gain switched regime, the pulse train has a repetition frequency of 1.13GHz and peak power of 400mW, which has overtaken the performance of nowadays commercial pulsed "blue" or "violet" diode laser sources.

References

[4.1] S. Strite and H. Morkoc, "GaN, AlN and InN: A review", *Journal of Vacuum Science and Technology.*, **B10**, 1237-1266, 1992

[4.2] H. Amano, M. Kito, K. Hiramatsu, and I. Akasaki, "p-type conduction in Ma-doped GaN treated with low-energy electron beam irradiation (LEEBI)", *Japanese Journal of Applied Physics*, **28**, L2112-L2114, 1989

[4.3] S. Nakamura, N. Iwasa, M. Senoh, and T. Mukai, "Hole compensation mechanism of p-type GaN films", *Japanese Journal of Applied Physics*, **31**, 1258-1266, 1992

[4.4] S. Nakamura and T. Mukai, "High-quality InGaN films grown on GaN films", *Japanese Journal of Applied Physics*, **31**, L1457-L1459, 1992

[4.5] M. A. Khan, J. N. Kuznia, A. R. Bhattarai, and D. T. Olson, "Metal semiconductor field effect transistor based on signal crystal GaN", *Applied Physics Letters*, **62**, 1786-1788, 1993

[4.6] S. Chichibu. T. Azuhata, T. Sota, and S. Nakamura, "Spontaneous emission of localized excitons in InGaN single quantum well structures", *Applied Physics Letters*, **69**, 4188-4190, 1996

[4.7] Y. Narukawa, Y. Kawakami, S. Fujita, S. Fujita, and S. Nakamura, "Reconbination dynamics of localized excitons in $In_{0.20}Ga_{0.80}N$-$In_{0.05}Ga_{0.95}N$ multiple quantum wells", *Physics Review*, **B55**, 1938R-1941R, 1997

[4.8] Y. Narukawa, Y. Kawakami, M. Funato, Sz. Fujita, Sg. Fujita, and S. Nakamura, "Role of self-formed InGaN quantum dots for the exciton localization in the purple laser diodes emitting at 420nm", *Applied Physics Letters*, **70**, 981-983, 1997

[4.9] http://www.nichia.com/

[4.10] S. Nakamura, M. Senoh, S. Nagahama, N. Iwasa, T. Yamada, T. Matsushita, H. Kiyoku, Y. Sugimoto, T. Kozaki, H. Umemoto, M. Sano and K. Chocho, *Japanese Journal of Applied Physics*, **37**, L1020, 1998

[4.11] S. Nakamura, M. Senoh, S. Nagahama, N. Iwasa, T. Yamada, T. Matsushita, H. Kiyohu, H. Umemoto, M. Sano and K. Chocho, *Japanese Journal of Applied Physics*, **37**, L627, 1998

[4.12] S. Nakamura, N. Iwasa, M. Senoh, T. Matsushita, Y. Sugimoto, H. Kiyohu, T. Kozaki, M. Sano, H. Matsumura, H. Umemoto, K. Chocho and T. Mukai, "High-power and long-lifetime InGaN multi-quantum-well laser diodes grown on low-dislocation-density GaN substrates", *Japanese Journal of Applied Physics*, **39**, L647-L650, 2000

[4.13] T. Tojyo, S. Uchida, T. Mizuno, T. Asano, M. Takeya, T. Hino, S. Kijima, S. Goto, Y. Yabuki and M. Ikeda, "High-power AlGaInN laser diodes with high kink level and low relative intensity noise", *Japanese Journal of Applied Physics*, **41**, 1829-1833, 2002

[4.14] T. Asano, T. Tojyo, T. Mizuno, M. Takeya, S. Ikeda, K. Shibuya, T. Hino, S. Uchida, and M. Ikeda, "100-mW kink-free blue-violet laser diodes with low aspect ratio", *IEEE Journal of Quantum Electronics*, **39**, 135-140, 2003

[4.15] S. Nakamura, M. Senoh, S. Nagahama, N. Iwasa, T. Matsushita and T. Mukai, *Applied Physics Letters*,**76**, 22, 2000

[4.16] S. Nakamura, S. Pearton and G Fasol, *The Blue Laser Diode, The Complete Story*, 2nd edition, Springer, Berlin, 2000

[4.17] W. Risk, R. Pon and W. Lenth, "Diode laser pumped blue-light source at 473nm using intracavity frequency doubling of a 946nm Nd: YAG laser", *Applied Physics Letters*, **54**, 1625-1627, 1989

[4.18] E. Lim, M. Fejer, R. Byer, and W. Kozlovsky, "Blue light generation by frequency doubling in periodically poled lithium niobate channel waveguide", *Electronics Letters*, **25**, 731-732, 1989

[4.19] L. Golberg and M. Chun, "Efficient generation at 421 nm by resonantly enhanced doubling of GaAlAs laser diode array emission", *Applied Physics Letters*, **55**, 218-220, 1989

[4.20] G. Dixon, C. Tanner and C. Wieman, "432-nm source based on efficient second-harmonic generation of GaAlAs diode-laser radiation in a self-locking external resonant cavity", *Optics Letters*, **14**, 731-733, 1989

[4.21] J. Ohya, G. Tohmon, K. Yamamoto, T. Taniuchi, and M Kume, "Generation of picosecond blue light pulse by frequency doubling of a gain-switched GaAlAs laser diode having saturable absorber", *IEEE Journal of Quautum Electronics*, **27**, 2050-2059, 1991

[4.22] http://www.ibh.co.uk/

[4.23] http://www.picoquant.com/

[4.24] http://www.laser2000.co.uk/

[4.25] S. Nakamura, M. Senoh, S. Nagahama, N. Iwasa, T. Yamada, T. Matsushita, Y. Sugimoto, and H. Kiyoku, "Longitudinal mode spectra and ultrashort pulse generation of InGaN multiquantum well structure laser diodes", *Applied Physics Letters*, **70**, 616-618, 1997

[4.26] C. Marinelli, I. Khrushchev, J. Rorison, R. Penty, I. White, Y. Kaneko, S. Watanabe, N. Yamada, T. Takeuchi, H. Amano, I. Akasaki, G. Hasnain, R. Schneider, S. Wang, and M. Tan, "Gain-switching of GaInN multiquantum well laser diodes", *Electronics Letters*, **36**, 83-84, 2000

[4.27] A. Siegman, *Lasers*, University Science Books, Mill Valley, CA, USA, 1986

[4.28] K. Lau, "Gain switching of semiconductor injection lasers", *Applied Physics Letters*, **52**, 257-259, 1988

[4.29] T. Sogawa and Y Arakawa, "Picosecond lasing dynamics of gain-switched quantum well lasers and its dependence on quantum well structures", *IEEE Journal of Quantum Electronics*, **27**, 1648-1654. 1991

[4.30] M. Demokan and A. Nacaroglu, "An analysis of gain-switched semiconductor lasers generating pulse-code-modulated light with a high bit rate", *IEEE Journal of Quantum Electronics*, **20**, 1016-1022. 1984

[4.31] E. Scholl, D. Bimberg, H. Schumacher, and P. Landsberg, "Kinetics of picosecond pulse generation in semiconductor lasers with bimolecular recombination at high current injection", *IEEE Journal of Quantum Electronics*, **20**, 394-399, 1984

[4.32] P. Paulus, R. Langenhorst, and D. Jager, "Generation and optimum control of picosecond optical pulse from gain-switched semiconductor lasers", *IEEE Journal of Quantum Electronics*, **24**, 1519-1523, 1988

[4.33] A. Kompa, "Numerical simulation of the generation of gain switched laser pulses", *Optical and Quantum Electronics*, **31**, 981-995, 1999

[4.34] O. Qasaimeh et al., "Bistability and self-pulsation in quantum-dot lasers with intracavity quantum-dot saturable absorbers," *Applied Physics Letters*, **74**, pp. 1654-1656, 1999

[4.35] H. Summers, D. Matthews, P. Smowton, "Laser dynamics in self-pulsation quantum dot systems," *Journal of Applied Physics*, **95**, pp. 1036-1041, 2004

[4.36] R. Conroy, J. Hewett, G. Lancaster, W. Sibbett, J. Allen, K. Dholakia, "Characterisation of an extended cavity violet diode laser", *Optics Communications*, **175**, 185-188, 2000

[4.37] D. Lonsdale, A. Willis and T King, "Extended tuning and single-mode operation of an anti-reflection-coated InGaN violet laser diode in a Littrow cavity", *Measurement Science and Technology*, **13**, 488-493, 2002

[4.38] K. Hayasaka, "Frequency stabilization of an extended-cavity violet diode laser by resonant optical feedback", *Optics Communications*, **206**, 401-409, 2002

[4.39] S. Gee and J. Bowers, "Ultraviolet picosecond optical pulse generation from a mode-locked InGaN laser diode", *Applied Physics Letters*, **79**, 1951-1952, 2001

[4.40] D. Seo and H. Liu, "Wavelength-tunable nearly transform-limited pulse generation by external injection-seeding of a gain-switched Fabry-Pérot laser", *Electronics Letters*, **33**, 2129-2130, 1997

[4.41] Y. Matsui, S. Kutsuzawa, S. Arahira, and Y. Ogawa, "Generation of wavelength tunable gain-switched pulses from FP MQW lasers with external injection seeding", *IEEE Photonics Technology Letters*, **9**, 1087-1089, 1997

[4.42] S. Nagiwa, Y. Kawaguchi, H. Ohta, and Y. Endo, "Generation of gain-switched optical pulses with low timing jitter by using external CW-light injection seeding", *Electronics Letters*, **36**, 235-236, 2000

[4.43] L. Barry, P. Anandarajah and A. Kaszubowska, "Optical pulse generation at frequencies up to 20GHz using external-injection seeding of a gain-switched commercial Fabry-Pérot laser", *IEEE Photonics Technology Letters*, **13**, 1014-1016, 2001

[4.44] D. Wang and X Fang, "Generation of electrically wavelength-tunable optical short pulses using a Fabry-Pérot laser diode in an external-injection seeding scheme with improved sidemode suppression ratio", *IEEE Photonics Technology Letters*, **15**, 123-125, 2003

[4.45] S. Li, K. Chiang, W. Gambling, Y. Liu, L. Zhang, and I. Bennion, "Self-seeding of Fabry-Pérot laser diode for generating wavelength-tunable chirp-compensated single-mode pulses with high-sidemode suppression ratio", *IEEE Photonics Technology Letters*, **12**, 1441-1443, 2000

[4.46] S. Li, K. Chiang and W. Gambling, "Wavelength tuning in self-seeded gain-switched Fabry-Pérot laser diode with Moiré grating", *Electronics Letters*, **35**, 2209-2210, 1999

[4.47] S. Li, K. Chiang and W. Gambling, "Generation of wavelength-tunable single-mode picosecond pulses from a self-seeded gain-switched Fabry-Pérot laser diode with a high-birefringence fiber loop mirror", *Applied Physics Letters*, **76**, 3676-3678, 2000

[4.48] S. Li, K. Chiang, W. Gambling, "Fast wavelength tuning of a self-seeded Fabry-Pérot laser diode with a Fabry-Pérot semiconductor filter", *IEEE Photonics Technology Letters*, **13**, 1364-1366, 2001

[4.49] M. Schell, D. Huhse, W. Utz, J. Kaessner, D. Bimberg, I. Tarasov, "Jitter and dynamics of self-seeded Fabry-Pérot laser diode", *IEEE Journal of Selected Topics in Quantum Electronics*, **1**, 528-534, 1995

[4.50] M. Schell, D. Huhse, A. Weber, G. Fischbeck, D. Bimberg, D. Tarasov, A. Gorbachov, and D. Garbuzov, "20nm wavelength tuneable single mode picosecond pulse generation at 1.3μm by a self-seeded gain-switched semiconductor laser", *Electronics Letters*, **28**, 2154-2155, 1992

[4.51] S. Bouchoule, N. Stelmakh, M. Cavelier, and J. Lourtioz, "Highly attenuating external cavity for picosecond tunable pulse generation from gain/Q-switched laser diodes", *IEEE Journal of Quantum Electronics*, **29**, 1693-1700, 1993

[4.52] D. Huhse, M. Schell, J. Kaessner, D. Bimberg, I. Tarasov, A. Gorbachov, D. Garbuzov, "Generation of electrically wavelength tunable ($\Delta\lambda$=40nm) singlemode laser pulses from a 1.3mm Fabry-Pérot laser by self-seeding in a fibre-optic configuration", *Electronics Letters*, **30**, 157-158, 1994

Chapter 5

Spectral filtering of high power diode laser pulses

In this chapter, we demonstrate experimental investigation of relaxation tail suppression of an overdriven pulsed 860nm DFB laser by spectral filtering. Tuneable fibre Bragg gratings worked as in-line spectral filters, and made the whole system robust and compact. As a result, the high energy undesired relaxation tail was substantially suppressed without suppression of the first peak energy. Due to poor side mode suppression ratio of the laser at high power pumping levels, the spectra of the filtered pulse were multimode and pulse chirp was nonlinear. Theoretical analysis together with our previous study of a 1550nm DFB laser shows more effective pulse compression after spectral filtering would have been achieved if the spectral components of the first peak of the pulse had been contained in only one single mode.

5.1 Introduction

Today, high power picosecond diode laser pulses are commonly generated by the approaches of gain-switching or Q-switching. Study of these high power diode laser pulses shows the possibility to improve the quality of high power pulses by appropriate tailoring of their spectra. A number of investigation shows spectral filtering is a simple and effective technique to suppress the relaxation tail [5.1-5.4] as well as to compress the pulse duration [5.3, 5.4] of high power pulses.

Gain-switched operation of diode lasers shows that when the laser is pumped at an excitation level where more than one relaxation oscillation is emitted, more than 50% of the total number of the longitudinal modes is emitted within the first relaxation peak and a certain amount of spectral shift to short wavelength was introduced. The large number of modes contained in the first relaxation peak is due to the large overshoot of the charge carrier density beyond the threshold density during the switch-on process. These modes are always composed of short-wavelength part of the pulse spectrum. The magnitude of the spectral shift is determined by the amount of carrier overshoot during transient switch-on process. Consecutive relaxation tails (or sub-pulses) are associated with a smaller carrier overshoot producing a narrower overall spectral linewidth. They are always composed of the long-wavelength part of the pulse spectrum. One study [5.5] shows that the transient spectrum broadening effect during the switch on process was so significant that simple spectral filtering allows the spectral mode for the first optical relaxation oscillation to be efficiently separated from the relaxation tail modes. Consequently, in the filtered pulses, the peak intensity of first spike could exceed that of emission tail by a few orders of magnitude.

As well as to suppress the tail, spectral filtering affects the duration and chirp of the laser pulses. It is well-known, that gain-switched laser diode pulses possess considerable chirp. Under the large-signal modulation the linewidth enhancement factor, α, changes during the pulse, and the chirp is not linear. Therefore, it is possible to compress duration of gain-switched laser pulses by selecting only the linearly-chirped components [5.3, 5.4]. After propagating through a certain length of fibre, the filtered laser pulses could be further compressed.

Spectral filtering of Q-switched diode lasers was also proposed. Both theoretical [5.6] and experimental [5.6, 5.7] work demonstrate that the spectral feature of Q-switched diode lasers is similar to intensively driven gain-switched lasers. The laser modes corresponding to the first oscillation peak are also located on the "blue" side of the spectrum. Comparably, the "tails" energy of Q-switched pulses is not so pronounced as gain-switched pulses. Effective suppression of the tails in Q-switched mode has been demonstrated using a band-pass filter [5.7].

Spectral filtering of pulsed DFB laser has aroused a lot of interest recently. Due to the mode discrimination nature of DFB lasers, the spectral components of the gain-switched DFB laser pulses were contained in only one mode. Pulses were strongly chirped, i.e. the frequency of the light varies substantially over the duration of pulse. T. Niemi et al. demonstrated optical filtering of gain-switched DFB lasers under moderate modulation condition using Fabry-Pérot filters [5.4]. By carefully adjusting wavelength window position of the Fabry-Pérot filter with its transmission peak scanned over the chirped spectral components, the output pulses were tailored with reduced pulse duration and narrowed spectral linewidth. Fourier-transform-limited pulses were generated by this means. There are also some disadvantages of this method. Firstly, the output power of the filtered pulses was low due to the electrical pumping power need to be kept at low levels in order to maintain single mode output and a large amount of energy was cut off by the filter. Secondly, the system's stability was poor due to the use of precision bulk-optics, Fabry-Pérot etalon.

In order to increase the output power of filtered gain-switched pulses, spectral filtering of an overdriven 1550nm DFB laser was demonstrated in our previous work [5.3]. At high pumping level, the spectra became multimode with a high peak located in the long wavelength part, which corresponded to the "tail" modes of the pulse. Simply eliminating this part of spectral components using tuneable fibre Bragg grating resulted in picosecond pulses output with substantially suppressed relaxation tail and high peak power. The whole system was simple and robust. In our study presented in this chapter, the similar spectral filtering technique was applied on a high power gain switched 860nm GaAs DFB laser.

5.2 Spectral filtering of GaAs DFB diode laser pulses

5.2.1 Laser characterisation

The laser samples are GaAs DFB lasers operating at a central wavelength of 860nm. The samples were produced at Glasgow University about 5 years ago. Three boxes of laser samples, 10 in each box have been supplied to Aston. Several lasers in box No. 2 were found to be in still good condition. There are five 900nm-long lasers and five 1.4μm-long lasers in this box. The experiments below were based on of a 1.4μm-long laser (sample No.1) and a 900nm-long laser (sample No. 2).

Fig. 5.1 shows the spectrum of laser No.1 under quasi-CW condition. The pumping signal had a peak current of 100mA, a pulse duration of 100ps, and a duty cycle of 1%. The spectrum shows a side band suppression ratio of more than 30dB. The unsuppressed sidebands occurred on the short wavelength side.

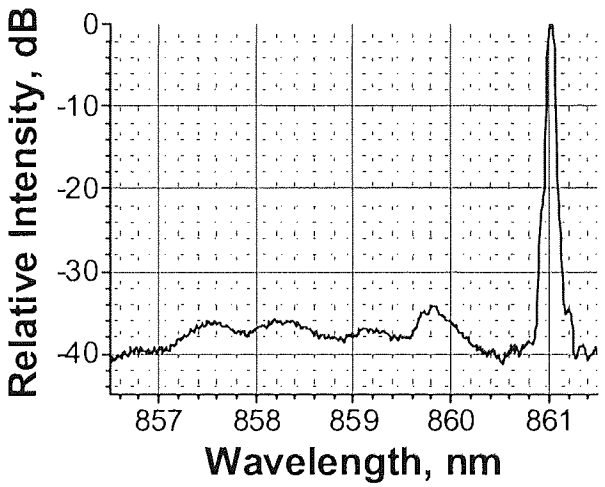

Fig. 5.1 Spectrum of GaAs DFB laser No.1 under quasi-CW pumping condition

For high power gain-switched operation, a Kentech avalanche pulse generator (APG-1) was used to drive the laser. The electrical pulse had a peak voltage of 780V, a rising time of 150ps, a falling time of 1ns, a repetition rate of 10kHz. The driving signal was attenuated before applied to the laser. Fig. 5.2 shows the temporal and spectral profiles of gain-switched pulses from laser No.1.

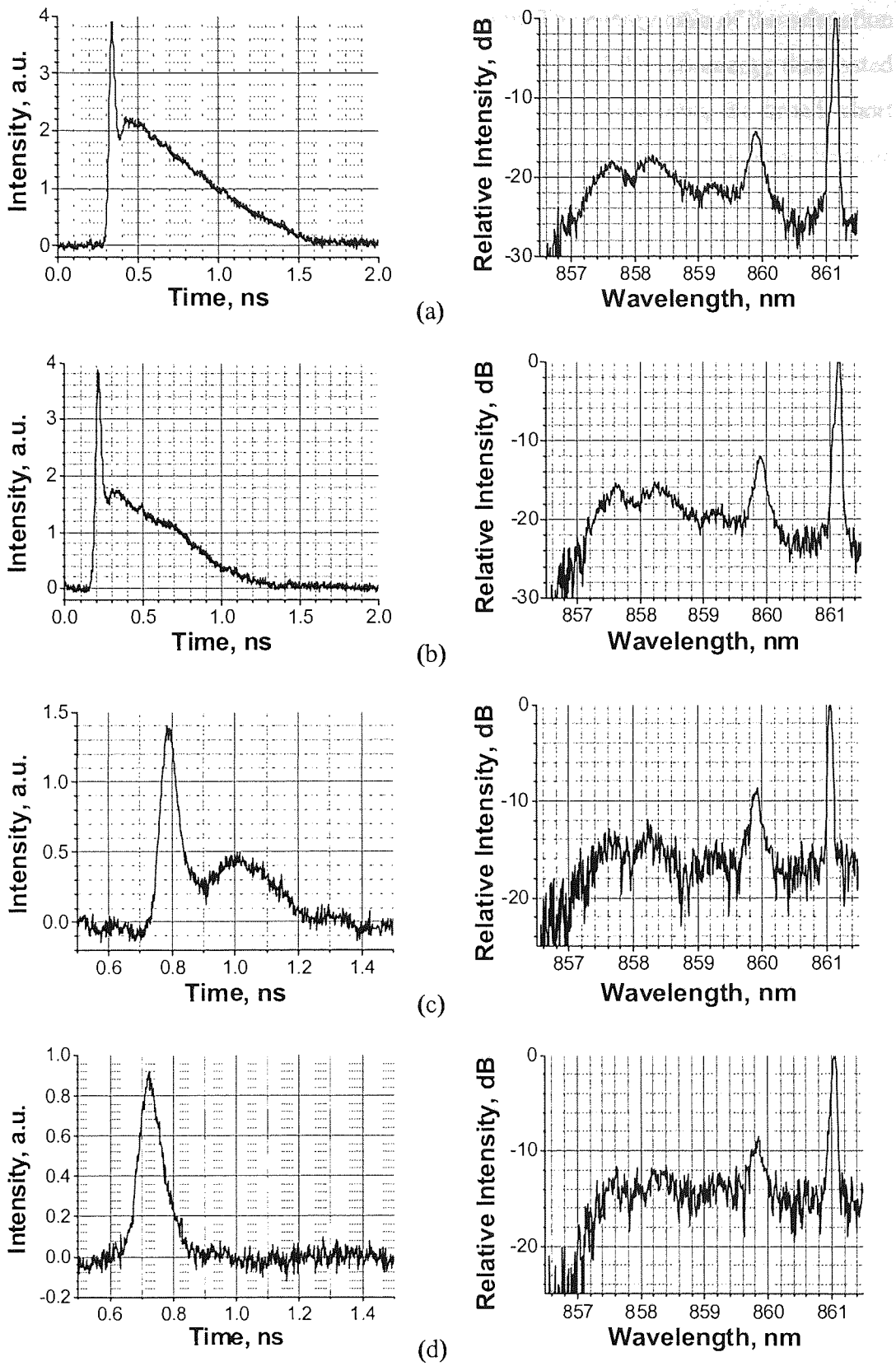

Fig. 5.2 Gain switched pulse (left) and the corresponding spectra (right) of GaAs DFB lasers under different electrical pumping conditions: (a) I_{peak}=620mA, (b) I_{peak}=550mA, (c) I_{peak}=440mA, (d) I_{peak}=390mA.

The laser showed a typical gain-switched operation. The energy ratio of the relaxation tail to the whole pulse increased with pumping levels, and the tail energy dominated the whole pulse energy at high pumping levels. At the same time, the broad, short wavelength, side band in the spectrum, ranging from 857nm to 860.5nm, became more and more pronounced. However, the broad short-wavelength band and the narrow long-wavelength band were clearly separated from each other. Side band suppression ratio increased from 8dB to 14dB, as the pumping signal increased from I_{peak}=390mA to I_{peak}=620mA.

Comparing the temporal and spectral profiles of the generated pulses, we suggested that the fast components (short, intensive spike) of the pulse corresponded to the wide side band in the spectrum and the slow components (long, high energy tail) of the pulse corresponded to the long wavelength narrow band in the spectrum. In order to justify the above suggestion, a monochromator incorporated in an optical spectral analyser (Hewlett-Packard 70950) was used to analyse the spectral components of the pulses. Fig. 5.3 shows the output laser pulses with spectra filtered by the monochromator at different wavelengths and bandwidths. Due to the big loss of the monochromator, only very weak signals were detected on the oscilloscope. However, from comparison of signal (a) and (b) in Fig. 5.3, spectral separation of the "fast" and "slow" components is evidently shown.

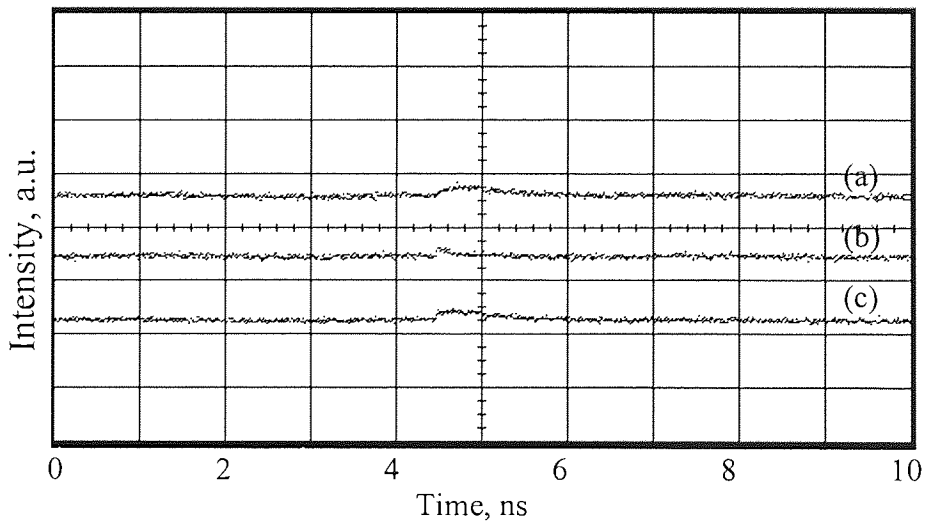

Fig. 5.3 Oscilloscope traces of gain-switched GaAs DFB laser filtered by a monochromator at different central wavelengths, λ, and window bandwidths Δλ. (a) λ=861.0nm, Δλ=5nm; (b) λ=858.0nm, Δλ=5nm; (c) λ=859.5nm, Δλ=10nm. Pumping condition: I_{peak}=620mA.

Laser No.2 has a similar feature for both quasi-CW operation and gain-switched operation. Its temporal and spectral profiles will be shown in the later sections.

5.2.2 Spectral filtering operation

For the spectral filtering operation, two 10mm-long, uniform period fibre Bragg gratings were fabricated in a Talbot interferometer setup [5.8]. Transmission spectra of the gratings are shown in Fig. 5.4. The insertion loss is ~3dB for grating No.1 and ~5dB for grating No.2. The gratings were subsequently glued to thin metal beams and strained by a four-point mechanical bending device, shown in Fig. 5.5. By bending the beams using a tuning rig [5.9], it was possible to adjust the grating resonance wavelength in the range 859nm to 864nm.

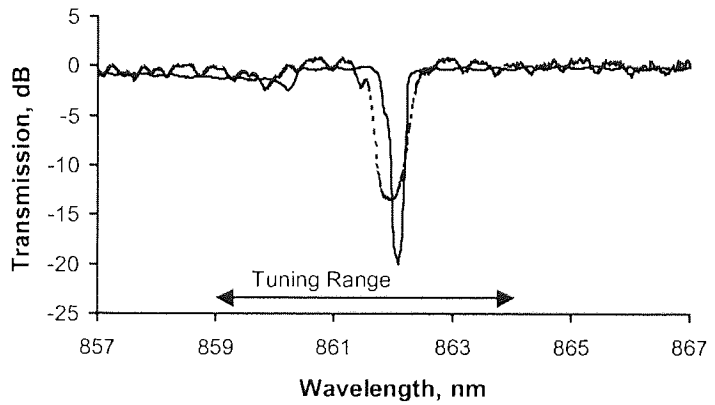

Fig. 5.4 Transmission spectra of two fibre Bragg gratings. Grating No.1 (solid line) and No.2 (dashed line) had -3dB bandwidths of 0.42nm and 0.68nm respectively.

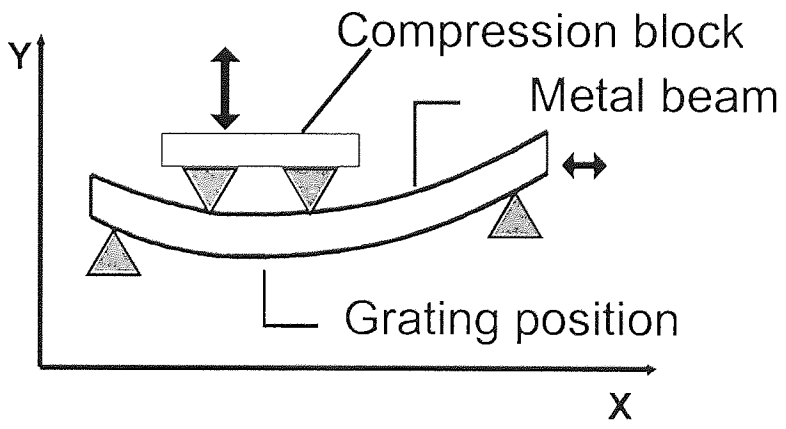

Fig. 5.5 Schematic draw of four point mechanical bending device for wavelength tuning of fibre Bragg grating.

The spectra of laser No. 2 under gain-switched operation comprises of three separate components, a short wavelength 2nm-wide band centred at 858.0nm, 0.4nm-wide band centred at 859.9nm, and a long- wavelength narrow band centred at 861.1nm. We are able to investigate the relation of spectral components to temporal pulse profiles with the aid of two wavelength tuneable gratings mentioned above. Experimental setup is shown in Fig. 5.6. The gratings were either used separately or connected in series for spectral filtering operation. The electrical pumping was provided by Kentech avalanche pulse generator as mentioned above.

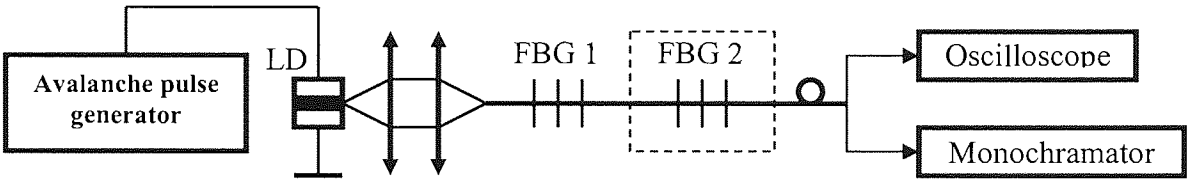

Fig. 5.6 Experimental set-up for pulse tail suppression

Plot 2 in Fig. 5.7 shows grating No.1 with wavelength tuned at 861.0nm substantially suppressed the long wavelength narrow band, resulting in a huge reduction of tail energy in temporal profile, but the pulse peak did not drop, which manifests that the long wavelength narrow band in spectrum only contributed to the huge pulse tail in temporal profile. However, a certain amount of pulse tail still remained.

Grating No.2 was then spliced to grating No. 1 with wavelength tuned to 859.5nm to suppress the central band in spectrum. It turned out to be that suppression of this band corresponded to energy drop of both pulse peak and pulse tail at the same proportion (plot 3 of Fig. 5.7).

At a lower electrical pumping level, I_{peak}=550mA, we obtained a similar result. A certain amount of unsuppressed tail energy still existed for the optimum spectral filtering, as is shown in Fig. 5.8.

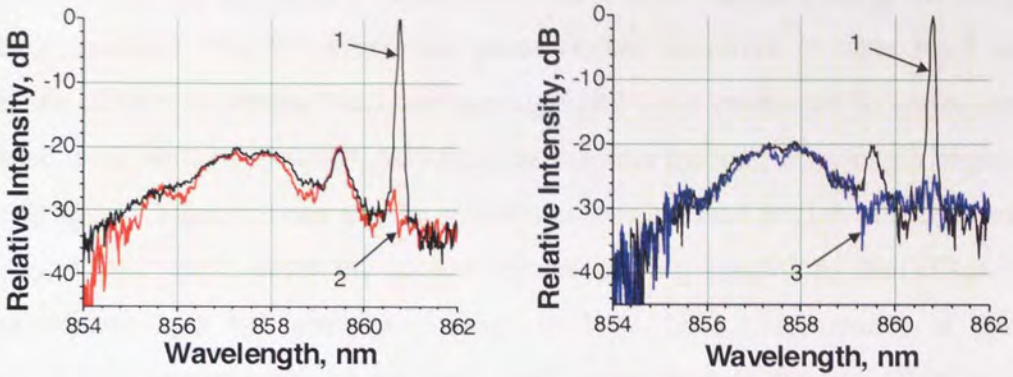

(a) (b)

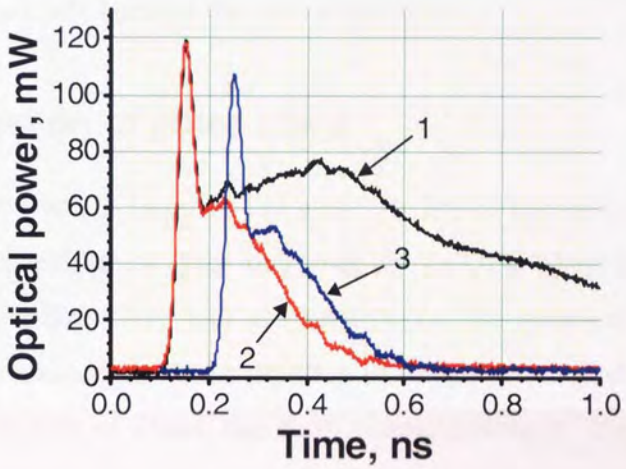

(c)

Fig. 5.7 Spectra (a), (b) and oscilloscope traces (c) of gain switched pulses from GaAs DFB laser No.1 (1) without spectral filtering, (2) filtered by grating No.1, (3) filtered by grating No.1 and No.2. Pumping condition: I_{peak}=620mA.

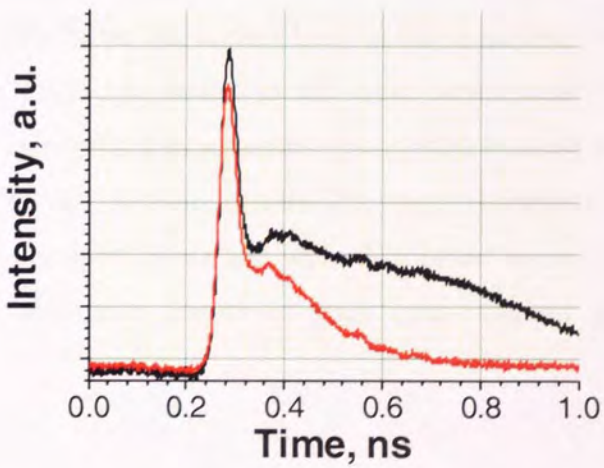

Fig. 5.8 Gain switched pulses from GaAs DFB laser No. 1 without (black line) and with (red line) spectral filtering by grating No.1 together with grating No. 2. Pumping condition: I_{peak}=550mA.

Spectral filtering operation of laser No.2 was also investigated using the same fibre Bragg gratings. Fig. 5.9 shows the gain-switched spectrum of laser No.2 has two separated bands. Grating No.1 and grating No.2 were connected in series and both tuned to the same wavelength, 859.8nm, to suppress the long wavelength narrow band in spectrum. Pulse tail can also be substantially suppressed at high driving conditions [Fig. 5.9(a), (b)]. However, at low power driving condition, the effect of tail suppression was not obvious. Similar to laser No.1, suppression of the long wavelength narrow band did not cause peak power drop of the gain-switched pulses. The incomplete suppression of pulse tail indicates there were some slow components existing in the broad side band of the laser's spectrum.

5.2.3 Investigation of pulse chirp

Another important work to improve the pulse quality of gain-switched DFB lasers is to compress the pulse duration. Previous work shows DFB lasers under gain-switched operation has linear-like chirp and are suitable for the simplest fibre compression [5.10, 5.11]. By measuring the pulse duration of the gain-switched pulses propagating through various lengths of fibres, the chirp characteristics of the initially generated pulses can be identified, thus, the optimum fibre length corresponding to the shortest pulse duration can be estimated.

Analyses in the above sections show the spectra of our DFB lasers under high power gain-switched condition are different from conventional gain-switched DFB lasers. With large signal modulation, the narrow band in the spectrum, which contains a large amount of energy, only contributed to the slow components (tail) of pulse. Fast components of the laser pulses experienced a long shift to short wavelength and were almost isolated from the slow components. The spectral components of the pulse did not remain in only one laser mode and were distributed to several short-wavelength modes. Therefore, the chirp feature of such gain-switched pulses can be quite different.

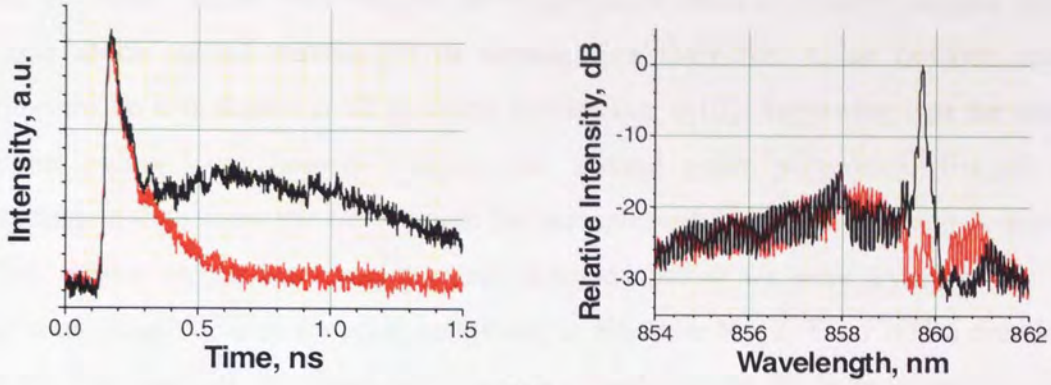

(a)

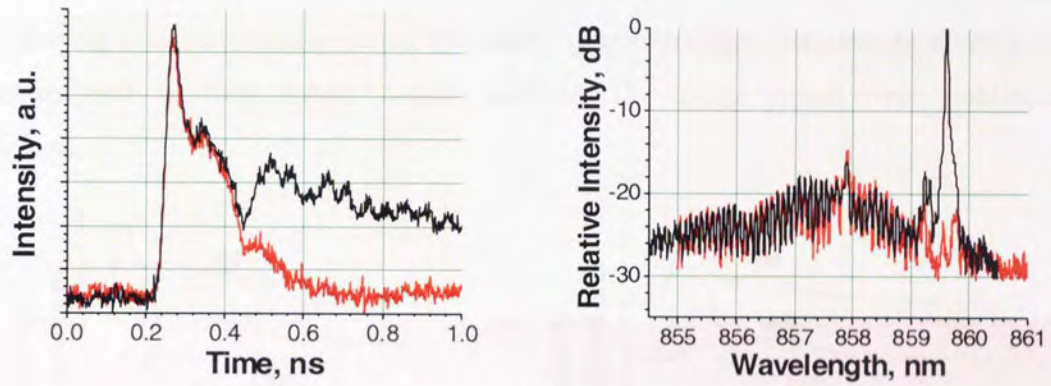

(b)

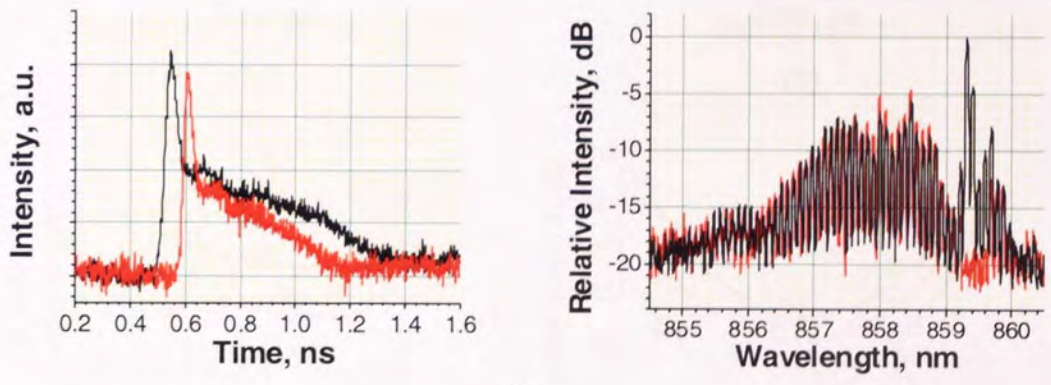

(c)

Fig. 5.9 Oscilloscope traces (left) and spectra (right) of gain switched GaAs DFB laser No.2 without (black line) and with (red line) spectral filtering at an electrical pumping level of (a) I_{peak}=880mA; (b) I_{peak}=550mA; (c) I_{peak}=350mA.

In our experiments, the electrical pumping pulse was attenuated to different levels, and the output signals were coupled into single mode fibres of different lengths with a single mode cut-off wavelength of 680nm. For laser No. 1, an obvious initial compression was shown at all pumping levels (Fig. 5.10). Supposing that the initial output pulses were linearly chirped, the second order polynomial fits of the experiment data show the fibre length for the optimum pulse compression is around 70m. However, the laser was severely degraded before we were trying to use the optimum length of fibre for pulse compression. For laser No. 2, The FWHM durations of the first peaks of the pulses were not measurable due to the huge relaxation tails. Hence, we characterise the pulses by their widths at 80% maximum. Fig. 5.11 shows pulses evolution at different driving conditions. Fig. 5.11 (d) shows output pulses at all driving conditions experienced a broadening-compression-broadening process with the increase of fibre length, which indicates the initial pulses were nonlinearly chirped.

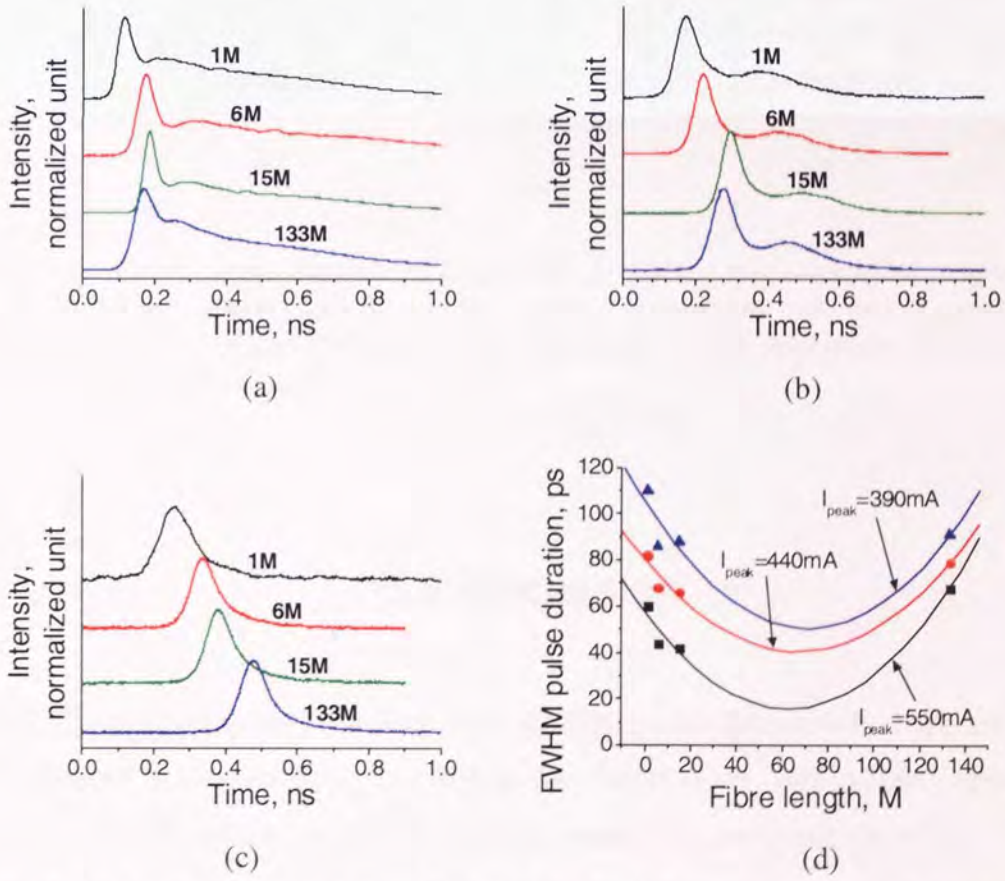

Fig. 5.10 Chirp characteristics of Laser No. 1: Pulses evolution after propagating over different length of fibres at driving conditions of (a) I_{peak}=550mA, (b) I_{peak}=440mA, (c) I_{peak}=390mA, and (d) Full width at half maximum (FWHM) pulse duration as a function of fibre length.

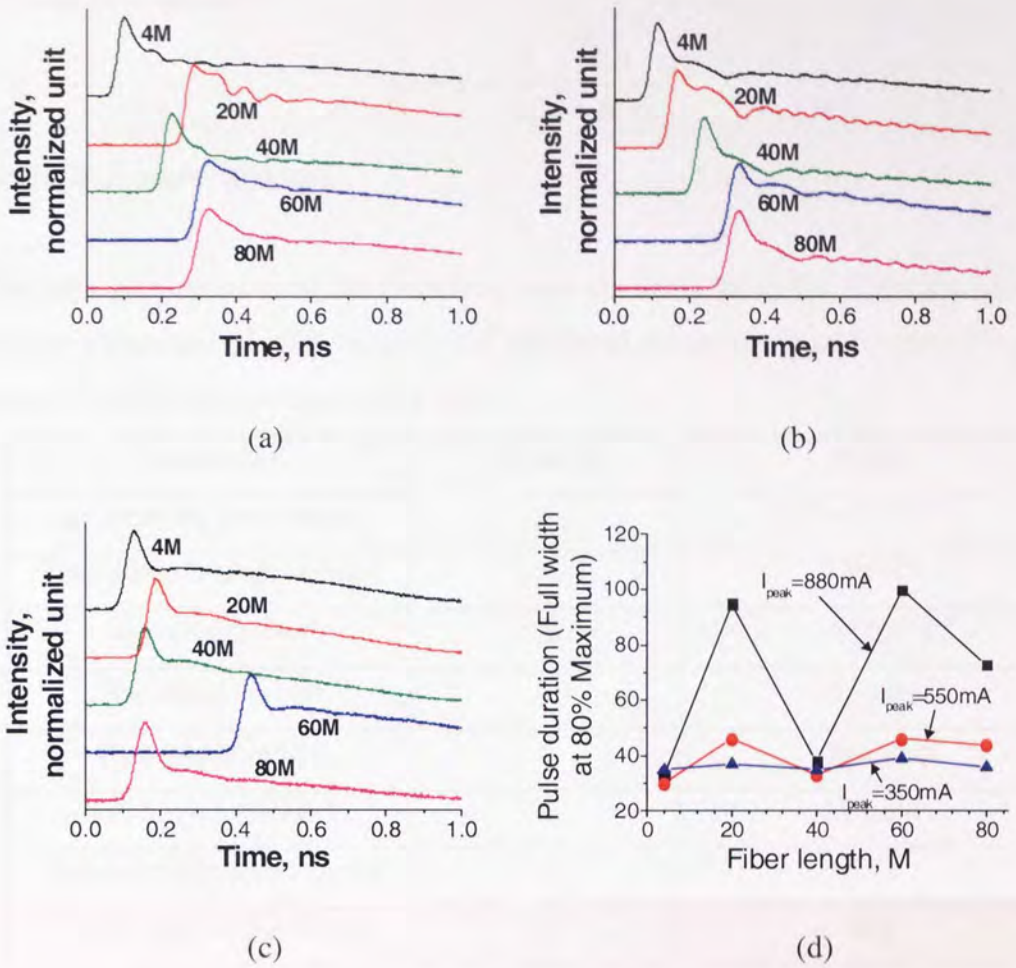

Fig. 5.11 Chirp characteristics of Laser No. 2: Pulses evolution after propagating over different length of fibres at driving conditions of (a) I_{peak}=620mA, (b)I_{peak}=550mA, (c)I_{peak}=350mA, and (d) Full width at 80% maximum of pulse width as a function of fibre length.

5.3 Discussion

Laser dynamics of GaAs DFB laser diode for high power gain-switched operation was investigated theoretically by modelling the laser diode with single mode rate equations (2.18). where, photon life time τ_{ph}, carrier life time τ_s are given by:

$$\tau_{ph} = 1/[v_g(\alpha_m + \alpha_i)] \tag{5.1}$$

$$\tau_s = 1/(A + Bn + Cn^2) \tag{5.2}$$

Loss factor is given by:

$$\alpha = \alpha_i + \frac{1}{2L}\ln\left(\frac{1}{R_1 R_2}\right) \tag{5.3}$$

where, α_i is absorption loss.

The laser parameters used for modelling were shown in table 5.1. They are taken for typical parameters of DFB lasers [5.18] Electrical pumping signal for modelling was taken directly from the experiment data.

Parameter	Symbol	Value
Differential gain factor	g_0	3.0e+16 [cm^{-1}]
Transparent carrier density	N_t	2.0e+18
absorption loss	α_i	14 [cm^{-1}]
Waveguide width	w	5 [μm]
Waveguide length	L	1000 [μm]
Active layer thickness	d	24 [nm]
Optical confinement factor	Γ	0.02
Current spread coefficient	sp	0.1
Wavelength	λ	850 [nm]
Group refractive index	n	3.55
Front mirror reflectivity	R_1	0.32
Back mirror reflectivity	R_2	1
Spontaneous recombination parameters	A	3e+8 [s^{-1}]
	B	1e-10 [$cm^3 s^{-1}$]
	C	1.28e-28 [$cm^6 s^{-1}$]
Spontaneous emission factor	β	1e-4
Nonlinear gain coefficient	ε	1.5e-17 [cm^3]

Table 5.1 Parameters used for numerical modelling of GaAs DFB laser diode

As we discussed in Chapter 2, the time dependence of the laser wavelength is related to the time dependence of the carrier concentration. The transient wavelength of the laser pulse is related to the refractive index as

$$\lambda(t) = \frac{\mu(t)}{\mu_0}\lambda_0 \tag{5.4}$$

where $\mu(t)$ and μ_0 are the refractive indices at times t and 0, respectively. The carrier-induced refractive index changes depends on a number of factors and the exact expression of μ as function of carrier density is very complicated [5.12, 5.18], for simplicity we can write,

$$\mu(t) \cong \frac{d\mu}{dn} n(t) \tag{5.5}$$

A typical value of $d\mu/dn$ is ~$2*10^{-20}$cm^3 [5/12, 5.18]. Combining equations (5.4) and (5.5) one obtains the wavelength chirp $\Delta\lambda$ during the gain-switched pulse,

$$\Delta\lambda(t) \cong \frac{\lambda_0}{\mu_0} \frac{d\mu}{dn} \Delta n(t) \tag{5.6}$$

Therefore, we are now able to obtain the transient wavelength of the gain-switched pulses. The above model is actually suitable for DFB lasers working at different wavelengths.

Fig. 5.12 shows the modelling results for different electrical pumping levels. As the pumping power increases, peak output power increased, pulse duration decreases, and relaxation oscillation tail becomes more and more pronounced. Almost linear chirp for the first relaxation peak was evidently shown, which was marked by red lines in the figures. However, the relaxation tail corresponds to comparably moderate wavelength chirp. As pumping power increases, the chirp for the first peak becomes more and more significant, but the chirp for relaxation tail is non-linear and always maintained at a moderate level and is located on the long wavelength side of the pulse.

The laser behaviour obtained from the above numerical modelling qualitatively agrees with our experimental results. Due to the small wavelength chirp of the relaxation tail, we are able to substantially suppress the tail using narrow band-pass filter with reflection peak tuned to the long wavelength side. In order not to substantially reduce the energy of the first relaxation peak from the output, the band-pass filter should have a reflection spectrum with a very sharp edge. The fibre Bragg grating used in this experiment had a reflection-curve slope in excess of 100dB/nm and proved to be an ideal element for spectrum trimming. In addition, the whole system for spectral filtering was robust and compact.

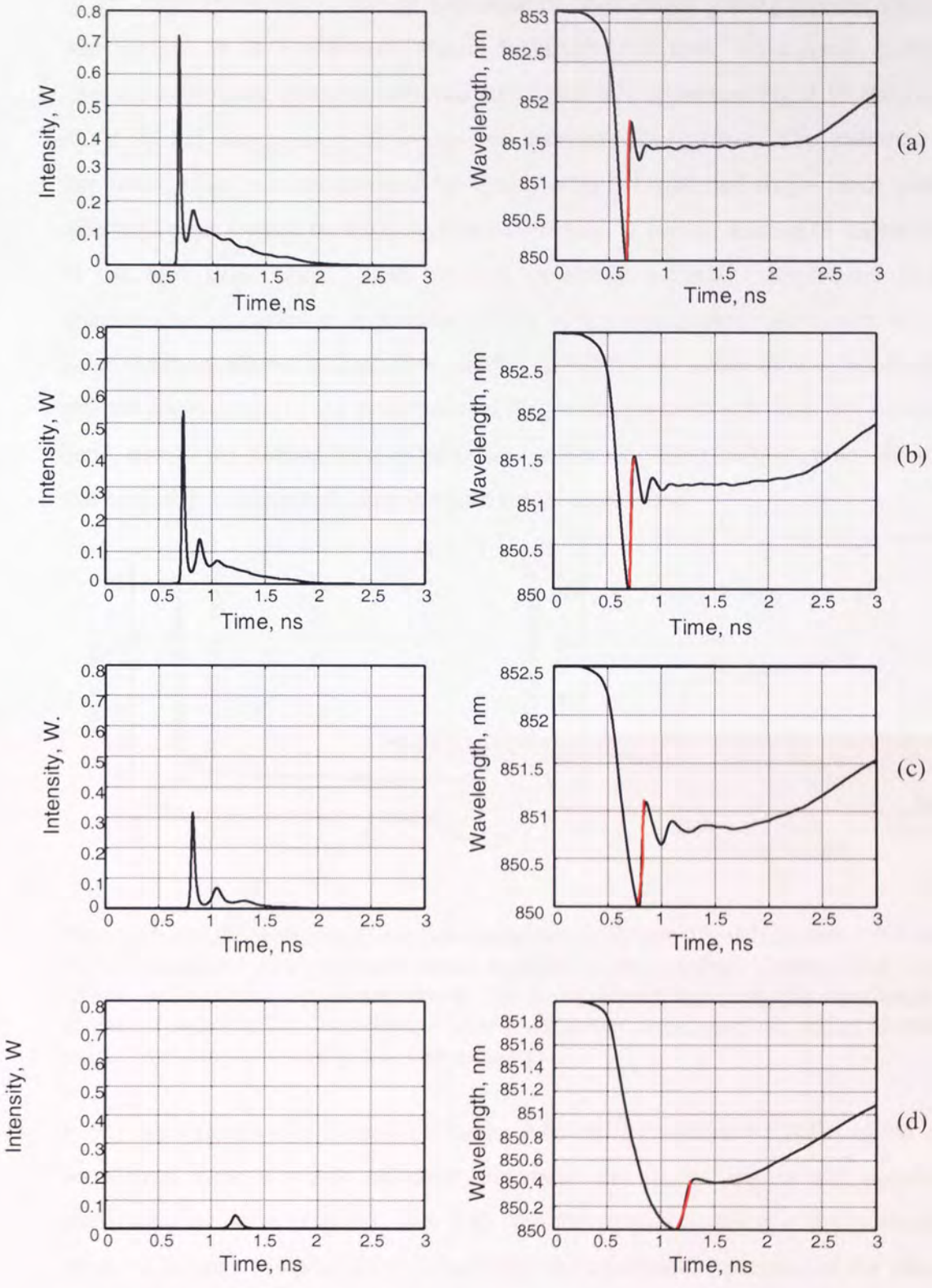

Fig. 5.12 Modelling results of 850nm single mode laser diode for pulsed operation. Temporal profiles (left column) and transient wavelength change (right column) were shown for different electrical pumping levels: (a) I_{peak}=2.0A; (b) I_{peak}=1.5A; (c) I_{peak}=1.0A; (d) I_{peak}=0.5A.

In an early experiment, a similar technique of fibre Bragg grating spectral filtering was applied on an overdriven 1550nm InGaAsP DFB laser. As a result, a 5-fold increase in the peak power is achieved for the tail-free operation. Fig. 5.13 shows the effect of tail suppression of overdriven gain-switched pulses. The spectrum of unfiltered pulse was characterised by a substantially broadened single mode profile with high peak located on the long wavelength side. A certain amount of suppression of the high peak, about 10dB, resulted in almost complete suppression of the relaxation tail. In addition, appropriate tuning of the grating gave rise to narrowing of pulse duration, shown in Fig. 5.14, which was due to the elimination of nonlinearly chirped components of the pulse located on the long-wavelength side. On the other hand, due to the filtered laser pulse is almost linearly down chirped, pulse duration can be further compressed using standard single-mode fibre.

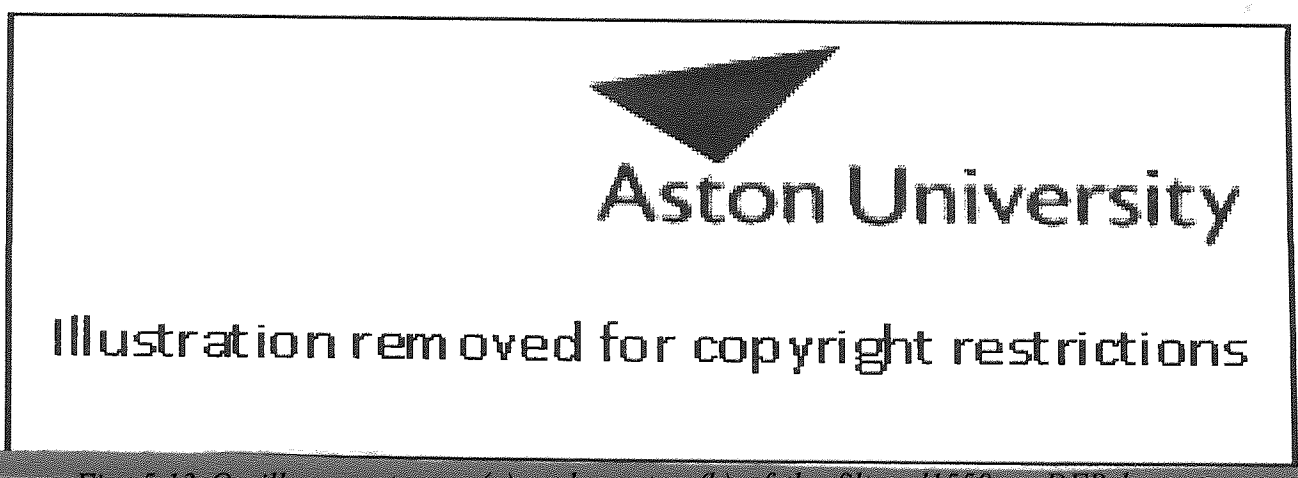

Fig. 5.13 Oscilloscope traces (a) and spectra (b) of the filtered1550nm DFB laser output measured with different strain applied to the grating. Dashed line - zero strain; solid line - optimised strain. Laser is overdriven and the amplitude of electrical pulses is 3A. Dotted line - laser is driven by low-amplitude (0.5A) electrical pulses, resulting in virtually tail-free output [5.3].

In our experiments with GaAs DFB lasers, substantial suppression (20dB) of the long wavelength peak was also achieved. However, the filtered pulses still possessed multimode spectrum (Fig. 5.7, Fig. 5.9), and the relaxation tail was not completely removed for any pumping levels. Therefore, the multimode spectrum of the filtered pulse contained both "fast" and "slow" components. In addition, our experimental investigation of pulse chirp after spectral filtering does not agree well with the linear chirp feature predicted from our theoretical model since single-mode model was not suitable in the case of our experiment.

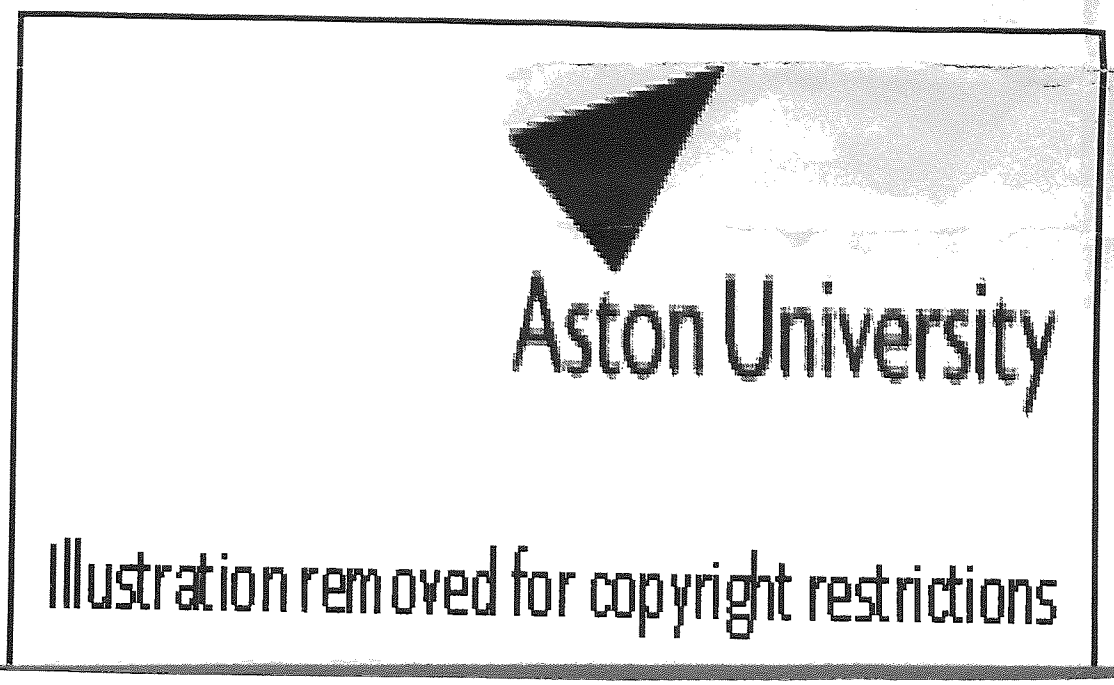

Fig. 5.14 Pulse duration and normalised relaxation tail energy E_{tail}/E_{total} of 1550nm DFB laser as functions of the grating strain. Closed symbols correspond to the unstrained fibre Bragg grating [5.3].

As a comparison, the spectral feature under overdriven pulsed condition shows the 1550nm InGaAsP DFB laser had a better quality than the 860nm GaAs DFB laser, which, as we considered, is mainly caused by the λ/4 phase shifted grating structure in the centre of the 1550nm DFB laser cavity. In the case of λ/4 phase shifted DFB laser, the lowest-loss mode is found to be located exactly at the Bragg wavelength. The gain margin between the main and side modes is much larger than that for conventional DFB lasers. It is such a large value of gain margin that makes the side mode suppression ratio phase-shifted DFB lasers advantageous for highly intensive electrical pumping. As a result, the pulsed spectrum of this type of laser is a broadened single mode one and the chirp is almost linear. Thus, such a linearly chirped single mode spectrum is extremely suitable for fibre compression.

In the spectrum of pulsed 1550nm InGaAsP DFB laser, shown in Fig. 5.13(b), Fabry-Pérot periodical structure is much less obvious than 860nm GaAs DFB laser. However, such a spectrum structure can not be strictly regarded as a single-mode one. Indeed, multimode spectrum always occurs in λ/4 phase shifted DFB lasers under large amplitude modulation. The reasons for that mainly come from longitudinal spatial-hole burning and small gain margin between TE and TM modes in this laser structure [5.12]. Further improved single-mode performance was observed in DFB

lasers with multiple phase-shifted regions [5.13-5.14] or gain-coupled DFB lasers [5.15-5.17]. We expected better spectral filtering and pulse compression results to be obtained by using this kind of DFB lasers.

5.4 Conclusion

We have experimentally demonstrated effective relaxation tail suppression of an overdriven pulsed GaAs DFB laser working at a wavelength around 860nm by means of spectral filtering. Tuneable fibre Bragg grating was utilized to suppress the relaxation tail of the output pulses. At different pumping levels, pulse tail energy was greatly reduced when the central reflection wavelength of the grating was tuned close to the long wavelength peak in the spectrum. However, there was still a certain amount of energy remaining in the tail even though the long wavelength peak was almost completely suppressed. The spectra of the output signal after spectral filtering were multimode and the pulse chirp was nonlinear.

Modelling of DFB laser using single mode rate equations shows, under overdriven condition, spectral components of first relaxation peak are located on the short wavelength "blue" side with linear down chirp and those of relaxation tail are separately located on the long wavelength "red" side with nonlinear chirp. It theoretically shows a suitable band-pass filter with deep enough band edge can be used to suppress the relaxation tail, and the filtered pulses can be further compressed. However, in practice, the effectiveness of spectral filtering and pulse compression depends on the quality of the laser pulses. Phase-shifted DFB lasers and gain-coupled DFB lasers, which show improved side-mode suppression ratio under large signal modulation, could probably demonstrate better spectral filtering effect.

References

[5.1] S. Vainshtein, G. Simin and J. Kostamovaara, "Deriving of single picosecond pulses from a high-power gain-switched laser diode by spectral filtering", *Journal of Applied Physics*, **84**, pp. 4109-4113, 1998

[5.2] G.Simin, S. Vainshtein, J. Kostamovaara, A. Kilpelä, K. Määttä, "Isolated picosecond pulses obtained by spectral selection from gain-switched semiconductor lasers", International conference on Lasers '97, New Orleans, Louisiana, USA, December 15-19, 1997, *Proceedings of the international conference on lasers '97*, STS Press, McLEAN, VA, pp. 71-77, 1998

[5.3] M. Dubov, D. Giannone, I. Khrushchev, I. Bennion, "Pulse tail suppression in laser diode output by tuneable notch filter", *Electronic Letters*, **37**, pp. 1404-1405, 2001

[5.4] T. Niemi, J. Zhang, H. Ludvigsen, "Effect of optical filtering on pulses generated with a gain-switched DFB laser", *Optics Communications*, **192**, pp. 339-345, 2001

[5.5] T. Sogawa and Y. Arakawa, "Picosecond spectral dynamics of gain-switched quantum-well lasers and its dependence on quantum-well structures", *Journal of Applied Physics*, **67**, pp. 2675-2677, 1990

[5.6] S. Vainshtein, V. Rossin, A. Kilpela, J. Kostamovaara, R. Myllyla, and K. Maatta, "Internal Q-switching in semiconductor lasers: high intensity pulses of the picosecond range and the spectral peculiarities", *IEEE Journal of Quantum Electronics*, **QE-31**, 1015-1021, 1995

[5.7] S. N. Vainshtein and J. Kostamovaara, "Spectral filtering for time isolation of intensive picosecond optical pulses from a Q-switched laser diode", *Journal of Applied Physics*, **84**, 1843-1847, 1998

[5.8] F. Floreani, A. Gillooly, L. Zhang, I. Bennion, X. Shu, K. Sugden, "A simple method for the fabrication of intrinsically apodized chirped fibre Bragg gratings", *Journal of Optics A*, **5**. pp. S59-S62, 2003

[5.9] B. A. L. Gwandu, L Zhang, K Chisholm, Y Liu, X Shu, I Bennion, "Compact FBG array structure for high spatial resolution distributed strain sensing", *Measurement Science and Technology,* **12**, pp. 918-921, 2001

[5.10] R. Hawkins, "Generation of <3ps optical pulses by fibre compression of gain-switched InGaAsP DFB laser diode pulses", *Electronics Letters*, **26**, pp. 292-294, 1990

[5.11] H. Liu, Y. Ogawa, and S. Oshiba, "Generation of an extremely short single mode pulse (~2ps) by fiber compression of a gain-switched pulse from a 1.3μm distributed-feedback laser diode", *Applied Physics Letters*, **59**, pp. 1284-1286, 1991

[5.12] M. Osinski and M. J. Adams, "Picosecond pulse analysis of gain-switched 1.55μm InGaAsP lasers", *IEEE Journal of Quantum Electronics*, **21**, pp. 1929-1936, 1985

[5.13] G. Agrawal, J. Geusic, and P. Anthony, "Distributed feedback lasers with multiple phase-shift regions", *Applied Physics Letters*, **53**, pp. 178-179, 1988

[5.14] J. Whiteaway, B. Garrett, G. Thompson, A. Collar, C. Armistead, M. Fice, "The static and dynamic characteristics of single and multiple phase-shifted DFB laser structures", *IEEE Journal of Quantum Electronics*, **QE-28**, pp. 1277-1293, 1992

[5.15] Y. Nakano, Y. Luo, and K. Tada, "Facet reflection independent, single longitudinal mode oscillation in a GaAlAs/GaAs distributed feedback laser equipped with a gain-coupling mechanism", *Applied Physics Letters*, **55**, pp. 1606-1608, 1989

[5.16] Y. Luo, Y. Nakano, K. Tada, T. Inoue, H. Hosomatsu, H. Iwaoka, "Fabrication and characteristics of gain-coupled distributed feedback semiconductor lasers with a corrugated active layer", *IEEE Journal of Quantum Electronics*, **QE-27**, pp. 1724-1731, 1991

[5.17] L. Olofsson, T. Brown, "The influence of resonator structure on the linewidth enhancement factor of semiconductor lasers", *IEEE Journal of Quantum Electronics*, **QE-28,** pp. 1450-1458, 1992

[5.18] P. P. Vasil'ev, *Ultrafast Diode Lasers: Fundamentals and Applications*, Artech House, 1 May, 1995

Chapter 6

Design of high-quality ultrafast diode laser sources

In this chapter, we present several ideas for design of compact and robust ultrafast diode lasers. We are trying to design a new type of device composed of two separate parts, a pulse generator and an auxiliary passive device, integrated in one compact chip. The approaches used for pulse generation are gain-switching and Q-switching techniques, which are appropriate for delivering high energy pulses. The passive devices for signal transformation are based on planar waveguide structures.

6.1 Introduction

Ultrafast diode lasers are the most compact, and probably the most cost-effective, existing type of generators of ultrashort optical pulses. Today, there is growing demand of such compact ultrafast laser sources for applications in telecommunication, sensing, medical diagnosis, spectroscopy, biological imaging, etc. However, there are several fundamental drawbacks of diode-laser-based pulse sources. Although it is relatively easy to produce optical pulses from a diode laser, generally, the quality of these pulses is usually low. Typically, diode lasers exhibit limited peak power, poor spectral and beam quality, presence of a pedestal, and relatively long pulse duration. Although some of these parameters can be improved simultaneously, as we discussed in the above chapters, it is currently impossible to obtain an ultrashort pulse signal from a diode laser that has a quality comparable with a pulsed fibre laser or a pulsed solid-state laser. Therefore, it will be highly advantageous to design diode-laser-based devices which are specifically used for pulsed operation and are able to replace the existing bulky pulsed laser systems.

Among the three basic approaches of generating ultrashort pulses from diode lasers, mode-locking produces the shortest pulse duration, the lowest timing jitter and the highest repetition frequency. The peak power of the pulse, which used to be relatively low compared with gain-switched or Q-switched devices, has now increased to more than 1W from passively mode-locked VCSELs with pulse duration shorter than 500fs [6.1, 6.2]. Hence, it is one promising way to design next-generation, high-quality ultrashort pulse generator based on mode-locked diode laser devices. One the other hand, gain-switching and Q-switching are simpler approaches for generation of high power short pulses, and it is possible to employ auxiliary devices that could improve the quality of the laser pulses dramatically. The auxiliary device can be represented by a dispersive delay line acting as a linear compressor [6.3], a spectral element [6.4], a nonlinear pulse compressor [6.5], or a nonlinear filter [6.6]. Indeed, the effect of the

auxiliary pulse transformer can be very significant. For example, a two-stage fibre-based pulse compressor is able to transform 20ps gain-switched laser pulses into 250fs, spectrally limited, pedestal free pulses [6.6]; an increase of peak power of a pedestal-free pulse by a factor of 5 was achieved using a fibre Bragg grating based notch filter, with precise tuning, to suppress the pulse tail [6.4]. In this chapter, we will present our design consideration for next-generation high-quality ultrafast diode laser sources with focus on the pulse generators and auxiliary devices respectively.

6.2 Design of pulse generators

6.2.1 Gain-switched devices

A large amount of nonlinear or linear chirp always appears in gain-switched pulses. It is possible to use auxiliary devices to compress the pulses to obtain Fourier-transform-limited pulses. However, the effect of compression is strongly dependent on the initially generated pulses. Here, the most appropriate pulse generators are single-longitudinal-mode devices, such as DFB or DBR lasers. As we discussed in Chapter 5, the pulse chirp is easy to control within only one laser mode. Our following discussion is based on this type of laser.

The pulse chirp is determined, to large extent, by the linewidth enhancement factor, α, of the material in the active region, defined by equation (2.21). Significant research efforts over several decades have been dedicated to realising structures with reduced α-factor, especially for applications in data transmission, involving high-speed modulation. However, a pulsed laser designed for subsequent pulse compression can benefit from a high α-factor. Indeed, a well-known way to linearly compress the output pulse of a gain-switched laser is to compensate the pulse chirp by transmitting it through a dispersive delay device. Assuming the chirp to be uniform, which is achievable in single-mode devices, the compressed pulse duration is simply inversely

proportional to the spectral bandwidth of the signal. A similar laser with increased α would generate longer pulses with wider spectral bandwidth, so better suited for linear compression. Thus, although greater α reduces, arguably, the pulse quality directly at the laser output, it improves the operation of the laser-compressor subsystem. Therefore, it would be possible to obtain femtosecond pulses simply by linear compression, which could only be achieved previously using multi-stage soliton pulse compression systems. It will substantially reduce the cost and spatial size and improve the stability of femtosecond pulse generation system.

Design of a large α-factor pulse generator can be based on the widely used single/multi-quantum-well structures. It is known that reducing the barrier height of the quantum well structure will increase the α-factor [6.7]. In shallower wells, the barrier states are more easily populated by carriers than in deep wells. The larger number of barrier carriers leads to a lower differential gain, higher differential refractive index changes and, therefore, larger α-factor values. It has also been reported that the number of quantum wells affects the α-factor [6.8]. Single quantum well structures produce high α-factors due to the high threshold carrier densities needed to attain lasing. Therefore, structures with lower barriers than the standard laser structure, and the effect of the number of quantum wells on the output pulses, are important issues for the design of high-α-factor pulse generators.

As we mentioned earlier, the high-α-factor pulse generators should ideally be single-mode devices, like DFB or DBR lasers. However, it may lead to low pulse energy as a result of small mode volume. From this point of view, this kind of laser design is not suited for high power pulse generation. Hence, we may turn to Q-switched devices to solve this problem.

6.2.2. Q-switched devices

Most of the previous work on Q-switched lasers with saturable absorbers aimed at increasing the output power and the Q-switching frequency. Relatively little effort has yet been applied to study the intrinsic (i.e. not involving external seeding or external feedback) spectral control in these devices, and only a small number of publications is available on this subject [6.9]. Generally, it is difficult to implement precise spectral control in Q-switched devices, as the feedback from spectral elements (gratings) reduces the contrast of the loss (on-off ratio) in the laser cavity. As a result, the laser cavity does not "lock" properly in the "off" state, and the Q-switching performance deteriorates.

Fig. 6.1 Schematic diagram of three contact MQW DFB laser [6.9]

Actually, internal spectral control is achievable in DFB and DBR lasers for Q-switched operation. It has been reported that Fourier-transform-limited Q-switched pulses can be achieved in a triple-contact DFB lasers [6.9]. In these lasers, there are two amplifier sections, with a saturable absorber located between them to facilitate carrier drift, shown in Fig. 6.1.

Optical loss in the cavity was altered by applying a reverse DC bias to the absorber section. Electron-hole pairs in the absorber section are transported rapidly by the

strong electric field back to the amplifier section. So, as the electron-hole pairs are accumulating in the amplifier the absorption coefficient of the central section remains constantly high and the Q-factor of the laser cavity is still low. The amplifier inversion population is occupying deeper and deeper levels in the bands due to the combined action of intraband thermalisation and the Paoli rule. When the injection carrier concentration becomes large enough, the absorber can not copy with the spontaneous photons so that it bleaches, the cavity is then "turned on", and giant picosecond pulse is generated. Meanwhile, spectral control was provided by the built-in distributed-feedback structure. As a result, the generated pulses had a peak power in excess of 200mW and a time-bandwidth product of 0.24, which is the lowest value ever reported in Q-switched devices.

Further investigation of multiple section Q-switched devices concerned with the number of contacts and the position and length of the absorber and amplifier sections [6.10] indicates there are many other multiple-section geometries, other than triple-contact devices with absorber section in the centre, which are also suitable for producing high energy Q-switched pulses. Therefore, with spectral control in mind, we intend to design a new type of Q-switched DFB or DBR devices based on optimised multiple-section geometry.

6.3 Design of auxiliary devices and subsystem integration

In this section, we will present our design consideration of linear and nonlinear transformation of pulses from directly modulated diode lasers (with or without the amplifying stage) by a passive optical device. A pulsed LD will produce picosecond optical pulses: the exact requirements on the pulse duration and peak power needed for compression will depend on the type of pulse compressor. The compressor can be

either made of fibre or based on a waveguide technology (planar or 3-D, non-resonant or resonant). Fibre devices have the advantage of long length and, hence, the ability to respond nonlinearly to low-intensity laser pulses. Effective nonlinearity as high as γ=550(W^{-1}*km^{-1}) has been measured in specialist fibres [6.11]. However, even a short fibre represents a relatively bulky element, incompatible with the on-chip integration strategy. It also requires special efforts for signal coupling.

We intend to transfer the fibre-validated techniques into new platforms, such as planar silica structures, to provide the foundation for future integrated subsystems. The problems to be addressed here arise, firstly, from the fact that planar elements are usually limited in size and, hence, can provide only limited effective nonlinear length. Thus, nonlinear processes in these elements only come into play if the optical signal intensity is significant. If we assume a length L of a singlemode waveguide inscribed in planar silica structure to be of the order of 10cm and an effective nonlinearity similar to that in photonic crystal fibres, then a nonlinear phase shift of π in such a structure demands a peak optical pulse power of $P = \pi/(\gamma L)$ ~20W. This level of power is not impossible to achieve from a LD, and there have been demonstrations of both lasers and amplifiers producing peak powers in this range. However, in practice the LD signal must be coupled to a tightly confined waveguide, demanding an exceptionally good quality laser beam. If the final goal is to obtain a femtosecond output from the pulse transformer, then the other prerequisites for the pulsed 'pump' would be reasonably short initial pulse duration, probably <10ps, and good spectral quality of the LD output. The approaches to achieve the required initial pulses have been discussed in section 6.2.

As far as materials are concerned, use of a resonant rather than a non-resonant interaction is attractive through the increased nonlinearity. Thus, materials with narrower bandgap, such as doped glasses, non-silica glasses, or semiconductors, rather than the more readily available silica-based glasses will be considered. The key element in the passive device could be fabricated by femtosecond pulse waveguide

inscription technology, which is currently being developed at Aston using a recently installed, state-of the art experimental installation. Femtosecond inscription in glass has been demonstrated by a number of groups worldwide during the past 6 years and is met with significant interest by the optoelectronic community [6.12, 6.13]. The known advantages of the technique are its ability to process a large variety of materials and exceptional device design flexibility. The latter is provided by the large refractive index difference achievable and, even more, by the possibility to control the refractive index, and so produce structures, in three dimensions. In our plan, femtosecond inscription will be employed to produce the dedicated passive elements for linear and nonlinear transformation of LD pulses. It is intended to attempt to integrate a passive device and a LD (or a LD-MOPA tandem) on a hybrid platform, most likely silica-based.

6.4 Conclusion

In conclusion, our design consideration of new type ultrafast diode laser sources includes: (1) A family of novel, pulsed (gain-switched or Q-switched) diode laser devices, dedicated to operation in conjunction with auxiliary passive elements. For gain-switched devices, single-mode lasers made of large α-factor materials are considered to be suited for generating highly linear chirped pulses so as to facilitate subsequent pulse compression. For Q-switched devices, multi-section DFB or DBR devices consisting of gain sections and absorption sections are considered to be suited for generating spectral controlled Q-switched pulses. (2) A range of compact passive elements suitable for hybrid integration with pulse generators. As a consideration of subsystem integration, planar waveguide structures are more preferable than fibre-based devices. (3) Prototype subsystems comprising a single or a tandem LD pump and a passive pulse transformer, generating high power, high-quality, ultrashort pulses on demand.

References

[6.1] A. Garnache, S. Hoogland, A. C. Tropper, I. Sagnes, G. Saint-Girons, J. S. Roberts, "Sub-500-fs soliton-like pulse in a passively mode-locked broadband surface-emitting laser with 100 mW average power", *Applied Physics Letters*, **80**, pp. 3892-3894, 2002.

[6.2] R. Haring, R. Paschotta, A. Aschwanden, E. Gini, F. Morier-Genoud, U. Keller, "High-power passively mode-locked semiconductor lasers", *IEEE Journal of Quantum Electronics*, **38**, pp. 1268-1275, 2002

[6.3] S. Arahira, S. Kutsuzawa, Y. Matsui, Y. Ogawa, "Higher order chirp compensation of femtosecond mode-locked semiconductor lasers using optical fibers with different group-velocity dispersions" *IEEE Journal of Selected Topics in Quantum Electronics*, **2**, pp. 480-486, 1996

[6.4] M. Dubov, D. Giannone, I. Khrushchev, I. Bennion, "Pulse tail suppression in laser diode output by tunable notch filter", *Electronics Letters*, **37**, pp. 1404-1405, 2001

[6.5] Y. Matsui, M. Pelusi, A. Suzuki, "Generation of 20-fs optical pulses from a gain-switched laser diode by a four-stage soliton compression technique", *IEEE Photnics Technology Letters*, **11**, pp. 1217-1219, 1999

[6.6] I. Khrushchev, I. White, R. Penty, "High-quality laser diode pulse compression in a dispersion-imbalanced loop mirror", *Electronics Letters*, **34**, pp. 1009-1010, 1998

[6.7] J. Stohs, D. Brossert, D. Gallant, and S. Brueck, "Gain, refractive index change and linewidth enhancement factor in broad-area GaAs and InGaAs quantum-well lasers", *IEEE Journal of Quantum Electronics*, **37**, pp. 1449-1459, 2001

[6.8] M. Hochholzer and V. Jordan, "Discussion of the linewidth enhancement factor α of GaAs/AlGaAs quantum well lasers", *IEE Proceedings-Optoelectronics*, **141**, pp. 311-315, 1994

[6.9] P. Vasil'ev, I. White and M. Fice, "Narrow line high power picosecond pulse generation in a multicontact distributed feedback laser using modified Q switching", *Electronics Letters*, **29**, pp. 561-563. 1993

[6.10] Z. Jiang, I. White, F. Laughton, H. Summers, R. Penty, P. Vasil'ev, "Optimization of high-power picosecond pulse generation in multicontact

semiconductor laser diodes", *Proceeding of Conference on Lasers and Electro-Optics 1995* (CLEO'95), pp. 14-15 (CMC7). Baltimore, MA, 1995

[6.11] D. Richardson, J. Lee, Z. Yusoff, W. Belardi, K. Furusawa, J. Prince, M. Kiang, K. Frampton, D. Hewak, J. Tucknott, R. Moore, H. Rutt, and T. Monro, "Holey fibers for nonlinear fiber devices", *Optical Amplifiers and Their Applications (OAA) 2002*,Vancouver, Canada, 14-17 July 2002

[6.12] C. Schaefer and E. Mazur "Micromachining using ultrashort pulses from a laser oscillator", *Optics and Photonics News*, April, 2001, pp. 20-23

[6.13] K. Hirao, T. Mitsuyu, J. Si, J. Qui, *Active glass for photonics devices*, Springer, 2001

Chapter 7

Thesis conclusions and future work

7.1 Thesis conclusions

This thesis presents experimental investigation of ultrashort pulse generation from semiconductor diode lasers with various materials, structures, and at different wavelength regions. Detailed experimental work, experimental results, and discussions for the generation of optical pulses with high-energy, short pulse duration, good pulse quality, good spectral quality, and wide wavelength tuneability are given. The ideas about the design of next-generation, compact, good-quality, and cost effective short pulse sources are also discussed. We employed very simple techniques and experimental configurations all through our experiments and achieved exceptionally good experimental results. We endeavoured to use simple and persuadable theories to explain the experimental phenomena and the achieved results. Some theories are adequate for the explanation of the experiments and for future laser design; however, some hypotheses are also given for the explanation of peculiar phenomena in the experiments. The achievements described in this thesis are summarised as follows:

At the beginning, we used a gain-switched, grating coupled surface emitting laser (GCSEL) to achieve generation of picosecond optical pulses with a remarkably wide tuning range of 100nm (from 900nm to 1000nm). The laser operated in a simple external cavity and produced pulses with duration in range 40-100ps and maximum

peak power of 0.88W. The narrow signal spectrum corresponded to the side-band suppression ratio in excess of 40dB and indicated single-frequency operation.

The demand for short pulse sources, operating at shorter wavelengths around 400nm, at the moment is constantly growing. More than 100 companies worldwide offer relevant products. However, a typical peak power delivered by commercial products is in range 0.1W to 0.5W. Some applications require precise spectral control, which also represents a technical challenge. We experimentally investigated the pulsed operation of InGaN violet diode lasers, paying particular attention to optimisation of the laser in terms of output power and/or spectral control.

In particular, we optimised the driving conditions for gain-switching of a commercial InGaN diode laser and obtained the record peak power in excess of 7W, representing an improvement by more than an order of magnitude compared with the known previous results. In another experiment, we achieved a stable operation of a self-seeded, gain-switched commercial InGaN diode laser in a simple external cavity. As a result, single-frequency, wavelength-tunable, picosecond pulses were achieved from a standard, uncoated diode laser with an external feedback by carefully adjusting the operation regime. The output laser pulses were characterised by the high peak power of 0.4W, narrow linewidth of 0.1 nm, spectral sideband suppression ratio in excess of 20 dB and wavelength tuneability over 3.5nm. The on-going part of this work aims at substitution of the bulk optical elements in the prototype with the new fibre components, currently being developed in the group.

In Chapter 5, the issue of relaxation tails suppression of high-energy ultrashort pulses is discussed. Our experiment demonstrated tuneable fibre Bragg gratings, as a spectral filtering element, could be used to suppress a large proportion (>80%) of the relaxation tail of laser pulses obtained from an overdriven GaAs DFB laser operating at 860nm. Theoretical analysis shows although fibre Bragg grating served as a high quality band-pass filter, the effectiveness of spectral filtering depends on whether the

spectral components of the first peak are completely separated from relaxation tail.

Finally, we present the idea of building compact, high quality ultrashort pulse sources comprising of pulse generators and auxiliary passive devices. The pulse generators for gain-switched operation could be singlemode lasers, like DFB or DBR lasers, with large value of line width enhancement factor. They are specifically designed in conjunction with subsequent pulse compressor. Q-switched pulse generators are designed to incorporate internal spectral control mechanism aiming to generate high-energy singlemode pulses. The design of auxiliary passive pulse transformers is largely dependent on the quality of initially generated pulses. Planar waveguide structure is highly preferred due to its compact size and the suitability for subsystem integration.

7.2 Future work

For future work of grating-coupled surface emitting lasers, we suggest to set up a model specially designed for the high power gain-switched behaviour of external cavity GCSEL. The spectral filtering mechanism would be included in the model. It will be instructive to know the dependence of temporal, spectral and spatial characteristics of the output pulses on laser structure parameters. We may modify the theoretical model by using different external feedback element, e.g. convex mirrors with different curvature or diffraction gratings. The wafer structure used in the model could also be modified, e.g. multi-quantum-well structure, tapered gain section, angled grating in the passive section, etc. For experimental work, we could design a new type of lasers made based on the proper laser parameters suggested by the above theoretical model. In addition, mode-locking of the GCSEL is also realistic task by using proper external cavity optics and thermal control devices.

For future work of violet InGaN lasers, we firstly suggested an improved self-seeding setup. As mentioned early, in our Littrow self-seeding setup, the 50/50 beam splitter reduced the power of feedback signal by a factor of 4. Alternatively, we may achieve high power feedback as well as stable output beam if a Littman configuration is used. This configuration was first designed for dye lasers, the only broadly tuneable lasers at that time, and later it proved useful when semiconductor lasers emerged [7.1]. Fig. 7.1 shows the simplest Littman configuration for self-seeding of gain switched InGaN laser. The most obvious advantage of this setup is substantial increase of feedback signal power without introducing angular displacement of output beam. With enough "quantity" of feedback signal, we are able to improve the "quality" of the feedback signal with even smaller bandwith. This can be achieved using a grating with higher resolution. We, therefore, expected a wider single frequency tuning range with improved side band suppression ratio to be achieved under both CW and pulsed modes with this setup.

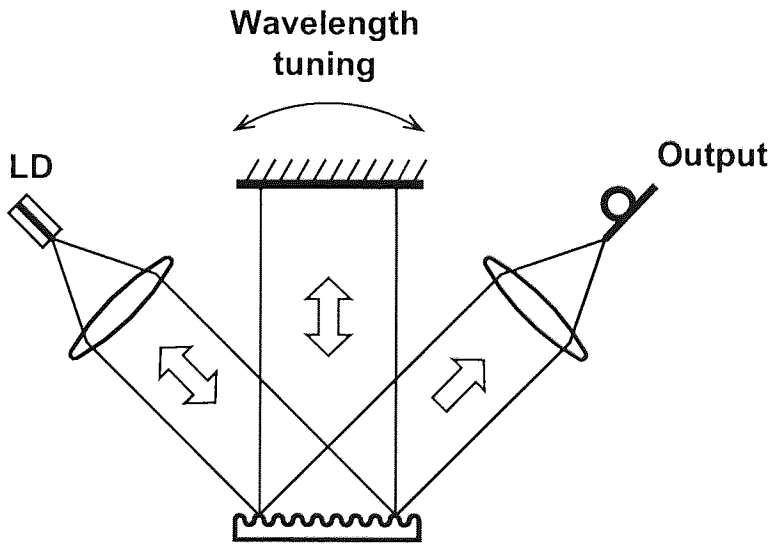

Fig. 7.1 Littman configuration for self-seeded operation

The other suggestion of future work is to improve spectral quality of highly intensive gain-switched pulses. It will be of great importance for applications if we can achieve single mode wavelength tuneable picosecond pulse from InGaN lasers with peak

power in excess of 7 Watts. CW seeding of gain switched operation may be one solution.

References

[7.1] D. Wandt, M. Laschek, A. Tunnermann, H. Welling, "Continuously tunable external-cavity diode laser with a double-grating arrangement", *Optics Letters*, **22**, pp. 390-392, 1997

Appendix

Publications

1. Y. Hu, A. Gubenko, G. Venus, I. Gadjiev, N. Il'inskaja, S. Nesterov, E. Portnoi, M. Dubov, I. Khrushchev, "Generation of an external cavity grating-coupled surface emitting laser with wide tunability", *Applied Physics Letters*, **82**, pp. 4236-4237, 2003.

2. Y. Hu, M. Dubov, I. Khrushchev, "Spectrally controlled gain-switched operation of an InGaN diode laser", *Electronics Letters*, **40**, pp. 702-703, 2004.

3. Y. Hu, A. Gubenko, G. Venus, I. Gadjiev, N. Il'inskaja, S. Nesterov, E. Portnoi, M. Dubov, I. Khrushchev, "Widely tunable gain-switched operation of external cavity grating-coupled surface emitting laser", *Ultrashort Photonics, Proceedings of the Fifty-Sixth Scottish Universities Summer School in Physics (SUSSP'56)*, poster sessions, pp. 342, St Andrews, UK, 1-13 Sep 2002,

4. Y. Hu, M. Dubov, I. Khrushchev, "High power gain-switched operation of an InGaN multi-quantum-well diode laser", under preparation.

5. Y. Hu, A. Gubenko, G. Venus, I. Gadjiev, N. Il'inskaja, S. Nesterov, E. Portnoi, M. Dubov, I. Khrushchev, "Widely tunable gain-switched operation of external cavity grating-coupled surface emitting laser", *Proceedings of the Society of Photo-Optical Instrumentation Engineerings (SPIE)*, **4913**, pp.145-148, Photonics Asia, Shanghai, P. R. China, 15-17 Oct, 2002.

6. Y. Hu, M. Dubov, I. Khrushchev, "Self-seeded gain-switched operation of an InGaN MQW laser diode", *Proceedings of the Society of Photo-Optical Instrumentation Engineerings (SPIE)*, **5452**, pp. 625-627, Photonics Europe, Strasbourg, France, 26-30 Apr, 2004.

7. Y. Hu, M. Dubov, I. Khrushchev, "High-power picosecond pulse generation from a gain-switched violet diode laser", *Conference on Lasers and Electro-Optics (CLEO) 2004*, **CThW2**, San Francisco, CA, USA, 17-21 May, 2004.

8. Y. Hu, M. Dubov, I. Khrushchev, "Spectrally controlled, picosecond pulse generation from an InGaN violet diode laser", *The 17th Annual Meeting of the IEEE Laser & Electro-Optics Society (LEOS)*, **MC 6**, Rio Mar, Puerto Rico, 7-11 Nov, 2004